Utrecht University

Utrecht University

Institute for Theoretical Physics

Master's Thesis

Large Scale Structure on the Light Cone

Author:
Michiel Zoomers
3856437

Supervisor:
Dr. Enrico Pajer

December 15, 2016

Abstract

In this thesis, we study the light cone effect when applying standard perturbation theory (SPT) of large scale structure to observations. We start by explaining how in SPT, the evolution of matter structure in the universe is assumed to be described by Newtonian dynamics, allowing for a hydrodynamic approach. The results for the fluid equations can be expanded perturbatively, which improves the accuracy of the description order by order. When applying SPT to observations, the light cone effect arises because galaxies are observed on the past lightcone. This induces a time dependence that is normally dealt with by dividing up the past lightcone into bins, where the time is set to the time corresponding to the center of this bin. However, because many high-precision experiments probing large scale structure are planned in the near future, the inaccuracy this approximation induces might become significant. Therefore, we include the light cone effect by evaluating the full time dependent results for observations in such bins. We show that the theoretical accuracy gained by this inclusion becomes significant (i.e. of order 1%) when probing large scale structure in surveys where the relative size of the redshift bin width with respect to the redshift of the center of the bin obeys $\Delta z \gtrsim 0.35(1+z)$.

Contents

Chapter 1

Introduction

1.1 Introduction

It is a familiar experience to practically every human being: gazing up at the stars in awe, wondering what those lights in our sky are and what our place is within the grand scheme of things. Since the earliest recorded history of mankind, people have been trying to find answers to those fundamental questions. Back in ancient times, people tried to explain the night sky using stories and parables, but as human civilization progressed, so did our understanding of the universe. The ancient Greeks were able to distinguish planets from stars, and later on Galileo Galilei conjectured (correctly) that we live in a solar system with planets revolving around the sun. It was only in the 20^{th} century however, that mankind understood that our solar system is but a single star among the many in the Milky Way galaxy, which itself is only one of the many galaxies in our universe.

Following this realization, we discovered that galaxies and intergalactic clouds form a web-like pattern of clusters, voids and filaments, an observation of which is given in figure 1.1 [15]. The study of *large scale structure* is the study of this pattern, or equivalently the study of matter structure within the universe.

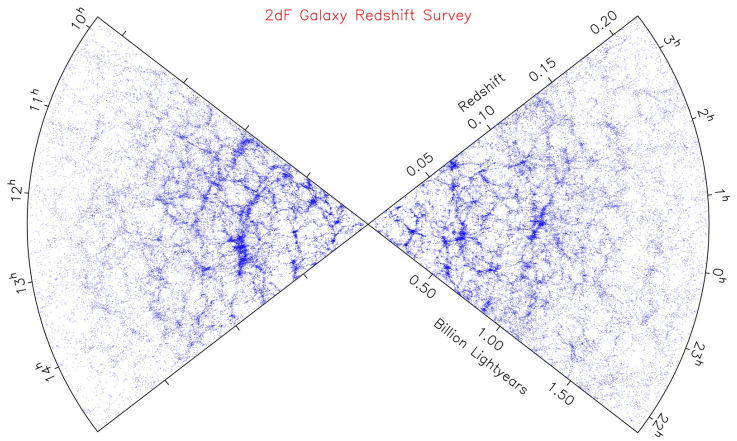

Figure 1.1: The large scale structure in the universe as observed in the 2dFGRS. Each blue dot marks an observed galaxy [15].

Why, then, would we want to study this pattern. Scientific interest alone is as worthwhile a reason as any, but the importance of studying large scale structure extends beyond that. Large scale structure turns out to be an excellent probe of parts of our universe we do not understand.

Current understanding of our universe is, at best, limited. Only 4% of it consists of stars, planets and other things we are familiar with. The other 96% of the universe consists of *dark matter* and *dark energy*, neither of which we can observe directly, and neither of which we understand. Moreover, we have not been able to explain conclusively why our universe is homogeneous. The theory of *inflation* is the most popular explanation, but it lacks experimental corroboration. Besides, one of the open question in physics is the size of the neutrino mass. Observations of large scale structure can probe these poorly understood phenomena and help us to understand our universe better [5, 6, 44]. Hence, it is imperative that the theory used to interpret observations is as accurate as possible. More specifically, our theoretical predictions need to be accurate at the 1% level to be in line with the next generation of large scale structure observations.

The theory used to describe our observations is called *Standard Perturbation Theory* (SPT). Usually, when applying SPT to observations, we use an approximation to deal with the fact that observations of large scale structure lie on the past light cone of an observatory on earth.[1]

Let us first consider the actual situation, with galaxies lying on the past light cone. Because galaxies (or cosmological objects in general) are observed on the past light cone, we typically see them at *different* times in the past, where the exact time depends on the radial distance from the earth. This can be seen in figure 1.2.

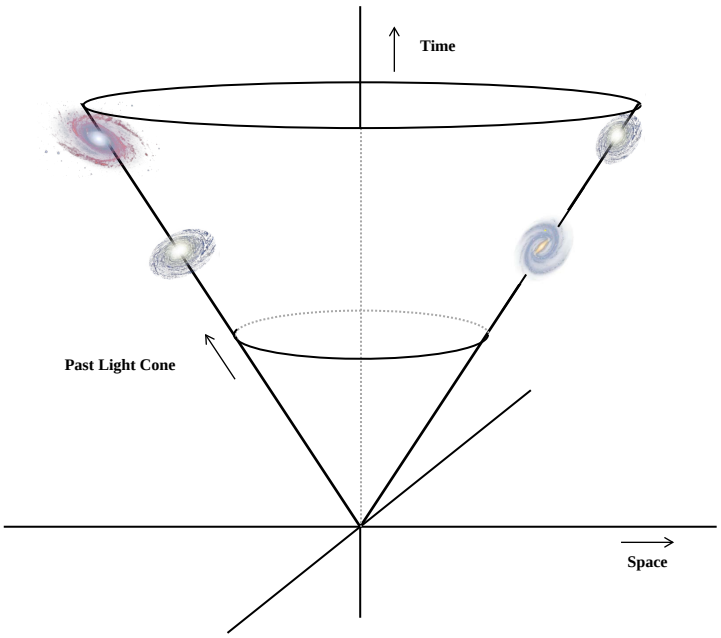

Figure 1.2: Galaxies are observed on the past light cone of the earth. Therefore, galaxies are observed at different times in the past, which correspond to the radial distance from the earth.

This effect is usually approximated by dividing up observations into bins along the line of sight. Galaxies within such radial distance bins typically have different time coordinates, which correspond to

[1] Or an observatory in space, but because we are considering large scales, the distance between the surface of the earth and an orbit around it is negligible.

their individual radial distance. Because these different time coordinates lead to complications when applying the theory to observations, galaxies are approximated to lie on the equal time hypersurface corresponding to the bin's center. In other words, the time coordinate of galaxies within a bin is set to the time coordinate corresponding to the radial distance of the center of the bin. This approximation is visualized in figure 1.3, where we applied it to the observation in figure 1.2. In the figure, all galaxies are assumed to lie in a single radial distance bin.

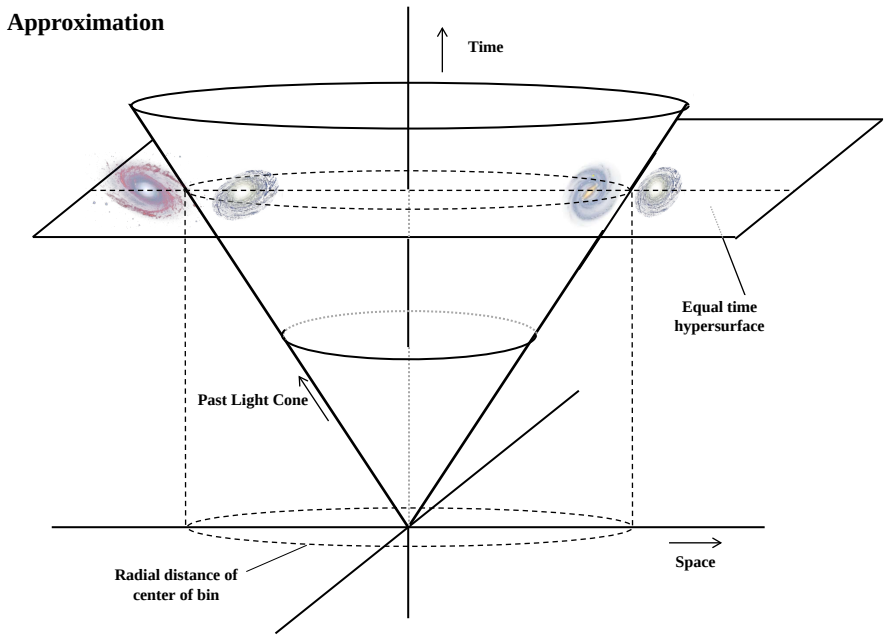

Figure 1.3: The approximation that is usually made for an observation (specifically, this is the approximated picture for the observation in figure 1.2). In observations, galaxies are divided up into radial distance bins. For galaxies within such a bin, the time coordinate is approximated by the time corresponding to the center of the bin. In the figure, this time is the equal time hypersurface that corresponds to the radial distance of the center of the bin.

This approximation causes inaccuracy in the theoretical description of observations. Therefore, we incorporate the light cone effect analytically in this thesis. We will divide up the radial distance into bins, and within these bins we will calculate the exact results for observations on the light cone. Doing this, we can calculate the size of the correction we have to make with respect to the approximated result. We will see that in the linear case there is no correction term. However, in first order perturbative terms we find an analytic expression for the correction, which is given in equation (5.51). We have plotted the relative size of this correction with respect to the approximated result in figure 1.4. Note that the axes give the bin width and radial distance to the center of the bin in terms of *redshift* z, which is a cosmological parameter that can be used to parametrize radial distance. We see that for wide bins (large Δz) at low redshift (small z) the correction is larger than 1% with respect to the approximated result. This implies that the light cone effect is significant for large scale structure surveys probing in this domain.

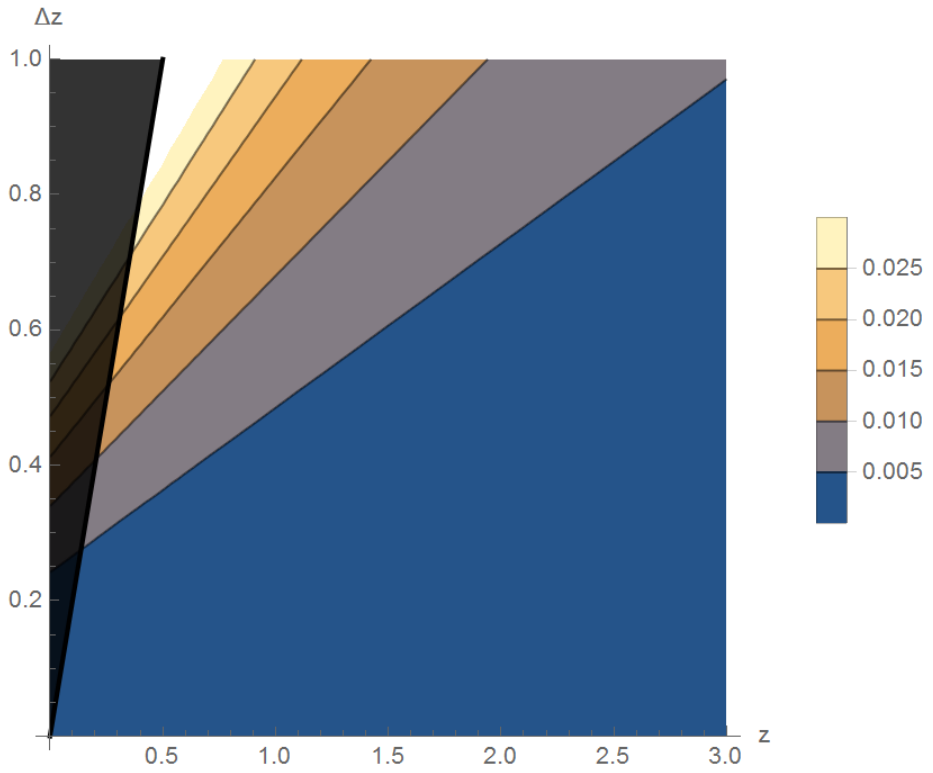

Figure 1.4: The size of the correction required because of the light cone effect. We see that corrections are significant ($> 1\%$) for observations with relatively large bin size Δz at relatively low redshift z. We have greyed out the area where $\Delta z > 2z$, because we cannot observe at negative z.

Outline of this thesis:

In chapter 2, we give a brief overview of the key concepts in modern cosmology. We will describe the expanding universe and state the Friedmann equations which govern this expansion. We will derive how different forms of energy affect the scale factor a, which parametrizes the expansion of our universe, and give an overview of the densities of different energy components of the universe.

After this, we will introduce Standard Perturbation Theory in chapter 3. We will derive the equations which govern the formation of structure, and work out the results in a matter-only cosmology. We will discuss how a stochastic treatment is required to come to meaningful results, and derive the power spectrum and corrections until the so-called one-loop order. After this, we will briefly discuss how observations of cosmological distance using redshift of observed objects can distort the picture we obtain.

Having explained the theoretical framework, we will move on to explain the value of large scale structure as a probe in chapter 4. We will describe how we can use large scale structure as a probe, and discuss the next generation of surveys.

In chapter 5, we apply SPT to observations without approximations to the light cone effect. We start by defining a finite volume Fourier transform along the line-of-sight, which is necessary because we will work in (finite volume) bins. We work out the implications of such a finite volume Fourier transform in a one-dimensional toy model. Following that, we develop our theory on the light cone. We derive results up to one-loop order and quantify the difference the light cone effect induces.

Finally, we summarize our findings and discuss the implications of our results in chapter 6. We give an outlook to additional research that can be done in the area, giving suggestions on how to extend our results to improve the theory further.

Chapter 2

Modern cosmology

2.1 Introduction

In order to give a theoretical description of large scale structure, we need to start at the basics of modern cosmology, which will underlie this theory. In this chapter, we will summarize that (and how) cosmology describes an expanding universe depending on its energy content, allowing us to describe its effects on large scale structure.

The basis of cosmology is found in the theory of an expanding universe. In the early 20^{th} century, it became known that the universe was expanding after observations of Edwin Hubble. As one could imagine, this expansion needs to be taken into account when doing physics related to the evolution of the universe. Therefore, we will introduce important cosmological quantities such as the Hubble rate H, the scale factor a and the comoving distance χ in this chapter. Moreover, we will discuss the Friedmann-Lemaître-Robertson-Walker (FLRW) metric, which was independently proposed by these four scientists around the same time as the observations of Hubble, basing the result on Albert Einstein's completion of his comprehensive theory of general relativity in 1915 [19].

Starting from the FLRW metric we can write down the Friedmann equations, named after Aleksandr Friedmann who derived them in 1922 [23] making use of Einstein's formalism. From these equations we learn that the energy content ρ of the universe is integral to the evolution of the universe. We will describe two toy models of the universe, to show the power of the Friedmann equations when trying to get a grip on the evolution of the universe.

In the following section, we will discuss the standard model of cosmology, which specifies the energy content of the universe to consist of baryonic matter, dark matter and dark energy. Moreover, we will give an overview of how this energy content of the universe changed in the past, leading to the introduction of the radiation and matter domination era of the universe. Both the current energy content and past energy content of the universe have an effect on large scale structure, which we will describe in the next chapter.

Note that in this chapter we will mainly follow Scott Dodelson's book on modern cosmology in our discussion of the key concepts [18].

2.2 Cosmological quantities and the FLRW metric

In the beginning of the 20^{th} century, Edwin Hubble was one of the first people to systematically map intergalactic objects. Using an ingenious application of the Doppler effect on the wavelength of emitted light, he was able to map relative speed as well as distance of these objects. In 1929 his work paid off,

giving evidence for what later would become known as Hubble's law: distant objects in the universe recede from us, and the further away they are, the faster they recede from us. In other words: the universe is expanding. The original diagram Hubble wrote down in his paper can be seen in figure 2.1, and since these types of diagrams have been called Hubble diagrams.

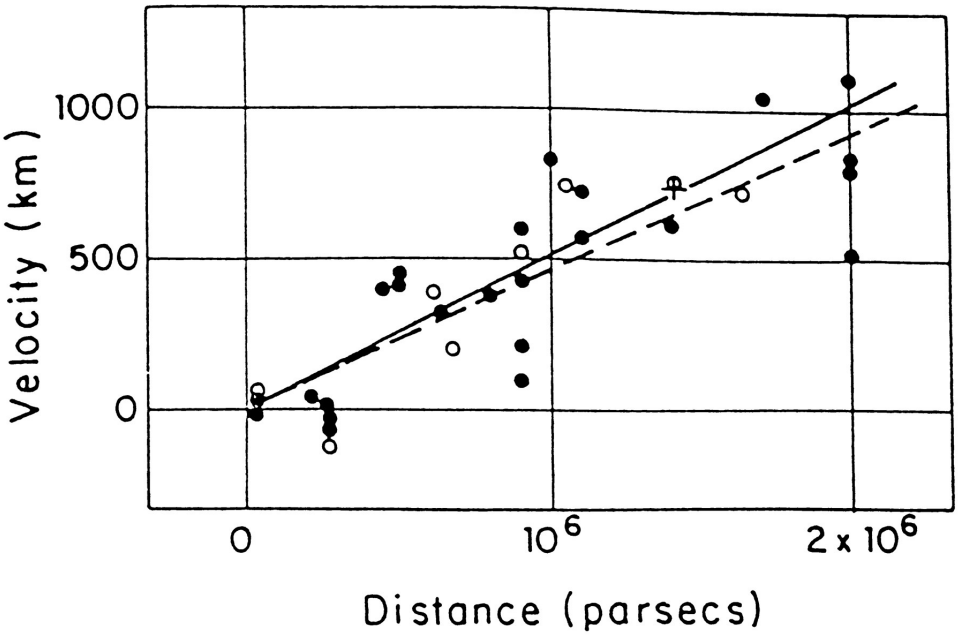

Figure 2.1: The original Hubble diagram as published in Edwin Hubble's 1929 paper [33]. On the horizontal axis we see the distance in units of parsecs (equivalent to about 3.26 light years), and on the vertical axis we see the recession velocity. Note that there is a mistake in the unit for the vertical axis, as it should be km/s. The solid line gives the best fit corrected for the motion of the sun within the milky way, the dashed line gives the best fit without taking this motion into account.

Mathematically, Hubble's law is described in terms of a linear relation between distance d and recession velocity v as given in equation (2.1), where the proportionality constant is called H_0 or the Hubble constant. As we can see from elementary dimensional analysis, the unit of the hubble constant is s^{-1}, but conventionally it is given in terms of km s^{-1}Mpc^{-1}. The latter unit is useful, because it immediately tells us how fast and object at a distance of one Mpc is receding from us in km/s.

$$v = H_0 d. \tag{2.1}$$

However, there is a more useful mathematical way to think about the expansion of the universe, especially because Hubble's law only holds for objects that are in relative proximity to our cosmological location in the universe. When objects are farther away, we need to take into account the composition of the universe in the past in ways that we will introduce later. Moreover, Hubble's law does not directly introduce a quantity with which we can easily describe the size of the universe in the past. In order to do that, we introduce a scale factor which describes the size of the universe in relation to the current size. Following conventions, we will call this scale factor $a(t)$, and normalize it such that its present day value is equal to one:

$$a(t_0) \equiv 1, \tag{2.2}$$

where t_0 is the current time. In this way, we get a simple and intuitive way to quantify the size of the universe at any given point in time.

In addition to the scale factor, we can define a quantity called *redshift*. As the universe is expanding, the wavelength of a photon travelling through the universe gets elongated proportionally. Because longer wavelengths correspond to the red end of the spectrum, this elongation is called *redshift*. This redshift z is what Hubble used to measure the recession speed of distant objects, and its current value is related to the scale factor by:

$$1 + z \equiv \frac{1}{a}. \tag{2.3}$$

This relation can easily be derived from the definition of redshift using wavelengths λ, and the relation between the observed wavelength λ_0 at time t_0, the emitted wavelength λ_1 at time t_1 and the scale factor:

$$z \equiv \frac{\lambda_0 - \lambda_1}{\lambda_1}, \tag{2.4}$$

$$\lambda_0 = \frac{a(t_0)}{a(t_1)}\lambda_1. \tag{2.5}$$

As the redshift is also a measure of distance (by Hubble's law) and a measure of the evolution of the universe, we will often use the redshift as a scale for both the age of the universe and the distance of objects. In the following chapter, we will also introduce *redshift space* which effectively is the space in which our observations live.

Having introduced the scale factor and redshift, we can also think of our coordinates in space in a different way. Of course the physical distance between two different objects might be growing in time, but that does not give us information as to the proximity of those two objects relative to the size of the universe. In order to get such a measure we introduce something called the *comoving distance*. We can think of the comoving distance as the distance measured in terms of a coordinate system within the universe. As the universe expands from time t_1 to time t_2, this coordinate system expands uniformly as well. So the comoving distance between two objects at fixed location in this coordinate system has remained the same, even though the physical distance has grown from a value d at t_1 to $d\frac{a(t_2)}{a(t_1)}$ at t_2. This is made visual in 2.2.

Let us make our formalism depending on the scale factor a little more rigorous. Even though we now have defined a factor that describes the size of the universe at any given point, we still do not know how that factor changes with time nor have we taken into account how quantities such as the comoving distance depend on this time dependence. Let us start from the point where we consider the scale factor $a(t)$ to be an arbitrary function of time. Then, we can define our comoving distance to an object at such a distance, that when it emitted its light the universe had (smaller) scale factor a. We will call this comoving distance $\chi(a)$, and it is defined using an integral, so that we will take into account the expansion of the universe while the light was moving toward us:

$$\chi(a) = \int_{t(a)}^{t_0} \frac{dt'}{a(t')}. \tag{2.6}$$

Moreover, we need to describe Hubble's law based on the scale factor to have it fit in our formalism as well. In order to achieve this, we will define the Hubble rate, which is given in equation (2.7):

$$H(t) \equiv \frac{da/dt}{a}. \tag{2.7}$$

We see that the correct unit for this quantity is s^{-1}, so this quantity can be used as an equivalent for the Hubble constant. If we then define the Hubble constant to be the value of the Hubble rate at the present day, so $H_0 = H(t_0)$, we regain Hubble's law for the recession of galaxies that are in our cosmological area. However, once again this does not take into account the previous time evolution of the universe. In order to say something sensible about the full time evolution of the universe, we then need to look at the equations from a perspective of Einstein's theory of general relativity. First, we recall

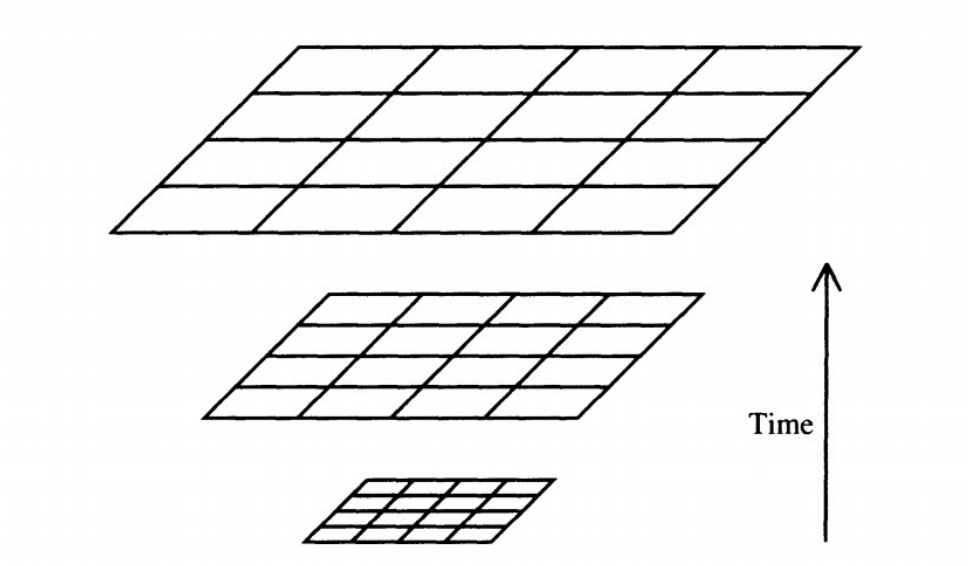

Figure 2.2: A visualization of the comoving coordinate frame. The physical distance between gridpoints increases with time, but as gridpoints describe comoving coordinates, the comoving distance remains the same. Taken from [1].

that in general relativity, the *metric* $g_{\mu\nu}$ is used to turn a coordinate distance into a physical distance. More formally, we can use the metric to define an invariant distance according to:

$$ds^2 = g_{\mu\nu} dx^\mu dx^\nu. \tag{2.8}$$

Starting from this point, Friedmann, Lemaitre, Robertson and Walker all indepently thought about a metric which would describe the universe at a large scale. They all were thinking about an expanding universe, and all came up with the idea of a scale factor a. After realizing that the 0^{th} coordinate describes time whereas the other three coordinates describe space, they came up with the metric that is now called the FLRW metric, given in equation (2.9). Please note that we are working in units of $c = 1$, and are assuming a flat universe. In the case of a curved universe, we can rewrite the spatial part of our metric to include a curvature parameter κ. However, as in this thesis we will be working in flat universes only, we will not do this here.

$$ds^2 = -dt^2 + a^2(t)(dx^i)^2. \tag{2.9}$$

We can also write the FLRW metric in a *conformal* way, which will be the form we use from chapter 3 onwards. To do this, we define the *conformal time* $\tau \equiv \int_0^t \frac{dt'}{a(t')}$ such that the metric becomes:

$$ds^2 = a^2(\tau)[-d\tau^2 + (dx^i)^2]. \tag{2.10}$$

We can also define the *conformal expansion rate* $\mathcal{H}$, which we will use instead of the Hubble rate from chapter 3 onwards as well:

$$\mathcal{H} \equiv \frac{d \ln a}{d\tau} = a(\tau) H(\tau) \tag{2.11}$$

From the FLRW metric, we can then use the toolbox of general relativity to come to a correct way of thinking about the expansion of the universe. Where Hubble's law gave the experimental proof that the universe is expanding, the actual rate of expansion at any given time follows from the application of general relativity to the FLRW metric. In the next section we will see the implications of this, and what they mean for the evolution of the universe in the past.

2.3 The Friedmann equations

The equations which we derive from general relativity based on the FLRW metric are called the Friedmann equations. These equations describe how the expansion of the universe took place as a function of the energy content of the universe. In order to arrive at these equations we need to look at Einstein's equations for the scale of the universe. We recall that Einstein's equations are given by equation (2.12):

$$G_{\mu\nu} \equiv R_{\mu\nu} - \frac{1}{2} g_{\mu\nu} R = 8\pi G T_{\mu\nu}. \tag{2.12}$$

Here, $R_{\mu\nu}$ is the Ricci tensor, a quantity depending on the metric and derivatives thereof. R is the Ricci scalar, a contraction of the metric with the Ricci tensor given by $R = g^{\mu\nu} R_{\mu\nu}$. $T_{\mu\nu}$ is the energy-momentum tensor, which describes the energy content of the universe, and G is Newton's gravitation constant. In order to start solving these equations, we need to define what the energy-momentum tensor looks like for the universe as a whole. This is done in equation (2.13), which describes a perfect isotropic fluid with energy density ρ and pressure P. That description makes sense for the universe on cosmological scale, as at that scale the universe is approximately isotropic and homogeneous, and the matter constituents of the universe indeed do behave as a fluid.

$$T^{\mu}_{\nu} = \begin{pmatrix} -\rho & 0 & 0 & 0 \\ 0 & P & 0 & 0 \\ 0 & 0 & P & 0 \\ 0 & 0 & 0 & P \end{pmatrix} \tag{2.13}$$

Now that we know the form of the energy-momentum tensor, we can derive the Friedmann equations. Without going into the full calculational difficulties, we see that when we calculate the time-component results of Einstein's equation the Ricci tensor time-time component takes the following form:

$$R_{00} = -3\frac{\ddot{a}}{a}. \tag{2.14}$$

Also, we can derive that the Ricci scalar is given by:

$$R = 6\left[\frac{\ddot{a}}{a} + \left(\frac{\dot{a}}{a}\right)^2\right]. \tag{2.15}$$

Combining these with the fact that the time-time component of the energy-momentum tensor simply is equal to the energy density ρ, the first Friedmann equation easily follows:

$$H^2(t) = \frac{8\pi G}{3}\rho, \tag{2.16}$$

or conformally:

$$\frac{\mathcal{H}^2(\tau)}{a^2(\tau)} = \frac{8\pi G}{3}\rho. \tag{2.17}$$

This first Friedmann equation describes the evolution of the size of the universe as a function of the energy density within the universe. In this equation ρ denotes all energy constituents of the universe, so it contains contributions from matter, dark matter, radiation and dark energy. We will use this equation to describe multiple (toy) models of the universe that can be used to expand our intuition. Moreover, because the composition of the energy density was different at different times in the past of the universe, this equation will help us describe the expansion rate in the past.

However, there is another equation that follows from the energy-momentum tensor. In the normal Newtonian case, we recall that the energy-momentum tensor is a conserved quantity:

$$\partial_\mu T^{\mu\nu} = 0. \tag{2.18}$$

In the general relativistic case, an equivalent of this equation continues to hold. However, because we need to take into account the metric here, it is the covariant derivative of the energy-momentum tensor that vanishes:

$$\nabla_\mu T^{\mu\nu} = 0. \tag{2.19}$$

Working out this equation using the known definition of the covariant derivative from general relativity, we find that the conversation law is given by (2.20), the second of Friedmann's equations:

$$\frac{\partial \rho}{\partial t} + \frac{\dot{a}}{a}[3(\rho + P)] = 0, \tag{2.20}$$

or conformally:

$$\frac{\partial \rho}{\partial \tau} + \mathcal{H}(\tau)[3(\rho + P)] = 0. \tag{2.21}$$

With the knowledge of both Friedmann equations, we now can continue to look for a quantitative expression for the expansion of the universe. We will consider the cosmological evolution of two different toy models, whose scaling properties will be important in our description of the actual cosmological history.

Einstein-de Sitter cosmology:

Let us first consider a toy model of a universe which consists only of matter, which is called the *Einstein-de Sitter* (EdS) Model. There, the right hand side in equation (2.16) is fully described by $\rho = \rho_m$. To understand how the Hubble rate changes in time, we then need to look at the implications of equation (2.20) for such a universe. As for matter $P = 0$, we see that the second Friedmann equation reduces to:

$$\frac{\partial \rho_m}{\partial t} + 3\frac{\dot{a}}{a}\rho_m = 0. \tag{2.22}$$

This tells us that ρ_m scales like a^{-3} with time, because:

$$\frac{\partial (a^3 \rho_m)}{\partial t} = 0. \tag{2.23}$$

This result makes sense if we think about it a little more deeply. After all, the energy density simply describes the amount of energy per unit of volume of the universe. As we are discussing energy in the form of matter, it then easily follows that if we make our volume larger by a factor of a^3, our density also decreases by a factor of a^{-3}. When we use this result in equation (2.16), we then see that the scale factor in such a matter-only universe needs to obey:

$$\dot{a}^2 = \frac{C}{a}. \tag{2.24}$$

Here C is some constant that is time independent, which results in the scale factor having the form $t^{\frac{2}{3}}$.

Because we will see in chapter 3 that an EdS cosmology is a very good description of the universe in the periods we are interested in when we discuss large scale structure, we will derive the implication of this result on other cosmological quantities. We find for conformal time that $\tau \propto \sqrt{a}$ such that $a(\tau) \propto \tau^2$. Moreover we find for the (conformal) Hubble rate that:

$$H(t) \propto \frac{2}{3t} \propto a^{-3/2}, \tag{2.25}$$

$$\mathcal{H}(\tau) \propto \frac{2}{\tau}. \tag{2.26}$$

In addition, we can calculate which form the comoving distance takes, as we will need a cosmologically well-defined radial distance scale when considering the light cone effect:

$$\chi(a) = \int_a^1 \frac{da'}{a'^2 H(a')} = \frac{2}{H_0}\left[1 - \sqrt{a}\right]. \tag{2.27}$$

Note that in the last derivation we used the first Friedmann equation (2.16) and the scaling of the Hubble rate.

Radiation-only cosmology:

We can also consider a toy model with radiation only. Again, we first look at the second Friedmann equation to see how radiation scales in time. It is known from a derivation we will not reproduce here that for radiation the following relation holds between density and pressure: $\rho = 3P$ [18]. Then, the second Friedmann equation reduces to:

$$\frac{\partial \rho_r}{\partial t} + 4\frac{\dot{a}}{a}\rho_r = a^{-4}\frac{\partial(a^4\rho_r)}{\partial t} = 0. \tag{2.28}$$

This means that the energy density of radiation scales as a^{-4}. Once again, if we think about this a little more deeply, we find that this result is quite logical. After all, the energy of a photon per unit volume is given by the inverse of its wavelength. As the universe expands, the volume grows by a factor a^3, and the wavelength also grows by a factor a. The factor a^{-4} for the energy density is simply a combination of those factors. Then, by making similar considerations about the first Friedmann equation (2.16) as we did for the EdS model, we see that for a universe which consists of radiation the scale factor a depends on time like $\sqrt{t}$. We will not calculate the implications this has on cosmological quantities for this cosmology, for we will see in the next section that a radiation-only model only approximates the universe well at very early times, which are not particularly relevant to this thesis.

2.4 The standard cosmological model

In the previous section we discussed the way in which we can think about the expansion of our universe using the Friedmann equations to determine the scale factor. We looked at the EdS and radiation only toy models in order to get a better intuition for the way in which this expansion scales with time, and saw that in a matter-only universe the scale of the universe grows like $t^{\frac{2}{3}}$ and that in a radiation-only universe the scale factor grows like $\sqrt{t}$. However, now we want to consider the growth of the universe as it depends on the actual constituents of the universe. Hence, we will first give a cosmic inventory and use this to describe which energy type was dominant at which cosmological time.

Moreover, we will also give a short description of some important events in the history of the universe. We will see that different types of energy interacted and decoupled at certain cosmological times, giving rise to effects that are important in the study of large scale structure. We will more specifically introduce *baryonic acoustic oscillations* (BAO), because they are an important reason why large scale structure is such an important cosmological probe.

Cosmic inventory and energy history:

To make a cosmological inventory, we need to get an idea of the constituents of the universe. In order to do this, we will first rewrite equation (2.16):

$$\frac{H^2(t)}{H_0^2} = \frac{\rho}{\rho_{\text{cr}}}. \tag{2.29}$$

Species	**Symbol**	**Fraction**
Dark energy	Ω_{de}	0.72 ± 0.03
Matter	Ω_m	0.27 ± 0.03
Baryons	Ω_b	0.045 ± 0.003
Dark matter	Ω_{dm}	0.23 ± 0.03
Radiation	Ω_r	0.000085 ± 0.000001

Table 2.1: An overview of the most important constituents of our universe, assuming a value of $h = 0.7$ [3, 25].

Here we used that ρ_{cr} is the current day energy density which is related to the present day Hubble constant:

$$\rho_{\text{cr}} \equiv \frac{3H_0^2}{8\pi G}. \tag{2.30}$$

Moreover, we will define the fraction of a type of energy with respect to the current day energy density as Ω_i, implying that:

$$\frac{\rho}{\rho_{\text{cr}}} = \sum_i \Omega_i. \tag{2.31}$$

This allows for us to present an inventory of the cosmic constituents of the universe. By finding the Ω_i for all sorts of energy that are present in the current universe, we can effectively derive what our universe consists of. However, here we still have a dependence on the experimental value we find for the Hubble constant H_0. In order to make the dependence of our result clear we define the small-h parameter h, which is defined by:

$$H_0 = 100h \text{ km s}^{-1}\text{Mpc}^{-1}. \tag{2.32}$$

Now, in order to find these fractions of energy, we can calculate the total energy density of a species using distribution functions, a method we will not explain further but which can be found in chapter two of [18]. However, we will list the fraction of the main species for the composition of energy in our universe in table 2.1 [3, 25]. In this table, we see that approximately 72% of the current energy density is attributed to *dark energy*, a mysterious type of energy responsible for the accelerating expansion of the universe. Also, approximately 27% of the universe consists of matter, and only 8.5×10^{-5} of the energy density in the universe is accounted for by radiation. Note that these estimates assume a value of $h = 0.7$, which is a reasonable value given the current bounds on H_0 [31, 45].

In table 2.1 an important distinction is made between baryonic matter and dark matter. Baryonic matter denotes most matter we are familiar with here on earth (i.e. atoms consisting of protons and neutrons).[1] However, we know from observations that there must be another type of matter that interacts gravitationally. Because we cannot see this matter in another way than by its gravitational signature, we denote it by *dark matter*. As it turns out, approximately 83% of all matter in the universe is dark matter, whereas only approximately 17% is baryonic matter. Luckily, we do not have to distinguish between dark matter and baryonic matter in our description of large scale structure.

Now that we have an indication of the current fractions of the several species of energy in our universe, we can also look back to see which form of energy was dominant in the past. It of course immediately is clear that dark energy is the current dominant force driving expansion in the universe. However, in order to see whether it was dominant in the past, we have to consider how the energy density of each

[1] Leptons, such as electrons, are not included in this inventory because their contribution to the total energy density is negligible.

component scales with time. Because the second Friedmann equation (2.20) tells us how species of energy scale in terms of a, we look at bounds on the parameter w from observation, where w is defined by:

$$w \equiv \frac{P}{\rho}. \tag{2.33}$$

The predominant theory that explains dark energy is called the ΛCDM model. This theory explains dark energy to be due to a cosmological constant Λ (changing Ω_{de} to Ω_Λ), which can be interpreted as a vacuum energy of the universe that causes our universe to expand. For such a cosmological constant we find that $w = -1$, which implies that the dark energy content is independent of the scale factor. This, in turn, implies that dark energy became the dominant energy species in the universe very recently on a cosmological timescale. To calculate the actual scale factors for which a different species became dominant, we will use that the cosmological constant Λ is a-independent, that matter scales like a^{-3}, and that radiation scales like a^{-4}. Then we find that dark energy became dominant at scale factor $a \approx 0.72$ or redshift $z \approx 0.4$:

$$\Omega_m a^{-3} = \Omega_\Lambda, \tag{2.34}$$

$$a = \left(\frac{\Omega_m}{\Omega_\Lambda}\right)^{\frac{1}{3}} \approx 0.72. \tag{2.35}$$

This means that we can approximate the universe will using the Einstein-de Sitter model from the last section for redshifts larger than $z \approx 0.4$. Because the results for cosmological quantities are relatively simple for EdS, this will be very helpful in our calculations in chapters 3 and 5.

However, this EdS approximation breaks down at the epoch of matter-radiation equality, an important time in the history of our universe for which the scale factor has been denoted a_{eq}. Doing that calculation, we find that $a_{\text{eq}} \approx 3 \times 10^{-4}$ and $z_{\text{eq}} \approx 3.2 \times 10^2$.

Having obtained this history of the universe in terms of the dominant species of energy helps us to make a timeline of the expansion of the universe. From this history, we can assert that after the big bang and a period of inflation, the universe expanded like $\sqrt{t}$ during a period of radiation domination. This period of radiation domination ended at the epoch of equality at z_{eq}, after which the period of matter domination began. During this period the universe expanded at a rate of $t^{\frac{2}{3}}$. Then, at redshift $z \approx 0.4$ the universe entered another period, in which dark energy dominated and presently continues to dominate.

Cosmological events:

In this part, we will describe some of the key cosmological events that influenced large scale structure within our universe. The way different types of energy (e.g. Dark matter, baryonic matter, photons etc.) interacted in the history of the universe has left a mark on its current realization. We will consider the coupling of four critical types of energy, which will give us a greater insight in the current structure of the universe.

We consider the interaction between dark matter, baryonic matter, neutrinos and photons during some key events in the history of the universe. We have listed the events with the corresponding cosmological time and redshift,[2] while we also denote which types of energy were still coupled to each other. Note that we assume that during the big bang all four energy types we describe here were coupled. An overview of key events and the coupling of energy types is given in table 2.2.

[2]Some events were so early in the history of the universe that redshift is not well-defined at those times

Events			**Coupling**[3]			
Event	time t	redshift z	Dark Matter	Neutrinos	Photons	Baryons
Big bang	0	?	Yes	Yes	Yes	Yes
Dark matter freeze-out	?	?	No	Yes	Yes	Yes
Neutrino decoupling	1 s	6×10^9	No	No	Yes	Yes
Matter-radiation equality	60 kyr	3200	No	No	Yes	Yes
Photon decoupling	380 kyr	1100	No	No	No	Yes

Table 2.2: A list of cosmological events and an indication which types of energy were coupled to baryonic matter. We see that the interactions between dark matter and baryons and the interactions between neutrinos and baryons were frozen out before photons decoupled from baryonic matter. We will see that the relatively late time of photon decoupling is responsible for baryonic acoustic oscillations. Note that photon decoupling is also the time since when photons have been able to travel freely. Hence, we cannot look back further than to 380,000 years after the big bang using photons. Taken from [2, 10].

We continue by giving a short description of the events from table 2.2, to give the reader some intuition for the mechanics responsible for the current state of our universe, and more specifically for the current realization of large scale structure.

Big bang: evidence shows that it is highly likely that the universe came into existence from a very dense region, corresponding to $a(0) = 0$, which canonically is known as the big bang. The mechanics at $t = 0$ are unknown, but we know from the Hubble diagram, the cosmic microwave background and the abundance of light elements predicted by the consequences of the big bang postulate that a big bang is the best candidate for the beginning of our universe. Most cosmologists assume that directly after the big bang a period of accelerating expansion called *inflation* took place, which would explain the observed homogeneity of the universe [10]. In these very earliest moments of our universe dark matter, neutrinos, photons and baryons were all coupled to each other. Note that after the big bang the universe started cooling down as it expanded.

Dark matter freeze-out: at some time shortly after the big bang and after the end of inflation, dark matter particles decoupled from other matter and radiation in the form of neutrinos and photons. This decoupling caused dark matter mechanics to be fully determined by gravitational dynamics, whereas the baryonic mechanics were mainly driven by their coupling to the cosmic plasma. Note that dark matter freeze-out is estimated to have occurred around the same time as neutrino decoupling under the assumption that dark matter consists of weakly interacting matter particles [2].

Neutrino decoupling: from the standard model, we know that the rate at which neutrinos couple to the components of the cosmic plasma (we assume that dark matter has already frozen out) becomes smaller than the expansion rate at the energy of 1 MeV, which corresponds to an age of the universe of 1 s. After this time, neutrinos travel freely throughout the universe.

Matter-radiation equality: as described in the previous section, radiation was the dominant energy type in the very early universe. Hence, expansion was driven by radiation during dark matter freeze-out and neutrino decoupling.[4] However, at redshift $z \approx 3200$ matter instead of radiation starts driving expansion. Note that during the epoch of equality baryons and photons are still coupled to each other.

Photon decoupling: at redshift $z \approx 1100$, photons decouple from baryons, and are able to travel freely through the universe. Hence, the earliest picture of the universe we can take using light corresponds to this time. Photons from before this time were constantly destroyed and created

[4] We assume that expansion immediately after the big bang was driven by inflation instead of radiation.

by the coupling to baryons after all. The *cosmic microwave background* (CMB) is the radiation (i.e. photons) we can observe from this time. Note that any structure in matter created after this time is due to gravitational interactions between both baryonic and dark matter. In general, the physics which governed our universe remained the same (matter-dominated) untill dark energy domination at redshift $z = 0.4$.

The coupling of different cosmic constituents throughout these major events and the physical mechanisms they were subjected to are the drivers which created our current universe. We give a specific description of the mechanism of *baryonic acoustic oscillations* (BAO), an effect which has a clear signature in large scale structure and which is a reason for the wealth of information about the universe we can probe with large scale structre.

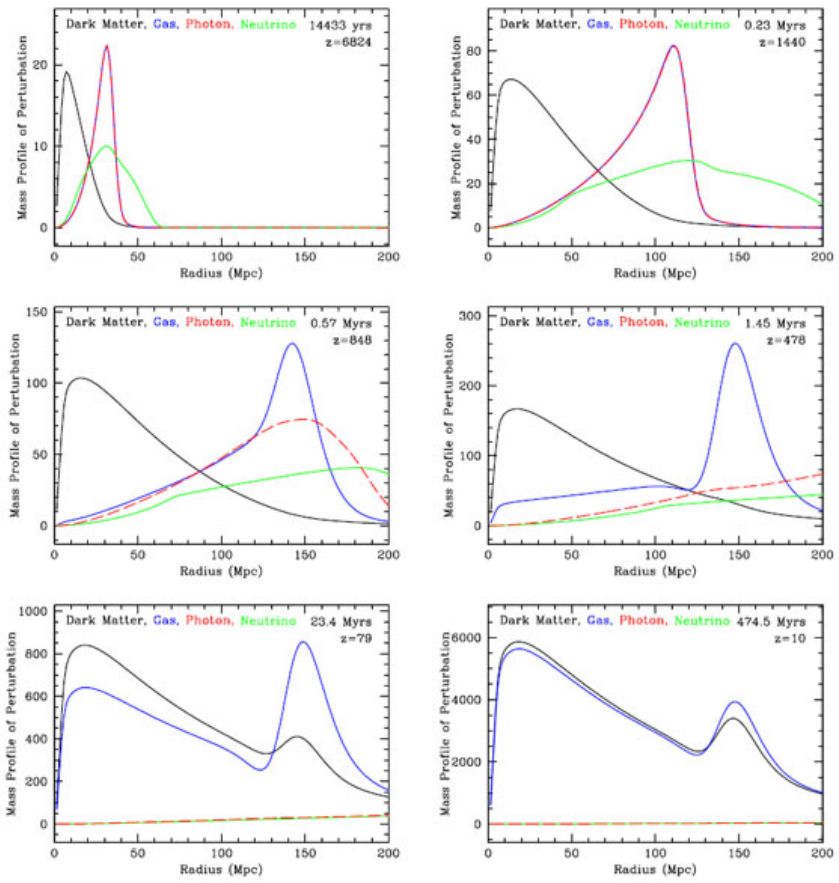

Figure 2.3: A visualization of the BAO. We can clearly see that the propagating photon wave pulls away the baryons radially as time evolves, while the dark matter only is subjected to a slight gravitational tug. After the photons decouple, the gravitational interaction between dark matter and baryonic matter leaves a distinctive peak in the density distribution of matter. Taken from [22].

The BAO were created because after dark matter freeze-out but before photon decoupling, baryonic matter was tightly coupled with photons whereas dark matter was evolving freely. If we assume a point-like density perturbation sourced by inflation, at first the density peak is located at that point for all energy species. However, the photons are overpressurized at this point, inducing a wave propagating away spherically. As the baryonic matter is coupled to the photons, the baryonic matter also propagates away spherically [22]. However, dark matter has frozen out, so it will approximately stay at the center,

only pulled away slightly in the radial direction becaus of the gravitational pull of the baryons. This mechanism continues until the photons decouple from the baryons, leaving the matter constituents to interact gravitationally. The full mechanism leaves a distinctive signature in density profile, which can be seen in figure 2.3.

The great value of the BAO lies in the fact that the distances from figure 2.3 are typical for the effect, and based on the duration of the coupling of photons and baryonic matter. Hence, the BAO can be used as a *standard statistical ruler* for observations [9]; in observations of distant cosmological objects we cannot know the angular distance for sure unless we have some referential scale. After all, redshift is useful for observations where we know the color objects should have and the radial distance is small enough that Hubble's law applies, but typically the redshift for distant objects depends on cosmology. This means that we cannot use redshift to probe cosmology. Therefore, if we observe a BAO peak in our range of observations, we can use the fact that this peak fixes a scale to probe cosmology.

2.5 Summary

In this chapter, we have given an introduction to some of the key concepts of cosmology which will be of use when describing large scale structure. Moreover, we have given some context about cosmology that gives the reader an idea of the sequence of events that led to our current universe.

We started by giving an introduction to the expanding universe, and described the manner in which the expanding universe paradigm can be included in our equations using the scale factor a. Moreover, we have written down the FLRW-metric, which describes our expanding universe on a cosmological scale.

Based on the FLRW metric, we have derived the Friedmann equations which govern the manner in which our universe expands. We have shown that Einstein's equations imply that the expansion of our universe is sourced by its energy content, and used the Friedmann equations to calculate this expansion for two important toy models. More specifically, we have shown that in an EdS-cosmology, the scale factor evolves like $t^{3/2}$ and that in a radiation-only cosmology the scale factor evolves like $\sqrt{t}$.

After describing these toy models, we explained the standard model of cosmology. First, we gave an inventory of the constituents of our universe and their implication for the history of its evolution. We showed that at early stages the expansion of the universe was driven by radiation, whereas at redshift $z \approx 3200$ matter became the driving force. Moreover, we showed that currently dark energy is the dominant force in the universe, which it became at redshift $z = 0.4$.

In addition, we gave an overview of some of the key events in the early universe that have left their mark on its current realization. We showed that dark matter, neutrinos and photons decoupled sequentially from the cosmic plasma, which leaves its mark on large scale structure. We explained these baryonic acoustic oscillations, and argued why they are such useful signatures in large scale structure observations.

In conclusion, we have introduced the key concepts of cosmology and are now able to move on to the main subject of the thesis: large scale structure.

Chapter 3

Standard perturbation theory of large scale structures

3.1 Introduction

Now that we have a good view of the paradigm of the expanding homogeneous and isotropic universe, we can continue to study the Large Scale Structure (LSS) of the universe. The framework in which calculations about this are usually done is called *Standard Perturbation Theory* (SPT), in which the *density contrast* δ of matter in the universe is expanded perturbatively to obtain results on the formation of structure. Note that in SPT, there is no distinguishment between dark matter and baryonic matter. In this chapter we will write down the results from SPT which are relevant to this thesis. Then, in chapter 5 we will have the toolbox to develop our theory of large scale structure on the light cone.

We will start by introducing our main quanitities and specifying our conventions. Then, we will write down the equations that govern the dynamics of matter in our universe. As these equations are equivalent to Euler's treatment of fluid dynamics, the set of equations governing matter dynamics is called *Eulerian theory*. We will make an assumption about the linearity of the behavior of our relevant quantities, and derive the way structures grow in a matter-only cosmology. Moreover, we will provide the basis needed for the nonlinear treatment.

After the linear Eulerian theory, we will extend our results to the perturbative regime. We will look at the density contrast in Fourier space, and start developing the density contrast perturbatively. Working out this formalism, we will see that the higher order density contrasts depend on the first order non-perturbative solutions by symmetric kernels.

In the following section, we will look at correlators between the density contrast at different wavelengths k and k', which will be our main way to probe the large scale structure. Related to this, we introduce the power spectrum, a quantity derived from these correlators to start our real theoretical discussion. We describe how Wick's theorem tells us how the power spectrum gets corrected at higher orders, and derive the one loop results. Moreover, we will also consider the three-correlators of density contrast in our universe. In a similar fashion as for the power spectrum, we can derive the bispectrum from this.

Following this, we will introduce the notion of redshift space. We will see how the peculiar velocities of distant objects modify our observations of their redshift, and we will motivate the correcting terms.

For much of this chapter, we will be closely following Bernardeau et al.'s review of the SPT formalism [11].

3.2 Linear Eulerian perturbation theory

To start our description of the large scale structure of the universe, we define this to be the structure of matter on larger than galaxy scales. Because we will be talking about the structure of matter on scales much shorter than the Hubble scale (though still much longer than galactic scales), we can describe the dynamics using Newtonian gravity.[1] Knowing this, we can continue to write down the equation which will govern the dynamics of matter in our universe:

$$\frac{d^2\vec{r}}{dt} = -\frac{\partial\phi}{\partial\vec{r}}. \tag{3.1}$$

In this equation ϕ is the total gravitational potential, which depends on the density of matter $\rho(\vec{r})$, and $\vec{r}$ is the physical location of matter within the universe. However, as we have seen in chapter 2, things get more complicated because we live in an expanding universe. To take this into account we choose to work in comoving coordinates $\vec{x}$ and conformal time τ:

$$\vec{x} = \frac{\vec{r}}{a(\tau)}, \tag{3.2}$$

$$d\tau = \frac{dt}{a(\tau)}. \tag{3.3}$$

Moreover, we once more need the Friedmann equations. To follow the conventions in literature, we choose to write these as a function of $\mathcal{H}$, the conformal expansion rate, which is given by:

$$\mathcal{H} \equiv \frac{d\ln a}{d\tau} = Ha. \tag{3.4}$$

Using these conventions and neglecting the effect of radiation we can write down the Friedmann equations in a different form, which is given in equation (3.5). Here, once more, we assume to have a universe without curvature ($\kappa = 0$). Besides, we have redefined our fractions Ω_i to be time-dependent, to avoid terms of H_0 in our equations.

$$\frac{\partial\mathcal{H}}{\partial\tau} = \left(\Omega_\Lambda(\tau) - \frac{\Omega_m(\tau)}{2}\right)\mathcal{H}^2(\tau). \tag{3.5}$$

Also, because we are interested in the effects of matter *structure*, it is instructive to describe our dynamics using equations that do not have a dependence on quantities such as the average matter density $\overline{\rho}(\tau)$. To do this, we define the *density contrast* $\delta(\vec{x})$, the *peculiar velocity* $\vec{u}(\vec{x},\tau)$ and the *cosmological gravitational potential* $\Phi(\vec{x},\tau)$:

$$\rho(\vec{x},\tau) \equiv \overline{\rho}(\tau)[1+\delta(\vec{x},\tau)], \tag{3.6}$$

$$\vec{v}(\vec{x},\tau) \equiv \mathcal{H}\vec{x} + \vec{u}(\vec{x},\tau), \tag{3.7}$$

$$\phi(\vec{x},\tau) \equiv -\frac{1}{2}\frac{\partial\mathcal{H}}{\partial\tau}x^2 + \Phi(\vec{x},\tau). \tag{3.8}$$

With these definitions, we are now able to describe the density contrast as influenced only by the cosmological gravitational potential Φ. The relation is given by a Poisson equation:

$$\nabla^2\Phi(\vec{x},\tau) = \frac{3}{2}\Omega_m(\tau)\mathcal{H}^2(\tau)\delta(\vec{x},\tau). \tag{3.9}$$

Now that we have given our definitions we can rewrite equation (3.1), which governs our dynamics in terms of our momentum $\vec{p} = am\vec{u}$:

[1] Of course, a full general relativity treatment is required for maximum accuracy. Some of the full GR results and their effects on LSS observables are given in [51].

$$\frac{d\vec{p}}{d\tau} = -am\nabla\Phi(\vec{x},\tau). \tag{3.10}$$

Then, if we consider some function $f(\vec{x},\vec{p},\tau)$ which describes our particle number density in the universe, we can require this function to be conserved in phase space:

$$\frac{df}{d\tau} = \frac{\partial f}{\partial\tau} + \frac{\vec{p}}{ma}\cdot\nabla f - am\nabla\Phi\cdot\frac{\partial f}{\partial\vec{p}} = 0. \tag{3.11}$$

This equation is called the *Vlasov equation*, and in general, it is not very instructive to our purposes. The equation itself is nonlinear and has many variables, so it does not allow for simple solutions. However, we can devise a method which will help us use the Vlasov equation to describe the dynamics of matter structure in cosmology. This method is called the method of moments, and it amounts to integrating out the part which we do not want to describe. As in the study of large scale structure we are interested in how matter is distributed at a given conformal time throughout space, we decide to integrate out the momentum. In this way, we obtain the momentum moments of our particle number density. We see that our density field is defined by the zero$^{\text{th}}$ order moment:

$$\int d^3\vec{p} f(\vec{x},\vec{p},\tau) \equiv \rho(\vec{x},\tau). \tag{3.12}$$

The first and second order moments of the particle number density define the *peculiar velocity flow* $\vec{u}(\vec{x},\tau)$ and the *stress tensor* $\sigma_{ij}(\vec{x},\tau)$:

$$\int d^3\vec{p}\frac{\vec{p}}{am} f(\vec{x},\vec{p},\tau) \equiv \rho(\vec{x},\tau)\vec{u}(\vec{x},\tau), \tag{3.13}$$

$$\int d^3\vec{p}\frac{p_i p_j}{a^2m^2} f(\vec{x},\vec{p},\tau) \equiv \rho(\vec{x},\tau)\vec{u}_i(\vec{x},\tau)\vec{u}_j(\vec{x},\tau) + \sigma_{ij}(\vec{x},\tau). \tag{3.14}$$

Having given a definition of the moments of our particle number density, we can apply these to obtain a manageable version of equation (3.11). Taking the first moment of the Vlasov equation yields us the *continuity equation*:

$$\frac{\partial\delta(\vec{x},\tau)}{\partial\tau} + \nabla\cdot[1+\delta(\vec{x},\tau)]\vec{u}(\vec{x},\tau) = 0. \tag{3.15}$$

Then, by taking the first moment of the Vlasov equation and combining the result with the continuity equation (3.15) we obtain the *Euler equation*:

$$\frac{\partial\vec{u}(\vec{x},\tau)}{\partial\tau} + \mathcal{H}(\tau)\vec{u}(\vec{x},\tau) + \vec{u}(\vec{x},\tau)\cdot\nabla\vec{u}(\vec{x},\tau) = -\nabla\Phi(\vec{x},\tau) - \frac{1}{\rho}\nabla_j(\rho\sigma_{ij}). \tag{3.16}$$

Now, we have a description of the dynamics of matter within the universe in terms of equations without all too terrible nonlinearities. Moreover, we can investigate the mechanics of our system by taking an Ansatz for the form of the stress tensor $\sigma_{ij}(\vec{x},\tau)$ based on models we know from nature. In other words, we can start from an equation of state which describes the matter ingredients of our cosmology and use that to derive the behavior of our system.

In the following, we assume that our stress tensor is vanishing $\sigma_{ij}(\vec{x},\tau) \approx 0$, which is a reasonable assumption for the evolution of structure on large scales. The stress tensor describes how much the velocity of matter disagrees with a single coherent flow after all, and this term only becomes relevant when structures start to collapse. For the scales of interest in this discussion we assume that structures are not collapsing as of the present, even though on smaller scales (e.g. galactic scales) the velocity dispersion is dominant.

Another assumption we will make about our large scale behavior is the *smallness* of the fluctuations. Where within a galaxy the density contrast becomes large, it remains very small on the lengthscales of large scale structure. In other words, we can consider the universe to become smooth at large scales. This assumption allows us to only consider first order terms in the fluctuations in equations (3.15) and (3.16).

If we introduce $\theta(\vec{x},\tau)$ for the divergence of the velocity field $\nabla\cdot\vec{u}(\vec{x},\tau)$, we see that we can write the continuity equation as:

$$\frac{\partial\delta(\vec{x},\tau)}{\partial\tau}+\theta(\vec{x},\tau)=0. \tag{3.17}$$

We can rewrite the Euler equation in a similar manner:

$$\frac{\partial\vec{u}(\vec{x},\tau)}{\partial\tau}+\mathcal{H}(\tau)\vec{u}(\vec{x},\tau)=-\nabla\Phi(\vec{x},\tau). \tag{3.18}$$

Now that we have this equation, it makes sense to write it in terms of the density contrast $\delta(\vec{x},\tau)$ and the velocity divergence $\theta(\vec{x},\tau)$. We do this by taking the divergence of this equation. Then we can use the Poisson equation (3.9) to write this equation as:

$$\frac{\partial\theta(\vec{x},\tau)}{\partial\tau}+\mathcal{H}(\tau)\theta(\vec{x},\tau)=-\frac{3}{2}\Omega_m(\tau)\mathcal{H}^2(\tau)\delta(\vec{x},\tau). \tag{3.19}$$

Now, we have a coupled system of equations in terms of $\theta(\vec{x},\tau)$ and $\delta(\vec{x},\tau)$, so that we can proceed to solve these. However, we need to take into account that by taking the divergence of equation (3.18), we lose some information about the peculiar velocity flow. This can be mitigated by also considering the vorticity of the peculiar velocity flow, because a vector field can be fully described by the combination of its vorticity and divergence. When we define the vorticity of $\vec{u}(\vec{x},\tau)$ as $\vec{w}(\vec{x},\tau)\equiv\nabla\times\vec{u}(\vec{x},\tau)$, we get the following equation to append equation (3.19):

$$\frac{\partial\vec{w}(\vec{x},\tau)}{\partial\tau}+\mathcal{H}(\tau)\vec{w}(\vec{x},\tau)=0. \tag{3.20}$$

Now that we have these equations, we can continue to look at the time evolution of the density contrast, the vorticity and of the divergence of the peculiar velocity flow. For the vorticity $\vec{w}(\vec{x},\tau)$ we immediately notice that its time evolution will scale like a^{-1}, so in the linear regime vorticity will decay with the growth of the universe.

Next we continue to look at the density contrast $\delta(\vec{x},\tau)$. We can combine equations (3.17) and (3.19) to obtain a second-order ordinary differential equation:

$$\frac{\partial^2\delta(\vec{x},\tau)}{\partial\tau^2}+\mathcal{H}(\tau)\frac{\partial\delta(\vec{x},\tau)}{\partial\tau}-\frac{3}{2}\Omega_m(\tau)\mathcal{H}^2(\tau)\delta(\vec{x},\tau)=0. \tag{3.21}$$

If we then assume that we can decompose the density contrast into a time dependent *linear growth function* $D_1(\tau)$ and a time independent density contrast distribution $\delta(\vec{x})$ such that $\delta(\vec{x},\tau)=D_1(\tau)\delta(\vec{x})$, we can use the combination of equation (3.21) and the evolution of our cosmology to analyze time evolution. Because equation (3.21) is a second order differential equation in conformal time, there will be two solutions for $D_1(\tau)$, which we will denote by the fastest growing mode $D_1^{(+)}(\tau)$ and the slowest growing mode $D_1^{(-)}(\tau)$. Then, our results for the density contrast will have the form:

$$\delta(\vec{x},\tau)=D_1^{(+)}(\tau)A(\vec{x})+D_1^{(-)}(\tau)B(\vec{x}), \tag{3.22}$$

where $A(\vec{x})$ and $B(\vec{x})$ describe the initial configuration of the density field.

Once we have calculated the evolution of the density contrast, we can also understand the time evolution for the velocity divergence using equation (3.17). More specifically, if we derive the result we find that the velocity divergence is given by:

$$\theta(\vec{x},\tau) = -\frac{\partial\delta(\vec{x},\tau)}{\partial\tau} = -\mathcal{H}(\tau)\frac{\partial\delta(\vec{x},\tau)}{\partial\ln a} = \\ -\mathcal{H}(\tau)\big[f(\Omega_m,\Omega_\Lambda)A(\vec{x}) + g(\Omega_m,\Omega_\Lambda)B(\vec{x})\big], \tag{3.23}$$

where

$$f(\Omega_m,\Omega_\Lambda) \equiv \frac{d\ln D_1^{(+)}}{d\ln a} = \frac{1}{\mathcal{H}}\frac{d\ln D_1^{(+)}}{d\tau}, \qquad g(\Omega_m,\Omega_\Lambda) = \frac{1}{\mathcal{H}}\frac{d\ln D_1^{(-)}}{d\tau}. \tag{3.24}$$

In the following we will calculate the time evolution for an Einstein de Sitter (EdS) cosmology. To do this, we take $\Omega_m = 1$ and $\Omega_\Lambda = 0$. Then, our equation (3.21) simplifies a lot, and we find that:

$$D_1^{(+)}(\tau) = a, \qquad D_1^{(-)}(\tau) = a^{-3/2}, \qquad f(1,0) = 1. \tag{3.25}$$

Because the fastest growing mode is dominant in the evolution of the density contrast, we see that our fluctuations will grow as the scale factor in an EdS cosmology. In more complicated cosmologies than EdS, it may not be possible to come to an analytic solution for the linear growth functions, but several approximations exist [13, 28, 38].

Having calculated the formulas which govern the dynamics of the matter fluid within the universe, this concludes our treatment of the linear Eulerian theory of large scale structure. We have fully described the dynamics and time evolution of the density contrast, which depend on the initial configuration given by $A(\vec{x})$ and $B(\vec{x})$ and the linear growth function given by equation (3.25). In the next section we will continue to develop this formalism in the non-linear case.

3.3 Non-linear Eulerian perturbation theory

To develop the evolution of our density in the non-linear regime we need to consider the full relations instead of the ones in which we simply set all of our nonlinear results to zero. This means that our relatively simple results from the last section do not apply anymore. More specifically, both elements of the decomposition of our velocity field into a divergence and vorticity part appear to be relevant once more. To deal with this, we need to take a look at the full[2] equation for the vorticity part of the velocity field, which we derive from the Euler equation (3.16). We then see that this equals:

$$\frac{\partial\vec{w}(\vec{x},\tau)}{\partial\tau} + \mathcal{H}(\tau)\vec{w}(\vec{x},\tau) - \nabla\times[\vec{u}(\vec{x},\tau)\times\vec{w}(\vec{x},\tau)] = 0. \tag{3.26}$$

Whereas in the linear case we could show that any primordial vorticity decays as the universe grows, we find that vorticity can indeed grow in the nonlinear case because of the third term in equation (3.26). In this thesis, however, we will assume no contribution from vorticity, which makes sense considering the fact that vorticity only contributes to the density at higher orders in perturbation theory than those we will consider.

Having gotten rid of the vorticity term in our system, we return to a coupled system of second-order differential equations in $\theta(\vec{x},\tau)$ and $\delta(\vec{x},\tau)$, given by equation (3.15) and the divergence of equation (3.16). A natural way to consider the equations we obtain in this manner is transforming them to *Fourier space*. Then, if we consider the linear perturbation theory from the previous section, we know that the different Fourier modes do not interact. Moreover, we also see that the interaction between Fourier modes describes the higher order terms of our perturbation theory. We use the following Fourier conventions:

[2] We continue to assume that the stress tensor does not contribute ($\sigma_{ij}(\vec{x},\tau) \approx 0$), so the observant reader will realize that this is not the full equation.

$$f(\vec{k}) = \int d^3\vec{x} f(\vec{x}) e^{-i\vec{k}\vec{x}}, \tag{3.27}$$

$$f(\vec{x}) = \int \frac{d^3\vec{k}}{(2\pi)^3} f(\vec{k}) e^{i\vec{k}\vec{x}}. \tag{3.28}$$

If we Fourier transform the equations we get from the continuity equation (3.15) and the divergence of the Euler equation (3.16), we get the following:

$$\frac{\partial\delta(\vec{k},\tau)}{\partial\tau} + \theta(\vec{k},\tau) = -\int \frac{d^3\vec{k}_1}{(2\pi)^3} d^3\vec{k}_2 \delta_D^3(\vec{k}-\vec{k}_{12})\alpha(\vec{k}_1,\vec{k}_2)\theta(\vec{k}_1,\tau)\delta(\vec{k}_2,\tau), \tag{3.29}$$

$$\begin{aligned}\frac{\partial\theta(\vec{k},\tau)}{\partial\tau} + \mathcal{H}(\tau)\theta(\vec{k},\tau) + \frac{3}{2}\Omega_m\mathcal{H}^2(\tau)\delta(\vec{k},\tau) = -\int \frac{d^3\vec{k}_1}{(2\pi)^3} d^3\vec{k}_2 \delta_D^3(\vec{k}-\vec{k}_{12}) \\ \times\beta(\vec{k}_1,\vec{k}_2)\theta(\vec{k}_1,\tau)\theta(\vec{k}_2,\tau).\end{aligned} \tag{3.30}$$

In these equations $\vec{k}_{12} \equiv \vec{k}_1 + \vec{k}_2$, and $\alpha(\vec{k}_1,\vec{k}_2)$ and $\beta(\vec{k}_1,\vec{k}_2)$ are given by:

$$\alpha(\vec{k}_1,\vec{k}_2) \equiv \frac{\vec{k}_{12}\cdot\vec{k}_1}{k_1^2}, \qquad \beta(\vec{k}_1,\vec{k}_2) \equiv \frac{k_{12}^2(\vec{k}_1\cdot\vec{k}_2)}{2k_1^2k_2^2}, \tag{3.31}$$

where these functions arise because of the relation:

$$\theta(\vec{k},\tau) = i\vec{k}\cdot\vec{u}(\vec{k},\tau). \tag{3.32}$$

Equations (3.29) and (3.30) fully describe our nonlinear dynamics. To develop our perturbation theory, we need to write our density contrast and velocity divergence perturbatively:

$$\delta(\vec{k},\tau) = \sum_n \delta^{(n)}(\vec{k},\tau), \qquad \theta(\vec{k},\tau) = \sum_n \theta^{(n)}(\vec{k},\tau). \tag{3.33}$$

In this perturbative expansion, the first terms ($\delta^{(1)}(\vec{k},\tau)$ and $\theta^{(1)}(\vec{k},\tau)$) are given by the solutions of the linear equations, so equations (3.29) and (3.30) with the right hand side set to zero. The next order in perturbation theory can be calculated by solving the equations for $\delta^{(2)}(\vec{k},\tau)$ and $\theta^{(2)}(\vec{k},\tau)$, where the interactions on the right hand side of the equations are only sourced by the linear order, so:

$$\frac{\partial\delta^{(2)}(\vec{k},\tau)}{\partial\tau} + \theta^{(2)}(\vec{k},\tau) = -\int \frac{d^3\vec{k}_1}{(2\pi)^3} d^3\vec{k}_2 \delta_D^3(\vec{k}-\vec{k}_{12})\alpha(\vec{k}_1,\vec{k}_2)\theta^{(1)}(\vec{k}_1,\tau)\delta^{(1)}(\vec{k}_2,\tau), \tag{3.34}$$

$$\begin{aligned}\frac{\partial\theta^{(2)}(\vec{k},\tau)}{\partial\tau} + \mathcal{H}(\tau)\theta^{(2)}(\vec{k},\tau) + \frac{3}{2}\Omega_m\mathcal{H}^2(\tau)\delta^{(2)}(\vec{k},\tau) = -\int \frac{d^3\vec{k}_1}{(2\pi)^3} d^3\vec{k}_2 \delta_D^3(\vec{k}-\vec{k}_{12}) \\ \times\beta(\vec{k}_1,\vec{k}_2)\theta^{(1)}(\vec{k}_1,\tau)\theta^{(1)}(\vec{k}_2,\tau).\end{aligned} \tag{3.35}$$

To calculate the higher-order perturbative expansions, we follow the same procedure. For example, $\delta^{(n)}(\vec{k},\tau)$ and $\theta^{(n)}(\vec{k},\tau)$ would be given by the couplings between all the different lower order terms up until $\delta^{(n-1)}(\vec{k},\tau)$ and $\theta^{(n-1)}(\vec{k},\tau)$.

Looking at these equations, it becomes quite obvious that these are not necessarily simple to solve. However, if we assume an Einstein-de Sitter cosmology, which is accurate for redshift $0.4 < z < 3200$, the equations simplify. We recall from chapter 2 that the scale factor $a(\tau)$ scales as τ^2 for this cosmology so that $\mathcal{H}(\tau) = \frac{2}{\tau}$. Then, when we consider the system of (3.29) and (3.30), we see that the differential equations become homogeneous in conformal time. In other words, any polynomial in conformal time

τ and as an extension in the scale factor $a(\tau)$ will solve the conformal time differential equations.This motivates us to write the velocity and density contrast perturbatively as:

$$\delta(\vec{k},\tau) = \sum_n a^n(\tau)\delta_n(\vec{k}), \qquad \theta(\vec{k},\tau) = -\mathcal{H}(\tau)\sum_n a^n(\tau)\theta_n(\vec{k}). \tag{3.36}$$

Note that in equation (3.36), we assumed that the time dependence of our density field is separable from its comoving coordinate. Theoretically this is true, but when we are observing the universe, any object we observe lies on the past light cone. Therefore, its time coordinate depends on the radial distance from the earth. In chapter 5, we will include this dependence explicitly at this step.

Following our assumption of separability of time and coordinate dependence, we recall that we know the linear order results and that the relation $\delta_1(\vec{k}) = \theta_1(\vec{k})$ holds. Now, we can expand until arbitrary order using equations (3.29) and (3.30). To actually solve these equations, we need to derive the Green's function for the combined system. The Green's function is defined by:

$$\frac{\partial^2 G(\tau,\tilde{\tau})}{\partial\tau^2} + \mathcal{H}(\tau)\frac{\partial G(\tau,\tilde{\tau})}{\partial\tau} - \frac{3}{2}\mathcal{H}^2 G(\tau,\tilde{\tau}) = \delta_D(\tau-\tilde{\tau}). \tag{3.37}$$

We can rewrite this equation in terms of the scale factor a:

$$a^2\mathcal{H}^2\frac{\partial^2 G(a,\tilde{a})}{\partial a^2} + \frac{3}{2}a\mathcal{H}^2\frac{\partial G(a,\tilde{a})}{\partial a} - \frac{3}{2}\mathcal{H}^2 G(a,\tilde{a}) = \delta_D(a-\tilde{a}). \tag{3.38}$$

We can show that this Green's function equals [42]:

$$G(a,\tilde{a}) = \frac{2}{5\mathcal{H}_0^2}\theta_H(a-\tilde{a})\left[\left(\frac{a}{\tilde{a}}\right) - \left(\frac{a}{\tilde{a}}\right)^{-3/2}\right]. \tag{3.39}$$

We can use this Green's function to calculate our higher order terms, because the Green's function solves the linear part of our equation. For instance, for the second order terms we can calculate $\delta_2(\vec{k})$ using the following:

$$\begin{aligned}\delta_2(\vec{k},\tau) = a^2\delta_2(\vec{k}) = \int d\tilde{a}\int\frac{d^3\vec{k}_1}{(2\pi)^3}d^3\vec{k}_2\delta_D^3(\vec{k}-\vec{k}_{12})G(a,\tilde{a})\Big(\beta(\vec{k}_1,\vec{k}_2)\theta^{(1)}(\vec{k}_1,\tilde{a})\theta^{(1)}(\vec{k}_2,\tilde{a}) - \\ \alpha(\vec{k}_1,\vec{k}_2)\mathcal{H}\left[1+\tilde{a}\frac{\partial}{\partial\tilde{a}}\right]\theta^{(1)}(\vec{k}_1,\tilde{a})\delta^{(1)}(\vec{k}_2,\tilde{a})\Big).\end{aligned} \tag{3.40}$$

We shall not do the further calculation for the second order explicitly, but we will remark that the Green's function exactly leaves an a^2 term on the right hand side as well, which is consistent with our time-separability assumption. This separation between the time variable and the spatial dependence motivates us to continue our discussion talking about the Fourier modes only. Then, following the procedure we explained here to arbitrary order, while explicity integrating out the $\tilde{a}$ gives us the following results for $\delta_n(\vec{k})$ and $\theta_n(\vec{k})$ [26]:

$$\delta_n(\vec{k}) = \int\frac{d^3\vec{q}_1}{(2\pi)^{3(n-1)}}\ldots\int d^3\vec{q}_n\delta_D^3(\vec{k}-\vec{q}_{1\ldots n})F_n(\vec{q}_1,\ldots,\vec{q}_n)\delta_1(\vec{q}_1)\ldots\delta_1(\vec{q}_n), \tag{3.41}$$

$$\theta_n(\vec{k}) = \int\frac{d^3\vec{q}_1}{(2\pi)^{3(n-1)}}\ldots\int d^3\vec{q}_n\delta_D^3(\vec{k}-\vec{q}_{1\ldots n})G_n(\vec{q}_1,\ldots,\vec{q}_n)\delta_1(\vec{q}_1)\ldots\delta_1(\vec{q}_n). \tag{3.42}$$

Here F_n and G_n are symmetrized kernels, which can be calculated recursively for $n \geq 2$. For their expressions, which depend on α and β as we could have expected from equation (3.40), see for instance [11, 26]. We will give the explicit expressions for $n = 2$ below, where we symmetrized in $\vec{q}_1$ and $\vec{q}_2$:

$$F_2^{(s)}(\vec{q}_1,\vec{q}_2) = \frac{5}{7} + \frac{1}{2}\frac{\vec{q}_1\cdot\vec{q}_2}{q_1 q_2}\left(\frac{q_1}{q_2}+\frac{q_2}{q_1}\right) + \frac{2}{7}\frac{(\vec{q}_1\cdot\vec{q}_2)^2}{q_1^2 q_2^2}, \tag{3.43}$$

$$G_2^{(s)}(\vec{q}_1,\vec{q}_2) = \frac{3}{7} + \frac{1}{2}\frac{\vec{q}_1\cdot\vec{q}_2}{q_1 q_2}\left(\frac{q_1}{q_2}+\frac{q_2}{q_1}\right) + \frac{4}{7}\frac{(\vec{q}_1\cdot\vec{q}_2)^2}{q_1^2 q_2^2}. \tag{3.44}$$

We see from these equations, and this will hold for the higher order results as well [11], that they only depend on the relative sizes and directions of $\vec{q}_1$ and $\vec{q}_2$. Therefore, if we calculate the higher order results, the integrations will have some complicated form which in general cannot be solved analytically. Hence, we need to start from the form of the linear solutions to proceed with numerical calculations. The methodology for this, and the relevant observables that play a role, will be described in the next section.

3.4 The power spectrum and bispectrum

To discuss the large scale structure we observe in the universe, the perturbative expansion we have derived by itself is not enough. Some omniscient observer that is able to observe the entire universe and its evolution instantaneously would be able to write down an explicit function $\delta(\vec{x},\tau)$ that describes all matter in the universe, but we are limited in our observations. We are unable to see distant objects in the universe as they are today, and even though our lifetime appears to last long in our subjective experience, it is but a dot on the cosmological timescale. We deal with these limitations by testing the large scale structure in the universe using statistical methods.

The basis of these statistical models lies in our assumption about the cause of structure formation in the universe. We have no a priori reason to assume that the structure in our universe is a given, so we may wonder what created this structure we observe. As we can assume that the fluctuations in our background density grow over time because of gravitational collapse, we can conjecture that the structure in our universe is sourced by relatively small primordial perturbations to the homogeneous background.

One of the natural candidates for these perturbations is a quantum effect. As we know from quantum mechanics, quantum systems give rise to miniscule random fluctuations. These fluctuations could be the source of our primordial perturbations, and be the cause of all the structure we observe in our universe. As it turns out, an initial period of inflation just after the big bang indeed causes such quantum effects, which take the form of Gaussian fluctuations which behave adiabatically [27, 47]. In our thesis, we will assume that the primordial fluctuations were indeed Gaussian and sourced by inflation, even though there are different models which also yield primordial Gaussian fluctuations [50].

Starting from the assumption of initial Gaussian fluctuations, we can look at the structure of matter throughout the universe using a statistical methodology. We first make explicit that we assume *statistical homogeneity* and *statistical isotropy* in this section. Statistical homogeneity implies that the correlation between two density contrast fields[3] $\delta(\vec{x}_1)$ and $\delta(\vec{x}_2)$ depends only on their relative distance $(\vec{x}_1-\vec{x}_2)$. Statistical isotropy is the assumption that the correlation between two density fields is rotationally invariant. It is important to realize that these assumptions do not always hold. If we look at correlators in redshift space, as we will do in the next section, we explicity break statistical homogeneity and isotropy.

We also assume for now that the spatial part of the density has no relation to its cosmological evolution. If we recall equation (3.36), we can simply take out the factors of $a^{(n)}(\tau)$ and only worry about the spatial part.[4] When discussing the light cone effect in chapter 5, this is not possible anymore.

[3] From here on, we will just call these density fields.

[4] Or, when working in a different cosmology than Einstein de Sitter, we could take out the fastest growing mode of the growth function $[D_1^{(+)}(\tau)]^n$ instead of $a^n(\tau)$.

We formulate our statistical description of large scale structure starting from the two-point correlation function. This function gives the ensemble average of the product of two density fields at Fourier modes $\vec{k}$ and $\vec{k}'$, and is denoted by $\langle\delta(\vec{k})\delta(\vec{k}')\rangle$. Because we are working in Fourier space, the density field is a complex variable here. However, because we know that the density field is in fact real in real space, we can derive:

$$\delta(\vec{k}) = \int d^3\vec{x}\delta(\vec{x})e^{-i\vec{k}\vec{x}} = \int d^3\vec{x}\delta^*(\vec{x})e^{i(-\vec{k})\vec{x}} = \delta^*(-\vec{k}). \tag{3.45}$$

Inserting our assumptions of statistical homogeneity and isotropy, we can then postulate that the correlation function should vanish for $\vec{k} \neq -\vec{k}'$, and otherwise only depend on the size of the vector $\vec{k}$. The resulting k dependence we find is quantified by the *power spectrum* $P(k)$:

$$\langle\delta(\vec{k})\delta(\vec{k}')\rangle \equiv P(k)(2\pi)^3\delta_D^3(\vec{k}+\vec{k}'). \tag{3.46}$$

Here, $k = |\vec{k}| = |\vec{k}'|$. To figure out in which units the power spectrum will be given, we do dimensional analysis:

$$\begin{aligned} [\delta(\vec{k})] = [\int d^3\vec{x}\delta(\vec{x})e^{i\vec{k}\vec{x}}] &= -3, \\ [\langle\delta(\vec{k})\delta(\vec{k}')\rangle] &= -6, \\ [P(k)] &= -3. \end{aligned} \tag{3.47}$$

Hence, the power spectrum will have the inverse unit of $\vec{k}$. Before we move on to perturbative calculations we first want to consider what the linear power spectrum (so the power spectrum only depending on $\delta_1(\vec{k})$ and no higher orders) looks like. This is not a trivial thing, because the form of the power spectrum depends on the evolution of the primordial quantum fluctuations throughout the entire history of the universe. It falls outside the scope of this thesis to discuss how different scales have evolved differently throughout time, but we will state the general form of the result from [18]:

$$P(k,a) = 2\pi^2\delta_H^2\frac{k^{n_s}}{H_0^{n_s+3}}T^2(k)\left(\frac{D_1(a)}{D_1(a=1)}\right)^2. \tag{3.48}$$

This is a complicated expression, depending on the transfer function $T(k)$, which describes how modes change when the universe evolves from radiation to matter domination, the spectral index n_s, which is related to inflationary mechanics and the density amplitude at horizon crossing δ_H.[5] We will discuss how inflation, dark energy and neutrinos affect equation (3.48) in chapter 4, where we motivate the importance of large scale structure as a probe. In essence, that importance is given by the terms in the transfer function, which are in itself probes of the universe. Within the context of this chapter, it is important to note that, even though this result is time-dependent through the growth functions, in our Einstein de Sitter case a factor of $a^2(\tau)$ drops out.

Evaluating equation (3.48) is usually done using numerical (Boltzmann) code. The linear power spectrum shown in figure 3.1 was generated using CAMB [32, 39]. Note that there are wiggles in the power spectrum around $k = 0.01$ in this figure. These wiggles are due to the baryonic acoustic oscillations, which we discussed in chapter 2.

Note that the linear power spectrum is defined by:

$$P_L(k)(2\pi)^3\delta_D^3(\vec{k}+\vec{k}') \equiv \langle\delta_1(\vec{k})\delta_1(\vec{k}')\rangle, \tag{3.49}$$

so only by the terms that are linear in $\delta(\vec{k})$.

[5] Quantum fluctuations leave the Hubble horizon during the accelerating expansion of inflation, and become sub-Hubble scale again during the further cosmological evolution.

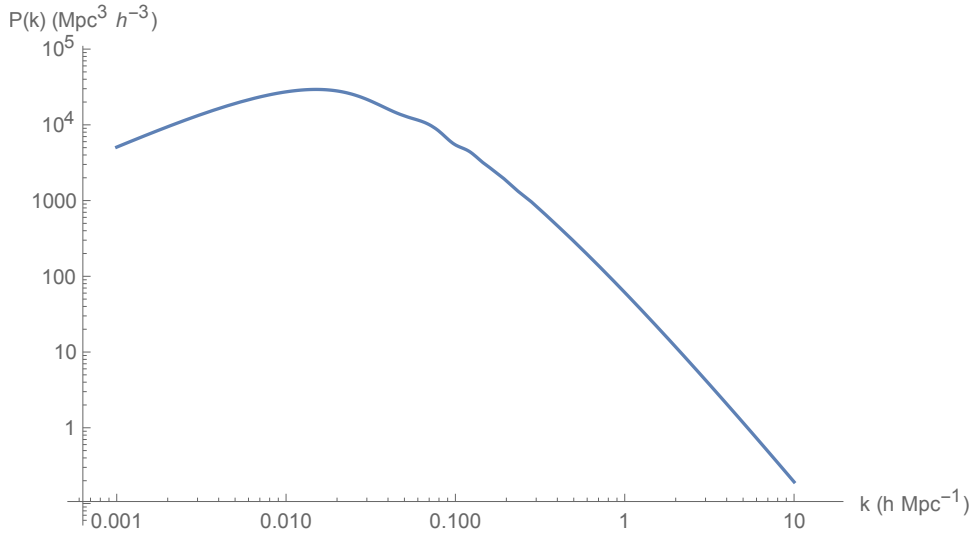

Figure 3.1: The linear power spectrum, generated using CAMB code [32, 39]. The wiggles around $k = 0.01$ are due to baryonic acoustic oscillations.

Let us now continue our discussion of the correlators between the density fields. Our assumption that the initial fields are Gaussian in their statistics becomes a central part of our theory because of the *Wick theorem*. This theorem describes the property that any ensemble average of a product of Gaussian fields can be described by the pairwise ensemble average of these fields. Mathematically:

$$\langle \delta(\vec{k}_1) \dots \delta(\vec{k}_n) \rangle = \begin{cases} 0 & \text{for } n \text{ is odd,} \\ \sum_{\text{all possible pairs}} \prod_{\frac{n}{2}\text{pairs } (i,j)} \langle \delta(\vec{k}_i)\delta(\vec{k}_j) \rangle & \text{for } n \text{ is even.} \end{cases} \tag{3.50}$$

Equation (3.50) is a very powerful tool for our description of large scale structure. We specifically chose to start from the two-point correlation function, because we see that for n-point correlation functions Wick's theorem will allow us to immediately discard terms that are odd in our initial Gaussian densities and write all other terms as a combination of two-point correlation functions. The key now, is to combine our knowledge about density perturbations from (3.41) with our statistical description.

First, we realize that we have to start from our initial density perturbations with their Gaussian statistics. We recall that these source fluctuations are quantified by our linear order results for $\delta(\vec{k}, \tau)$, so that Wick's theorem holds for $\delta_1(\vec{k})$. Then, because equation (3.41) specifies that every order in perturbation theory can be expressed as a product of the linear density fields, we can write our perturbations as n-point correlation functions in the Gaussian fields. This also implies that we can calculate the corrections to our two-point correlation function in terms of integrals over the linear order two-point correlation function.

However, before we start doing perturbation theory on the two-point correlation function, we will define the *bispectrum*. The bispectrum is an observable related to the three-point correlation function, which can be a more useful probe than the two-point correlation function in cases when one would like to extend his theory to primordial non-gaussianity [8]. We define the bispectrum as follows:

$$\langle \delta(\vec{k}_1)\delta(\vec{k}_2)\delta(\vec{k}_3) \rangle \equiv B(\vec{k}_1, \vec{k}_2, \vec{k}_3)(2\pi)^3 \delta_D^3(\vec{k}_1 + \vec{k}_2 + \vec{k}_3). \tag{3.51}$$

For the bispectrum there *is* a dependence on the separate Fourier modes, although statistical homogeneity still requires that the sum of the Fourier modes should equal zero. This is logical, as correlation should only depend on the relative position of the densities. This relative position is also exactly the

source for this dependence on the Fourier modes.

If we then consider the actual dependence of the bispectrum on the power spectrum using Wick's theorem, we see that the bispectrum of three linear fields vanishes. Therefore, the dependence on the Fourier modes is given by the second order kernel (3.43) [24]:

$$\langle \delta(\vec{k}_1)\delta(\vec{k}_2)\delta(\vec{k}_3)\rangle = \langle \delta_2(\vec{k}_1)\delta_1(\vec{k}_2)\delta_1(\vec{k}_3)\rangle + \text{cycl.}, \tag{3.52}$$

$$= (2\pi)^3\delta_D^3(\vec{k}_1+\vec{k}_2+\vec{k}_3)2F_2(\vec{k}_2,\vec{k}_3)P_L(k_2)P_L(k_3) + \text{cycl.}, \tag{3.53}$$

so that:

$$B(\vec{k}_1,\vec{k}_2,\vec{k}_3) = 2F_2(\vec{k}_2,\vec{k}_3)P_L(k_2)P_L(k_3) + \text{cycl.}. \tag{3.54}$$

We iterate once more that the second order kernel only depends on the relative size and direction of its arguments, giving the dependence we expected from our bispectrum.

Now that we have considered the linear results for both the power spectrum and the bispectrum, we will continue to consider perturbation theory results for our power spectrum. Having done the bispectrum example we already have some intuition how the first order perturbation theory results will arise. First of all, Wick's theorem demands that the sum of the orders of our two density fields is even. If we denote this sum as k, we find that we have our linear result at $k = 2$, our first perturbative results at $k = 4$, and further perturbative results at $k = 6, 8, \ldots$.

We can think about these perturbative results in a diagrammatic way as well. First, let's develop the ground rules for our correlation functions. *Rule 1* is the rule that for an n-point correlation function, we draw n dots. *Rule 2* is the rule that for every correlation we draw a line between the densities within our correlator. *Rule 3* is the rule that for a density field that is n^{th} order in perturbation theory, n lines have to emanate from the point that describes this density field. We now put these rules into practice, where we take our drawings from [11]. The simplest example for our diagrammatic description is given by the first order two-point correlation function as in figure 3.2.

Figure 3.2: The diagram for the linear two-point correlation function. As both densities (denoted by the points) have only one line emanating from them, this diagram describes the $\langle \delta_1\delta_1\rangle$ correlation function, so this is the $k = 2$ case.

We could also draw the diagram for the correlation function on the right hand side of equation (3.52), given in figure 3.3.

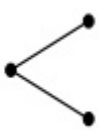

Figure 3.3: The diagram for the linear bispectrum. As the left most point has two lines emanating from it, this point describes a second order density δ_2. The other two densities only have one line emanating from them, so this diagram describes the $\langle \delta_2\delta_1\delta_1\rangle$ correlation function. For the bispectrum this is the linear order result, so for the bispectrum results start at $k = 2 + 1 + 1 = 4$.

These diagrams are very useful, because they provide us with an insightful way to develop our perturbation theory. If we want to calculate an n-point correlation function up to linear order, we can simply draw the diagram(s) for n densities. Rule 2 then requires that the diagram(s) need to be connected, and because linear order is the lowest k order we ensure that the diagram(s) have no loops in it, because each loop adds an unnecessary higher order for the densities. Having drawn the diagram(s), we can simply calculate the correlation function by calling point i in our diagram $\delta(\vec{k}_i)$, inserting a power spectrum $P(k_i)$ for each line between two points $\delta(\vec{k}_i)$ and $\delta(\vec{k}_j)$ and adding the required kernels for our points with multiple lines emanating from them. We also need to take into account the degeneracy we introduce in drawing these diagrams as a numerical factor in our results.

The fact that loops add extra orders in perturbation theory then motivates us to think of higher orders in terms of these loops. We see, using the parameter k we defined earlier, that adding a loop would increase k to $k+2$. Then, if we want to calculate our $k+2$ perturbative results, we can simply write down the one-loop diagrams and calculate these. Therefore, the n^{th} perturbative correction is also called the n-loop result.

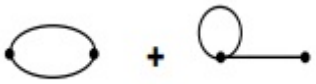

Figure 3.4: The diagrams for the one-loop two-point correlation function, where the left diagram describes P_{22} and the right diagram describes P_{13}.

Coming back to our two-point correlation function, we start by writing down the one-loop diagrams in figure 3.4. We see that there are two different ways to do this, and we will distinguish the different diagrams by indices in the related power spectrum P_{ij}. Hence, we will denote the diagram which has two lines emanating from both points by P_{22} and the diagram which has an additional loop on one of the points with respect to the linear case by P_{13}.

Using our formalism, we can write down the expressions for these one-loop corrections to the power spectrum. Note that the numerical factor of two for P_{22} comes from the two ways of connecting the two lines emanating from the two-vertices, and the numerical factor of 6 for P_{13} comes from the three choices of choosing which line to connect from the three-vertex, multiplied by the two choices we have for choosing which point in the diagram or equivalently which density corresponds to the three vertex.

$$P_{22}(k) = 2\int d^3\vec{q}[F_2^{(s)}(\vec{k}-\vec{q},\vec{q})]^2 P_L(|\vec{k}-\vec{q}|)P_L(q), \tag{3.55}$$

$$P_{13}(k) = 6\int d^3\vec{q} F_3^{(s)}(\vec{k},\vec{q},-\vec{q})P_L(k)P_L(q). \tag{3.56}$$

Here, for P_{13} we use the symmetrized kernel $F_3^{(s)}(\vec{k}_1,\vec{k}_2,\vec{k}_3)$ which can be obtained by symmetrizing F_3 [26]:

$$\begin{aligned} F_3(\vec{k}_1,\vec{k}_2,\vec{k}_3) = {} & \frac{1}{3k_1^2k_2^2k_3^3|\vec{k}_1+\vec{k}_2|^2}\left[\frac{1}{21}\vec{k}_1\cdot\vec{k}_2|\vec{k}_1+\vec{k}_2|^2+\frac{1}{14}k_2^2\vec{k}_1\cdot(\vec{k}_1+\vec{k}_2)\right] \\ & \times\left[7k_3^2(\vec{k}_1+\vec{k}_2)\cdot(\vec{k}_1+\vec{k}_2+\vec{k}_3)+\vec{k}_3\cdot(\vec{k}_1+\vec{k}_2)|\vec{k}_1+\vec{k}_2+\vec{k}_3|^2\right] \\ & + \frac{\vec{k}_1\cdot(\vec{k}_2+\vec{k}_3)|\vec{k}_1+\vec{k}_2+\vec{k}_3|^2}{3k_1^2k_2^2k_3^2|\vec{k}_2+\vec{k}_3|^2}\left[\frac{1}{21}\vec{k}_2\cdot\vec{k}_3|\vec{k}_2+\vec{k}_3|^2+\frac{1}{14}k_3^2\vec{k}_2\cdot(\vec{k}_2+\vec{k}_3)\right] \\ & + \frac{\vec{k}_1\cdot(\vec{k}_1+\vec{k}_2+\vec{k}_3)}{18k_1^2k_2^2k_3^2}\left[\vec{k}_2\cdot\vec{k}_3|\vec{k}_2+\vec{k}_3|^2+5k_3^2\vec{k}_2\cdot(\vec{k}_2+\vec{k}_3)\right]. \end{aligned} \tag{3.57}$$

Looking at these expressions, it is not very surprising that there is no analytic method to solve these. For starters, the linear power spectrum is a very complicated function, but we also see that the kernels are very hard to simplify. Usually, the calculations are approached starting from the isotropy of the universe. Then, we can integrate out the full angular dependence for P_{13} and the azimuthal dependence for P_{22} [30]. After this, we calculate the loop corrections numerically. From these calculations, we plot the P_{22} and P_{13} terms of the power spectrum in figure 3.5.

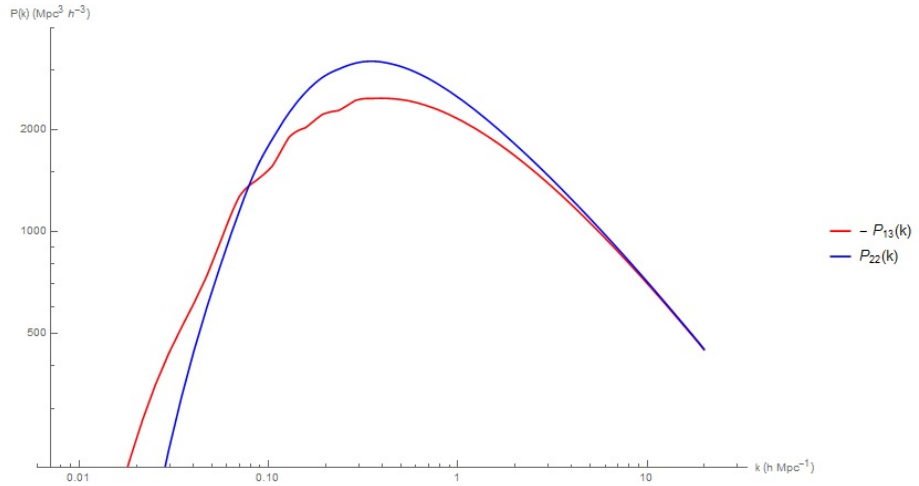

Figure 3.5: The one-loop corrections to the Power Spectrum. Note that the P_{13}-contribution is negative. Calculations based on the linear power spectrum generated using CAMB code [32, 39].

If we look at this plot for our one-loop corrections, a couple of things stand out. First of all, we see that for large k, the values of P_{22} and P_{13} approach each other. This means that for the very small-scale (or large wavenumber) results our perturbation theory does not affect the linear results. However, we already have reasons to be suspicious about our results for small scales. After all, our derivations depend on the assumption that there is no highly nonlinear behavior, which is exactly what we would expect for these scales.

We can also consider the effect of one-loop perturbations on the total power spectrum, which we have plotted in figure 3.6. We see that the contribution is significant for $0.1 \leq k$. Therefore, we can consider the one-loop results as an augmentation of linear theory for this scale, and this needs to be taken into account for terms at that scale in observations. For scales smaller than the scale defined by $k = 1$ (i.e. $k \geq 1$), the perturbations continue to be the dominant term in the total power spectrum. However, at this scale the behavior of the system is highly nonlinear, and therefore our theory cannot be trusted there.

Note that we need to be aware of the nonlinear scale when we extend our theory. When we include the light cone effect in chapter 5, we thus need to take into account whether our corrections are significant at linear or nonlinear scale. If we see that our corrections only become significant at scales $k \geq 1$, we cannot trust our extension at all.

3.5 Redshift space

If we want to couple our results from perturbation theory to observations, we recall that a lot of difficulties arise because of the distances and timescales involved. Often, redshift is used as a measure of distance in surveys, which implies that we have to take into account effects that distort the redshift we observe [11]. In general, these effects are due to peculiar velocities of the objects we observe. After all,

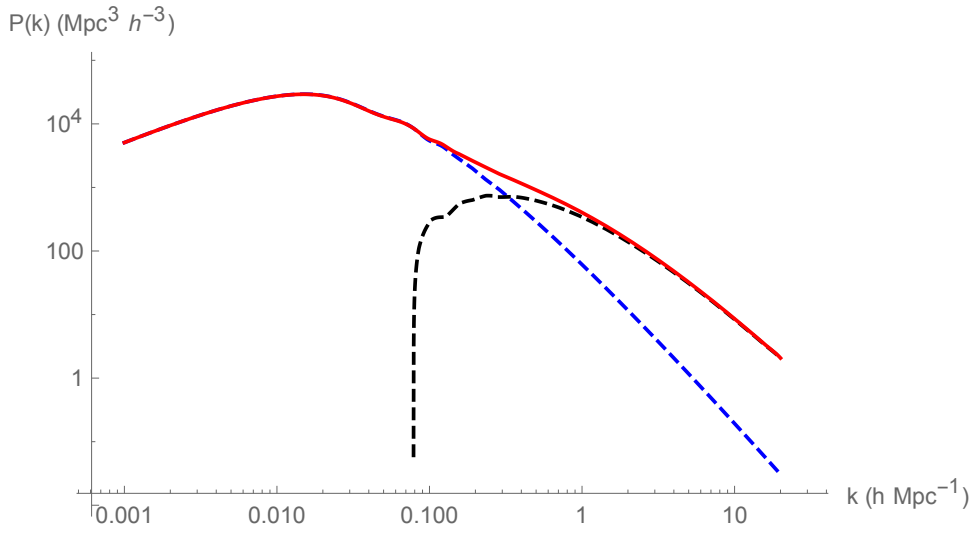

Figure 3.6: The power spectrum with one-loop corrections included. The red line denotes the full power spectrum, the blue dashed line denotes the linear power spectrum and the black dashed line denotes the perturbative contribution. We can clearly see that the perturbative effects become important for k larger than $k \approx 0.1$. Hence, we can consider the non-linear scale to start at $k_{\mathrm{NL}} \approx 0.1$. The effects become increasingly more dominant for larger k, but on scales with $k > 1$, or equivalently on such small scales, we cannot trust our theory anymore because gravitational effects become highly nonlinear. The linear power spectrum was generated using CAMB code [32, 39].

if an object is receding from us due to the expansion of space *and* due to a peculiar velocity away from us, we will see that the redshift of such an object is larger than the redshift that is accounted for by the expansion of space. If we use the redshift of this object to determine its distance, we would assume this object to be farther away than it actually is.

How, then, do we typically observe these peculiar velocities in galaxy surveys? It turns out that there are two main effects we need to consider. First of all, we observe redshift space distortions when we observe galaxies that are falling into a cluster, also called the *Kaiser effect* after [36]. Suppose we observe a galaxy that is closer to us than the cluster it is falling into. This causes the galaxy to have a peculiar velocity towards the cluster, leading us to observe it at a larger redshift. The opposite happens for a galaxy that is farther away than the cluster it is falling into. Then, a peculiar velocity that is directed towards us leads to a smaller redshift observation. The combination of these distortions leads to an observation of galaxies around a cluster that is squashed along the line of sight with respect to the real space case.

The other redshift space distortion effect that is important to take into account is called the *Finger of God* effect [34]. This effect takes place at smaller scales than the squashing effect, and it originates from the velocity dispersion of galaxies within clusters. These peculiar velocities then make the galaxies appear elongated in redshift space, thus causing an effect as if they are pointing at the observer.

We have plotted a visualization of both the Kaiser effect and the Finger of God effect together in figure 3.7.

Let us describe how to take these redshift space distortions into account. First, we shall make explicit that we decompose any coordinate $\vec{x}$ in real space into a redshift space coordinate. In this coordinate system, we take our origin to be the location of the earth, and we define our redshift space coordinate by:

$$\vec{s} \equiv \vec{x} + \frac{\vec{u}(\vec{x})}{\mathcal{H}(\tau)} \cdot \hat{x}. \tag{3.58}$$

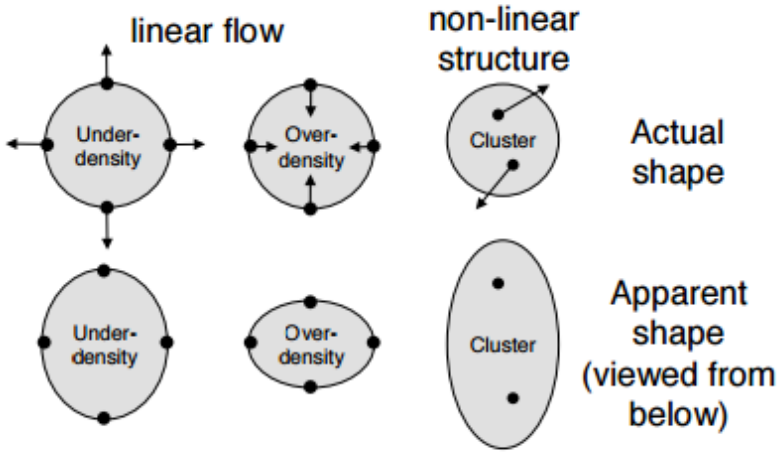

Figure 3.7: A visualization of redshift space distortions. The left column denoted linear flow shows how the Kaiser effect distorts the real space coordinates (top row) in a redshift space observation (bottom row). The right column illustrates the Finger of God effect. Taken from [44].

Here $\hat{x}$ is the direction of the line of sight. We start from the realization that any region should hold the same number of galaxies irrespective of coordinate system [36]. Therefore, we know that:

$$n(\vec{s})d^3\vec{s} = n(\vec{x})d^3\vec{x}. \tag{3.59}$$

From this, we see that:

$$n(\vec{s}) = n(\vec{x})J(\vec{x}). \tag{3.60}$$

Therefore, we proceed to calculate our Jacobian. We start from the volume element in the angular decomposition for real and redshift space coordinates:

$$\begin{aligned} d^3\vec{x} &= x^2 \sin\theta dx d\theta d\phi, \\ d^3\vec{s} &= s^2 \sin\theta ds d\theta d\phi. \end{aligned} \tag{3.61}$$

Because both ϕ and θ are competely equivalent for redshift space and real space, we then see that:

$$d^3\vec{s} = \frac{s^2}{x^2}\frac{ds}{dx}d^3\vec{x} \equiv J^{-1}(\vec{x})d^3\vec{x}. \tag{3.62}$$

This gives us a way to calculate our Jacobian. We proceed to calculate:

$$\frac{ds}{dx} = 1 + \frac{d}{dx}\left(\frac{\vec{u}(\vec{x})}{\mathcal{H}(\tau)} \cdot \hat{x}\right) = 1 + \frac{\nabla_x(\vec{u}(\vec{x}) \cdot \hat{x})}{\mathcal{H}(\tau)}, \tag{3.63}$$

and

$$\frac{s^2}{x^2} = \frac{\left(\vec{x} + \frac{\vec{u}(\vec{x})\cdot\hat{x}}{\mathcal{H}(\tau)}\right)^2}{x^2} = \left(\frac{\vec{x} + \frac{\vec{u}(\vec{x})\cdot\hat{x}}{\mathcal{H}(\tau)}}{x}\right)^2 = \left(1 + \frac{\vec{u}(\vec{x}) \cdot \hat{x}}{\mathcal{H}(\tau)x}\right)^2. \tag{3.64}$$

Then, we find that our Jacobian equals:

$$J(\vec{x}) = \left(1 + \frac{\nabla_x(\vec{u}(\vec{x}) \cdot \hat{x})}{\mathcal{H}(\tau)}\right)^{-1} \left(1 + \frac{\vec{u}(\vec{x}) \cdot \hat{x}}{\mathcal{H}(\tau)x}\right)^{-2}. \tag{3.65}$$

We can in fact explain the physical meaning of these terms in the Jacobian. We recall that peculiar velocities cause objects to appear closer (or farther) away in redshift space. The inverse quadratic order term can be explained because an object that is moving away at peculiar velocity $\vec{u}(\vec{x})$ appears to be at a distance $\left(1 + \frac{\vec{u}(\vec{x})\cdot\hat{x}}{\mathcal{H}(\tau)x}\right)\vec{x}$ in redshift space. Because the volume element is given by the area on the sphere at distance x which scales like x^2, we observe a larger area which scales like $\left(1 + \frac{\vec{u}(\vec{x})\cdot\hat{x}}{\mathcal{H}(\tau)x}\right)^2 x^2$. The Jacobian corrects for this distortion, which we visualize in figure 3.8.

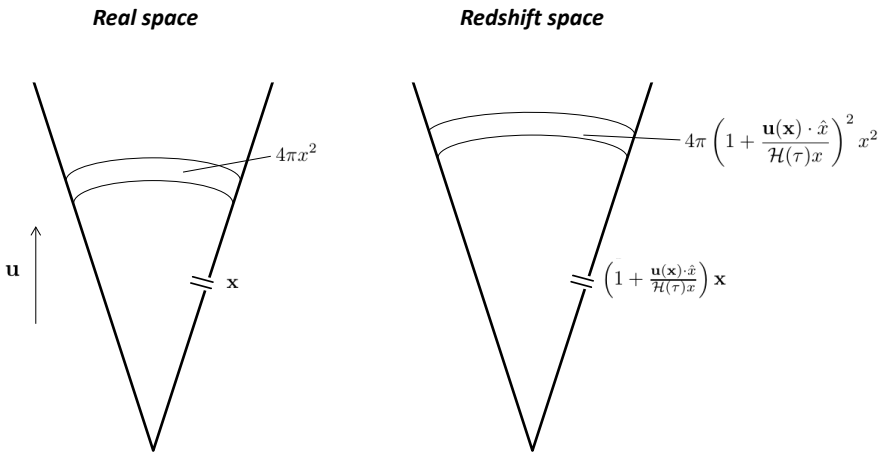

Figure 3.8: A visualization of the distortion of the volume element at distance $\vec{x}$ with recession velocity $\vec{u}(\vec{x})$ in redshift space.

Before we will explain the first term in the Jacobian, we will move to an approximation in which the quadratic terms do not contribute. The reason for this is that it in general is difficult to work with the radial components. Our power spectrum would obtain a dependence on the vector of the Fourier mode $\vec{k}$ instead of dependence on the norm alone, and this would require a different approach to our Fourier decomposition [29, 55]. Therefore, we take all our radial components to be in the same direction $\hat{x}$. This is also called the *plane parallel approximation*. Moreover, to comply with literature we redefine our redshift space coordinate in terms of $f(\Omega_m, \Omega_\Lambda) \equiv \frac{d \ln D_1(a)}{d \ln a}$ and $\vec{v} \equiv -\frac{\vec{u}(\vec{x})}{\mathcal{H}(\tau) f}$:

$$\vec{s} = \vec{x} - f\vec{v}(\vec{x}) \cdot \hat{x}. \tag{3.66}$$

This results in a Jacobian in which only the first order term is important, which we have rewritten as follows:

$$J(\vec{x}) = |1 - f\nabla_x(\vec{v} \cdot \hat{x})|. \tag{3.67}$$

This term can be explained by once more considering the fact that distortions are caused by a peculiar velocity along the line of sight, which in our approximation is fixed in the direction $\hat{x}$. If an area of the universe has a constant peculiar velocity along the line of sight, this would imply that only the distance is changed but the volume element remains the same size in either coordinate system. However, for an area of the universe in which the peculiar velocity has a gradient, this area appears stretched or compressed in redshift space. Even stronger, this gradient effect can lead to singularities in the observed density in redshift space, which are called *caustics* [41]. Let us first write down the density analog of equation (3.60) where we used $\delta(\vec{s}) = 1 + n(\vec{s})$:

$$\begin{aligned}(1 + \delta(\vec{s}))d^3\vec{s} &= (1 + \delta(\vec{x}))d^3\vec{x}, \\ (1 + \delta(\vec{s}))J(\vec{x})d^3\vec{x} &= (1 + \delta(\vec{x}))d^3\vec{x}.\end{aligned} \tag{3.68}$$

Rewriting this, we see that:

$$\delta(\vec{s}) = \frac{\delta(\vec{x}) + 1 - J(\vec{x})}{J(\vec{x})}. \tag{3.69}$$

Thus, the observed density is divergent for zeroes of the Jacobian, which occur when:

$$\nabla_x(\vec{v} \cdot \hat{x}) = \frac{1}{f}. \tag{3.70}$$

Physically, this exactly describes the points where the differential in peculiar velocity because of gravitational collapse is as large as the differential in Hubble flow. In other words, if we consider a galaxy at real distance $\vec{x}$ and another galaxy at real distance $\vec{x} + \Delta\vec{x}$, the *combination* of Hubble flow and peculiar velocity will map both galaxies to the same point in redshift space even though the *individual* Hubble flow and peculiar velocity differ. A visualization of this is given in figure 3.9.

Having understood the physical meaning of the intricacies in the redshift space Jacobian, we move on to once more do perturbation theory. Following [46] we can write the Fourier transform of the density in redshift space (denoted by $\delta_s(\vec{k})$) as:

$$\begin{aligned}\delta_s(\vec{k}) &\equiv \int d^3\vec{s}\delta(\vec{s})e^{-i\vec{k}\vec{s}}, \\ &= \int d^3\vec{x}e^{-i\vec{k}\vec{x}}e^{ifk_x v_x(\vec{x})}\left[\delta(\vec{x}) + f\nabla_x v_x(\vec{x})\right].\end{aligned} \tag{3.71}$$

Here the subscript x means the direction among the line of sight, and we have assumed that only points where $\nabla_x v_x(\vec{x}) < 1$ contribute to our density. This expression gives the full non-linear result when taking into account both the plane parallel assumption and the assumption that caustics do not occur. We can continue to develop a perturbation theory for our redshift density by expanding the second exponential [46]. We will however only state the famous linear result due to Kaiser [36]:[6]

$$\delta_s(\vec{k}) = \delta(\vec{k})\left[1 + f\left(\frac{\vec{k} \cdot \hat{x}}{k}\right)^2\right]. \tag{3.72}$$

This then affects the linear power spectrum according to:

$$(P_s)_L(\vec{k}) = \left[1 + f\left(\frac{\vec{k} \cdot \hat{x}}{k}\right)^2\right]^2 P_L(k), \tag{3.73}$$

[6] Kaiser used $\mu \equiv \frac{\vec{k}\cdot\hat{x}}{k}$ to describe the angular dependence. The use of μ is also the convention in literature.

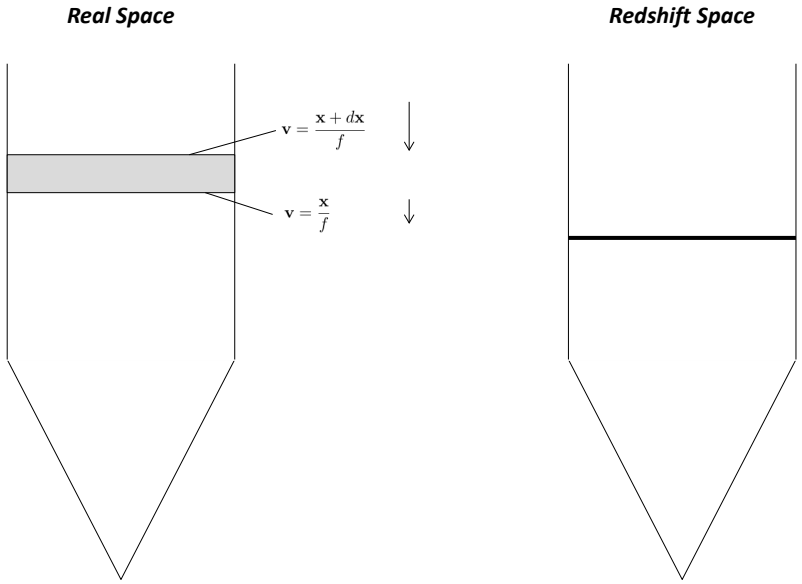

Figure 3.9: A visualization of the emergence of caustics in redshift space. The part that is farther away in real space has a larger peculiar velocity towards us than the part that is closer. The difference is exactly large enough to generate a caustic in redshift space.

which gives an adjustment to wave vectors that have components along the line of sight. This is of course exactly what one would expect. Concluding, we see that redshift space distortions are important to take into account when we consider results from observations that use redshift as a distance measure. Distortions such as the finger of God effect and the Kaiser effect have an impact that changes the measurements with respect to real space. Luckily, there are methods to adjust for this mathematically, as is done in equation (3.73).

3.6 Summary

We have seen that we have a framework in which we can describe the evolution of large scale structure in the universe. This framework starts from a Newtonian description of the gravitational physics that determine the way in which (dark) matter interacts gravitationally. If we insert the cosmological parameters, we obtain the Vlasov equation from which we can take the moments to derive the continuity equation and the Euler equation which will govern our density evolution. Following this, we can choose to linearize in the density contrast and velocity divergence to obtain results for the linear case.

If we want to include nonlinear results into our considerations, we need to follow the same procedure as before but without estimating away the nonlinear parts. Then, by performing a Fourier transformation, we can calculate the coupling between modes. We see that for an EdS cosmology we can derive analytic results up until arbitrary order, effectively giving us a working perturbation theory to describe large scale structure.

However, when we want to have a useful measure for the results our perturbation theory gives us, we need to take into account that we are seriously limited in our observations of the universe. We can only

observe at timescales of the order of a couple of years, which is for all practical purposes a fixed point in time in a cosmological context, and the objects we do observe are only observed as they were in the past because of nature's speed limit of c. Therefore, we need to look at our density fields as statistical objects. Assuming our primordial density fluctuations to be Gaussian stochastic variables, we can define useful observables such as the power spectrum and bispectrum. Using the strength of Wick's theorem and combining this with our perturbation theory results then gives us a way to develop the power spectrum and bispectrum perturbatively.

We are also limited in our observations because we often use cosmological redshift z to determine the distance of objects. In these redshift space coordinates, our observations are distorted by the peculiar velocity of objects. We have described a way to quantify this Kaiser effect and Finger-of-God effect so that we have a formalism which takes into account these distortions and relates it to the real space results.

Now that we have developed our standard perturbation theory, we will return to the relevance of large scale structure in chapter 4. We now possess the theoretical tools to show how information is contained in large scale structure. After returning to large scale structure as a probe, we move on to discuss the light cone effect in chapter 5.

Chapter 4

Large scale structure as a probe

4.1 Introduction

Now that we have discussed the basic quantities in cosmology and have formulated the standard theory that is used to describe large scale structure evolution, we can return to our claim that large scale structure can be an important probe for our universe. In this chapter, we will explain how certain cosmological effects leave a signature in the large scale structure we observe, and describe some of the key current large scale structure observations. Moreover, we will list some of the relevant observations that will start in the following 5-10 years. We will motivate that the accuracy and wealth of data from those experiments warrant an in depth study of large scale structure.

We start this chapter by describing three signatures of physical effects that are currently poorly understood (dark energy, neutrinos) or poorly probed (inflation). We will start by qualitatively explaining how inflation generates primordial fluctuations. After that, we will discuss the subject of primordial non-gaussianity, and show that it can be used to restrict the eligible models of inflation.

After this, we will discuss how large scale structure can be used to obtain a better understanding of dark energy. As we have seen in chapter 3, large scale structure is sensitive to cosmological evolution. Hence, the form of current structure can be used to probe the several models that have been proposed to explain dark energy.

Finally, we will describe how massive neutrinos leave their trace in the large scale structure of the universe. We will see that the early decoupling of massive neutrinos will leave a signature in the power spectrum below free-streaming scales.

After having described these important signatures, we list some of the key current observations. In addition, we discuss some next generation observations, and how they will help us to understand inflation, dark energy and massive neutrinos. The combination of a wealth of data, sensitivity to cosmological quantities and improved accuracy will provide a strong indication that large scale structure is an exciting field for the future.

4.2 Cosmological signatures in large scale structure

In this section, we will give a short qualitative discussion of the signatures inflation, dark energy and massive neutrinos leave in the large scale structure of the universe. We will state some of the key results, and make explicit how large scale structure observables depend on parameters from underlying theories.

Inflation:

In this part, we will be following Baumann's lecture notes on inflation [2, 10].

Inflation is the name given to a period of accelerating expansion ($\ddot{a}(\tau) > 0$) that took place just after the big bang, which solves the horizon problem; inflation explains why causally disconnected parts of the universe in the CMB are almost perfectly unifrom. We will see in this section that inflation provides us with the primordial seeds for large scale structure, which we already briefly referred to in chapter 3. This also means that large scale structure can be used to probe different models of inflation. To be more specific, we will show that we can use effects from primordial non-gaussianity in the bispectrum to restrict inflationary models.

To start our discussion, we define two parameters that can be used to check whether a model is suitable to sustain inflation for a long enough period to solve the horizon problem. As it turns out, this is only possible when the parameters ϵ and η are small, as is described in equations (4.1) and (4.2):

$$\epsilon \equiv -\frac{\dot{H}}{H^2} < 1, \tag{4.1}$$

$$\eta \equiv \frac{|\dot{\epsilon}|}{H\epsilon} \ll 1. \tag{4.2}$$

To avoid overcomplicating the discussion, we will at first limit it to *slow-roll* inflationary models, although many more models of inflation have been proposed [2]. When we move on to primordial non-gaussianity, we extend our range to different models. Slow-roll inflation is inflation driven by an *inflaton* field that is minimally coupled to gravity, giving rise to the following action:

$$S = \int dt d^3\vec{x}\sqrt{-g}\left[\frac{M_{pl}^2}{2}\mathcal{R} - \frac{1}{2}g^{\mu\nu}\partial_\mu\phi\partial_\nu\phi - V(\phi)\right]. \tag{4.3}$$

This action gives rise to slow-roll inflation if the potential has the required form given in figure 4.1. The flat shape of the potential is required to sustain inflation for a long enough period.

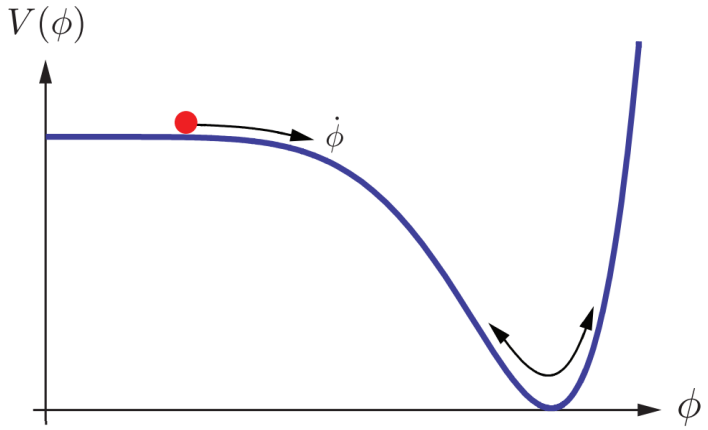

Figure 4.1: The form of the potential that is required for slow-roll inflation. The field rolls down into the potential well slowly enough to sustain the inflationary phase for a long enough period. Taken from [2].

We can derive the Hubble rate during inflation from equation (4.3), which is given by:

$$H^2 = \frac{1}{3M_{pl}^2}\left[\frac{1}{2}\dot{\phi}^2 + V(\phi)\right], \tag{4.4}$$

and which allows us to write down our conditions for inflation from equations (4.1) and (4.2) in terms of the potential. Therefore, any information we can obtain about the parameters ϵ and η will also tell us something about the potential used in the inflationary model.

How, then, does structure emerge from this inflationary model? It turns out that the energy density ρ of the early universe is governed by the evolution of the inflaton field. This implies that fluctuations in the inflaton field lead to fluctuations in the primordial energy density. By including quantum fluctuations in the action, it is possible to derive perturbations to the background. In fact, for a slow-roll model it can be shown that quantum fluctuations induce gaussian curvature fluctuations ζ.[1] Computing the power spectrum for these fluctuations in a systematic expansion in the slow-roll equivalents of ϵ, η yields the following scaling [2]:

$$P_\zeta \sim \frac{k^{-2\epsilon-\eta}}{k^3} \equiv \frac{k^{n_s-1}}{k^3}. \tag{4.5}$$

Recalling from chapter 3 that the matter power spectrum is sourced by primordial fluctuations, this implies we can measure the inflationary parameters ϵ and η using the large scale structure. Because ϵ and η depend on the potential $V(\phi)$ in slow-roll inflation, this will allow us to restrict inflationary models.To make the relation to current day structure specific, we write down the scaling of the current day matter power spectrum with P_ζ, where we recall equation (3.48):

$$P(k,a) \sim \left(\frac{k}{aH}\right)^4 T^2(k) \left(\frac{D_1(a)}{D_1(a=1)}\right)^2 P_\zeta(k). \tag{4.6}$$

We recall that the dependence of the current day power spectrum on the primordial power spectrum depends on the evolution of differently sized modes. This has to do with the time at which modes cross the *particle horizon* which is defined by $\tau = \int_0^t dt' \frac{1}{a(t')}$. On subhorizon scales modes evolve, whereas on superhorizon scales they behave adiabatically.

Primordial non-gaussianity:

Inflationary models can be restricted even further when we look at deviations from gaussianity for the curvature fluctuations. We recall that Wick's theorem allows us to set all correlations between an odd number of gaussian fields to zero, but for non-gaussianity this is not the case. In particular, this leads to a signature in the bispectrum because a non-gaussian B_{111}-term contributes:

$$\langle \delta_1(\vec{k}_1)\delta_1(\vec{k}_2)\delta_1(\vec{k}_3)\rangle \neq 0. \tag{4.7}$$

There are two different ways in which non-gaussianity arises in inflationary models, namely because of quantum effects within the horizon, and because of classical non-linear evolution outside of the horizon; the latter is only possible for non-adiabatic modes. We will not go into detail for either of the mechanisms, because they involve a lot of technical details. A review can be found in [2, 14]. Here, we will shortly refer to the formalism and state a key result.

To calculate the non-gaussian contributions due to quantum effects, one needs to apply the *Schwinger-Keldysh in-in* formalism, a review of which can be found in [2, 14]. When applying this formalism to quantum fluctuations, it is possible to derive the non-gaussian terms in the bispectrum. Maldacena did this first for general single-field inflationary models, and his calculation showed that no appreciable non-gaussianity can be observed for single field slow-roll models in the bispectrum [14, 40]. More specifically, the non-gaussian contribution scales like the slow-roll parameters ϵ and η, which are small [14]:

$$\langle \zeta(\vec{k}_1)\zeta(\vec{k}_2)\zeta(\vec{k}_3)\rangle \sim P_\zeta^2 \left[\frac{\epsilon}{8}F(k_1,k_2,k_3) + \frac{\eta}{8}G(k_1,k_2,k_3)\right], \tag{4.8}$$

[1] We will not consider tensor perturbations in this discussion, but an extension to include these needs to be made to be complete. See for instance [2, 10] for discussion of additional modes.

where $F(k_1, k_2, k_3)$ and $G(k_1, k_2, k_3)$ depend only on the relative sizes of the modes. Note that the slow-roll parameters are typically of order $\mathcal{O}(0.01)$, while effects of non-linearity of large scale structure observations are of order $\mathcal{O}(1)$. Hence, we will not find non-gaussianity induced by slow-roll inflation [14].

The result from equation (4.8) allows us to restrict our range of inflationary models if we measure primordial non-gaussianity. If we measure a signal that can be lifted above the induced non-gaussianity from nonlinear gravitational effects, we can discard the single-field slow-roll model. Moreover, models beyond single-field slow-roll tend to predict non-gaussianity, so a measurement would restrict the other candidates as well. Conversely, if we find no appreciable non-gaussianity, the likelihood of a single-field slow-roll inflation increases.

We will not discuss the way in which non-gaussianity arises due to classical superhorizon effects, but the interest reader may consult [2] for a review.

In conclusion, we have introduced inflation, and motivated that large scale structure can be used to probe models of inflation. More specifically, the observed large scale structure is the signature of quantum fluctuations during inflation. In addition, we have shown that primordial non-gaussianity can be used to restrict the range of models, and stated the important result that a slow-roll model will not induce a significant amount of primordial non-gaussianity.

Dark energy:

One of the largest mysteries in current cosmology is the nature of dark energy. We recall from chapter 2 that the universe is currently undergoing a phase of accelerated expansion, which is attributed to dark energy. The exact nature of this dark energy remains elusive however. Several explanations for dark energy have been conjectured, and it turns out these can be probed using large scale structure [6].

Some of the key models for dark energy that have been proposed are quintessence [12], k-essence (kinetic quintessence) [7], and modified gravity, the latter of which is problematic as an observable [37]. It turns out that these models have some properties that could be probed by observations of large scale structure. More specifically, these models tend to modify the dependence of the current power spectrum on the primordial perturbations, because they affect cosmological evolution [6]. The way in which equation (3.48) from chapter 3 changes because of different models can help us to obtain insight in the nature of dark energy. We recall the usual form of equation (3.48) below:

$$P(k, a) = 2\pi^2 \delta_H^2 \frac{k^{n_s}}{H_0^{n_s+3}} T^2(k) \left(\frac{D_1(a)}{D_1(a=1)} \right)^2 . \tag{4.9}$$

Different models of dark energy all change equation (4.9) in a specific way, allowing us to probe the parameters of these models.

Massive neutrinos:

In physics, very little is understood about the nature of neutrinos. One of the ways to increase our understanding about these particles would be to measure their mass. Already, the current bounds on neutrino mass are provided by cosmological data from both the CMB and large scale structure [16, 43]. In this part, we shortly discuss how massive neutrinos leave a signature in large scale structure observations, which can therefore be used to further constrain neutrino mass.

In general, neutrinos leave a signature that suppresses the power spectrum below the massive neutrino free-streaming length [35]. Typically this induces a suppression of order 1% for the short scale power spectrum [21]. Once more, we recall that the current realization of large scale structure depends on many factors, given in equation (4.9). To make the neutrino suppression for the power spectrum a little more

specific, we will give a result for the growth function on shorter scales than the free streaming length for massive neutrinos, so for $k > k_{\text{fs}}$ [48]:

$$D_\nu(z) \propto (1 - f_\nu)D^{1-p}(z), \tag{4.10}$$

where $f_\nu \equiv \frac{\Omega_\nu}{\Omega_m}$ and $p \equiv (5 - \sqrt{25 - 24f_\nu})/4$. The result influences power through equation (4.9).

Because the result depends on the neutrino mass fraction, it can be used to probe neutrino masses. Given that the effect is relatively small, once more the need for an accurate theoretical description of observations becomes clear.

4.3 Observations

In the previous section, we have given a motivation for studying large scale structure in detail. If we are able to accurately observe large scale structure, this will then give us more insight into some of the major questions in contemporary physics. Luckily, we will see that observations of large scale structure are becoming increasingly accurate. In this section, we list two of the most important current observations, and shortly discuss some of the observations we can look forward to in the coming 5-10 years.

Recently, there have been two experiments about large scale structure which have given unprecedented amounts of information, namely the *Sloan Digital Sky Survey* (SDSS) [20,54] and the *Baryon Oscillation Spectroscopic Survey* (BOSS), which is an experiment that is part of the third iteration of the SDSS experiment [17]. An older experiment which is worth addressing in passing without going into the results is the *2-degree Field Galaxy Redshift Survey* (2dFGRS) [15], which produced the remarkable image in our introduction in chapter 1; figure 1.1.

SDSS: we first discuss some power spectrum results from SDSS. We follow [49] in our discussion here, which is based on the 4^{th} data release from SDSS. Using the observations of a total of approximately 300,000 galaxies at distances up until $z \approx 0.5$, a number of physical parameters are constrained using the relation between these parameters and the power spectrum from equation (4.9). Moreover, in the analysis of the results they differentiate in the dataset between the bulk of the observed galaxies and a so-called *Luminous Red Galaxy* (LRG) sample, where the latter is a dataset which is optimized for estimating the power spectrum based on statistical technicalities. The results are plotted together with the theoretical value for the power spectrum for $0.01 < k < 0.2$ in figure 4.2. The reason the power spectrum is specifically evaluated for those values of k, is the fact that baryonic acoustic oscillations (BAO) leave a signature in that domain. Because the BAO are a standard statistical ruler, they can be used to constrain cosmological parameters. From this data release of the SDSS experiment, we see for instance for inflation that the spectral tilt has value $n_s = 0.953 \pm 0.016$, which means that the slow roll parameters are indeed of order $\mathcal{O}(0.01)$. Also, neutrino masses are constrained to < 0.94 eV in this SDSS data release [49].

BOSS: the results from SDSS were further improved on by the BOSS experiment, which probes galaxies with redshift $0.2 < z < 0.75$ and looks at correlator results at wavelengths $0.01 < k < 0.03$ [4].[2] The BOSS experiment produced reliable information on the power spectrum magnitude and standard deviation as shown in figure 4.3. Moreover, as we can easily see from its name, the BOSS experiment is optimized to measure baryon acoustic oscillations (BAO). We recall the importance of the BAO because they are standard statistical rulers, and their measurement can be used to probe cosmology.The measurements in the BOSS experiment were used to further refine the results on our cosmic inventory from table 2.1 with respect to the results from SDSS [4,49]. Quite impressively, within the BOSS experiment, accuracy in measuring the dark energy equation of state

[2]The BOSS experiment is in itself also a part of the SDSS of course, but we distinguish it in particular for its separate importance.

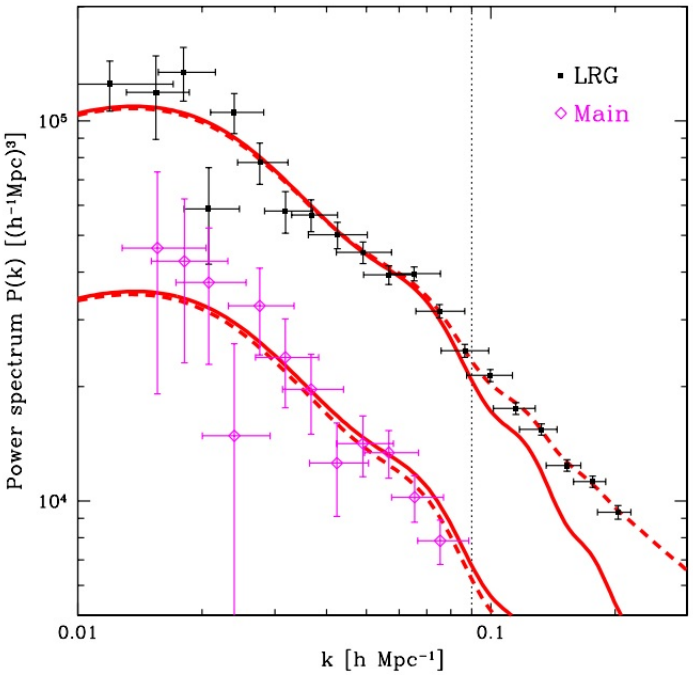

Figure 4.2: The results from SDSS for the power spectrum, based on both the optimal LRG sample and the main dataset. The solid curves give the linear theoretical value of the power spectrum, whereas the dashed curves describe nonlinear correction. We see that the nonlinear corrections become important at $k_{\mathrm{NL}} \approx 0.1$. Taken from [49].

w is determined up to 5% at specific redshift. Also, BOSS results restrain the sum of the neutrino masses to < 0.16 eV at the 95% limit, showing the power of large scale structure observations. More importantly, it shows the rapid increase of observational power of large scale structure surveys. In the ten years between [49] and [4], constraints on neutrino mass have improved by a factor 5.

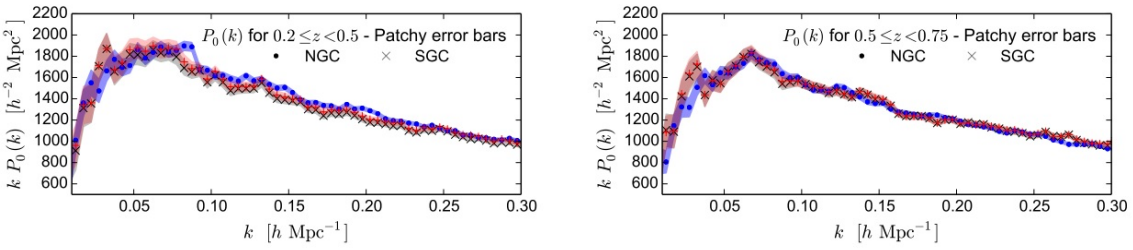

Figure 4.3: The results from BOSS for the reduced linear power spectrum $kP(k)$. NGC and SGC stand for North (South) Galactic Cap, and the shaded area denotes the error bars. Taken from [4].

It is important to note the large increase in both precision and maximum observed redshift in the timeframe between SDSS and BOSS. The error bars decrease with an order of magnitude, and the maximum redsift probed increased as well. Moreover, the accuracy in probing neutrino mass has increased by a factor of 5 between the two observations. Given that [49] was published in 2006 and [4] was published ten years later, this clearly gives motivation why the progress in the field of observational cosmology

is so exciting. We shall see that the next generation of observations probes unprecedented redshifts, which will provide us with observations that are increasingly sensitive to cosmology. This is a strong motivation why large scale structure is this important. Already, observations about large scale structure give us extra accuracy in probing inflation, dark energy and neutrino masses, and the increased precision of future experiments will give us strong observational bounds on models explaining these phenomena.

To be more specific about the expected experiments, we will list a couple of them. We can look forward to further surveys from the extended BOSS experiment that will ultimately probe large scale structure at redshifts up until $z \approx 2.5$. Moreover, we can look forward to the *Dark-Energy Spectroscopy Instrument* (DESI) which will probe tens of millions of galaxies using the Mayall telescope. Most impressive perhaps is the outlook we have to ESA's Euclid experiment, a mission which will increase the precision of measurements with two orders of magnitude or more [44]. For a review of the expected accuracy of Euclid (generally better than 1%), and the way in which it can be used to probe a range of models on dark energy, inflation, dark matter and other physical concepts, see [6].

4.4 Summary

In this chapter, we have shown that large scale structure can be used to learn about our universe. We have shortly discussed the signatures large scale structure contains from inflation, dark energy and from massive neutrinos, and motivated that observing large scale structure can lead to new insights. Moreover, we discussed some of the current large scale structure observations in detail, and listed some of the upcoming experiments.

Having shown that large scale structure contains invaluable information about the universe, and having discussed that the amount of data available on large scale structure will explode in the coming decade, we now have motivated the necessity to include the light cone effect when applying theory to observations. This is especially relevant because increased observational accuracy needs to be matched by the theory. We move on to the calculation of the light cone effect in chapter 5.

Chapter 5

Large scale structure on the light cone

5.1 Introduction

In the past chapters we have introduced and explained the framework in which the large scale structure of the universe is usually considered, and we have motivated why studying large scale structure is indeed very relevant. However, there is a major complication that is not taken into account in the standard theory. As alluded to in chapter 3, we are limited in our observations of the universe by a number of effects, one of which is the fact that we observe galaxies on the light cone. Therefore, we do not see far away galaxies where they currently are, but instead see a representation of their past. If we then recall that we have to take into account the time evolution of the universe for practically all assertions we make in cosmology, we are presented with a problem.

Usually, this problem is dealt with in observations by dividing up the radial distance component of the observed galaxies into bins [52]. Then, for each individual bin the state of cosmological evolution is approximated by the average state of cosmological evolution within that specific bin. In other words, galaxies are put on the equal time hypersurface that corresponds to the radial distance of the center of the bin. We recall the visualization of this from the introduction in chapter 1 in figure 5.1. Because this approximation induces an error, we are motivated to do a calculation which quantifies the full light cone effect.

The methodology is quite simple: we will follow standard perturbation theory (SPT), but when we actually calculate the correlation functions between two fourier modes we give a special role to the radial distance χ, because this parameter is also the parameter that defines conformal time for the galaxy observed. This will then allow us to get exact results for the power spectrum including the light cone effect. Our normal definition of the Fourier transform is problematic for this, because it assumes we can observe objects that are infinitely far away. In reality, however, we cannot see farther than the *particle horizon*, the maximum distance from which particles could have travelled to an observer on earth since the big bang, which is given by $c\tau_0$, where τ_0 is the current conformal time.[1] Moreover, because we want some way to compare our results to the results we would get with the normal approximation on an equal time hypersurface, we would like to expand our results around the average radial distance $\overline{\chi}$ of the bin, which parametrizes this equal time hypersurface. To make this possible, we define a finite volume Fourier transform within a bin.

[1] In an EdS cosmology this would yield a particle horizon of $\frac{2c}{H_0} = 6$ Gpc h^{-1}, but in reality the particle horizon is a bit farther away because of the other cosmic components.

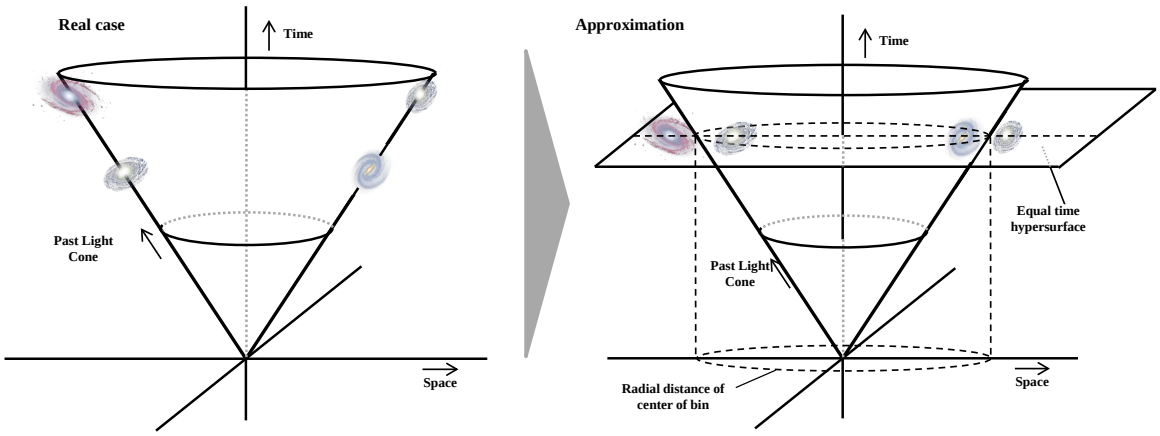

Figure 5.1: The approximation that is usually made when dealing with the light cone effect.

To get an intuition for the implications of our finite volume Fourier transform, we start by considering a one-dimensional toy model. We will calculate how the results for the two-point correlation function within this model would be affected, and discuss at which scales we can trust the finite volume Fourier transform.

Following this, we will calculate the light cone effect within an Einstein-de Sitter cosmology. We will see that the effect is trivial for the linear order result, but we will see that the one-loop order results give rise to correction terms. Because we will be breaking homogeneity along the line of sight, we will also introduce phase factors which make our solutions complex, but as we want to compare to the normal results we will look at specific Fourier coordinates in which the result is real. Because we develop our formalism as depending on the average distance $\overline{\chi}$ and an expansion parameter we will call $\Delta\chi$, we will consider the size of the effects of time dependence for typical values of $\overline{\chi}$ and $\Delta\chi$ of current and next generation experiments.

Finally, we will summarize our results and discuss the size and significance of this light cone effect with respect to the normal approximation.

5.2 Finite volume 1d toy model

In general, the definition of the Fourier transform as given in equations (3.27) and (3.28) is something we cannot measure. The integrals are taken over infinite space, whereas for our purposes we cannot look out into space infinitely far. Instead, we cannot see beyond the particle horizon. Moreover, we want to estimate the size of the correction we have to make for the light cone effect with respect to the usual division of galaxies into radial distance bins along the line of sight. This motivates us to give a new definition for the Fourier transform along the line-of-sight direction:

$$f(p) = \int_{\overline{\chi}-\frac{\Delta\chi}{2}}^{\overline{\chi}+\frac{\Delta\chi}{2}} d\chi f(\chi) e^{-ip\chi}. \tag{5.1}$$

The definition we give in equation (5.1) is useful, because it is defined over a radial distance bin parametrized by the comoving distance χ. Because we know how comoving distance and redshift are

related in an EdS cosmology from chapter 2, we can relate these bins to the redshift bins that are usual in observations.

However, we might have lost some properties in this new finite volume definition of the Fourier transform. We will test this by Fourier transforming a function which is constant and equal to the value at $\overline{\chi}$. In the normal definition of the Fourier transform this would then yield a Dirac delta function times this constant. For our finite volume Fourier transform we instead find:

$$f(p) = f(\overline{\chi})\frac{2\sin\left(\frac{p\Delta\chi}{2}\right)}{p}e^{-ip\overline{\chi}}. \tag{5.2}$$

Then, the departure from the normal result by equation (5.2) gives a measure of the implications of defining a finite volume Fourier transform. We recall that the normal Fourier transform would have yielded the following solution:

$$f(p) = 2\pi f(\overline{\chi})\delta_D(p). \tag{5.3}$$

Let us proceed to compare the two results. We know that the Dirac delta function is in fact a distribution instead of a function, whereas equation (5.2) is a function. Before we will formally fix this however, we will naively look at the function from equation (5.2). Doing a Taylor expansion, we see that the function is peaked at $p = 0$ with $f(0) = f(\overline{\chi})\Delta\chi$, and that it falls off like $(p\Delta\chi)^2$ away from $p = 0$. Thus, we see that the width of this function can be approximated by $\frac{1}{\Delta\chi}$. If we then want to restore the normal Fourier transform, we have to take the limit $\Delta\chi \to \infty$ we get an infinitely thin peak with width $\frac{1}{\Delta\chi} \to 0$ and height $\Delta\chi \to \infty$. From this, we see that our function is similar to the Dirac delta function in the limit $\Delta\chi \to \infty$.

Now, we want to formally compare equation (5.2) with the Dirac delta function. To do that, we have to do a trick so that we can compare a function with a distribution. If we integrate a function $g(p)$ times either a distribution or a function, we can consider them in the same manner. So, to really compare our finite volume Fourier transform to the standard Fourier transform, we need to look at the way they act on another function when integrated. We will do so, for obvious reasons, by looking at a correlation function.

We will consider a one-dimensional system in which we have a density field $\delta(\chi)$ and a power spectrum which is defined in the same way as usual:

$$2\pi\delta_D(p + p')P(p) \equiv \langle\delta(p)\delta(p')\rangle. \tag{5.4}$$

From this system, we will look at the impact our change to the finite volume Fourier transform will have. Of course, the result from equation (5.4) is what we will get when calculating the correlator with the standard Fourier transform. Therefore, we will now continue to calculate the correlator for the finite volume Fourier transform:

$$\langle\delta(p)\delta(p')\rangle_{\mathrm{FV}} = \int_{\overline{\chi}-\frac{\Delta\chi}{2}}^{\overline{\chi}+\frac{\Delta\chi}{2}} d\chi d\chi' \langle\delta(\chi)\delta(\chi')\rangle e^{-i(p\chi+p'\chi')}. \tag{5.5}$$

We can proceed with this calculation by inverse Fourier transforming the correlation function inside the integral, using our standard inverse Fourier transform from equation (3.28). We also assume that the density fields are *ergodic*, meaning that their form within the finite volume is representative of their entire shape. This allows us to perform the integrals over χ and χ', so that we are left with:

$$\langle\delta(p)\delta(p')\rangle_{\mathrm{FV}} = \int_{-\infty}^{\infty} \frac{d\tilde{p}}{2\pi}\frac{d\tilde{p}'}{2\pi}\frac{2\sin\left(\frac{(p-\tilde{p})\Delta\chi}{2}\right)}{p-\tilde{p}}\frac{2\sin\left(\frac{(p'-\tilde{p}')\Delta\chi}{2}\right)}{p'-\tilde{p}'}\langle\delta(\tilde{p})\delta(\tilde{p}')\rangle e^{-i(p+p')\overline{\chi}}. \tag{5.6}$$

Because the ergodic theorem allowed us to replace the finite volume correlator with the full correlator, we can then enter the power spectrum from the definition given in (5.4). This will give us the following result:

$$\langle\delta(p)\delta(p')\rangle_{\mathrm{FV}} = \int_{-\infty}^{\infty}\frac{d\tilde{p}}{2\pi}P(\tilde{p})\frac{4\sin\left(\frac{(p-\tilde{p})\Delta\chi}{2}\right)\sin\left(\frac{(p'+\tilde{p})\Delta\chi}{2}\right)}{(p-\tilde{p})(p'+\tilde{p})}e^{-i(p+p')\overline{\chi}}. \tag{5.7}$$

At this point, we cannot continue without making assumptions. Equation (5.7) is complex and the integration depends in some complicated manner on $\tilde{p}$. Therefore we have no way to compare this to the normal case from equation (5.4), because even when we could take into account the integration, we are still left with a phase factor. Moreover, we are comparing a distribution in equation (5.4) with the function in equation (5.7). Before we proceed to our computation we define:

$$f(p) \equiv \frac{2\sin\left(\frac{p\Delta\chi}{2}\right)}{p}, \tag{5.8}$$

to simplify our expressions.

Now, we first have to deal with our phase factor in equation (5.7). Because we can actually take this phase factor out of the integrand, we see that the only way to get rid of this factor is by demanding $p = -p'$ for the finite volume case. This is equivalent to demanding homogeneity along the line of sight. Then, that leaves us to compare:

$$\langle\delta(p)\delta(p')\rangle = 2\pi\delta_D(p+p')P(p), \tag{5.9}$$

with

$$\langle\delta(p)\delta(-p)\rangle_{\mathrm{FV}} = \int_{-\infty}^{\infty}\frac{d\tilde{p}}{2\pi}P(\tilde{p})f^2(p-\tilde{p}), \tag{5.10}$$

where in the last equation we used that $f(p) = f(-p)$. Note that in the standard case we did not set $p = -p'$ by hand, because homogeneity is ensured there.

Having done this step, we are still faced by the difficulty that the normal result includes a distribution whereas the finite volume result takes the form of a function. To deal with these difficulties we perform a double integration over p' and χ and we include a phase factor $e^{i(p+p')(\chi-\overline{\chi})}$.[2] The reason for these strange choices will become clear quickly when doing the computations. We first compute the double integral for the normal result:

$$\begin{aligned}\int_{\overline{\chi}-\frac{\Delta\chi}{2}}^{\overline{\chi}+\frac{\Delta\chi}{2}}d\chi\int_{-\infty}^{\infty}dp'\langle\delta(p)\delta(-p)\rangle e^{i(p+p')(\chi-\overline{\chi})} &= \int_{\overline{\chi}-\frac{\Delta\chi}{2}}^{\overline{\chi}+\frac{\Delta\chi}{2}}d\chi\int_{-\infty}^{\infty}dp'2\pi\delta_D(p+p')P(p)e^{i(p+p')(\chi-\overline{\chi})},\\ &= \int_{\overline{\chi}-\frac{\Delta\chi}{2}}^{\overline{\chi}+\frac{\Delta\chi}{2}}d\chi 2\pi P(p),\\ &= 2\pi\Delta\chi P(p).\end{aligned} \tag{5.11}$$

Then, we do the same computation for the finite volume result:

[2] Our finite volume result does not depend on p' anymore, so p' is just an arbitrary Fourier mode for the finite volume, which we include using an exponent, and which we integrate over.

$$\begin{aligned}\int_{\overline{\chi}-\frac{\Delta\chi}{2}}^{\overline{\chi}+\frac{\Delta\chi}{2}} d\chi \int_{-\infty}^{\infty} dp' \langle\delta(p)\delta(p')\rangle_{\mathrm{FV}} e^{i(p+p')(\chi-\overline{\chi})} =,\\ &= \int_{\overline{\chi}-\frac{\Delta\chi}{2}}^{\overline{\chi}+\frac{\Delta\chi}{2}} d\chi \int_{-\infty}^{\infty} dp' \int_{-\infty}^{\infty} \frac{d\tilde{p}}{2\pi} P(\tilde{p}) f^2(p-\tilde{p}) e^{i(p+p')(\chi-\overline{\chi})},\\ &= \int_{\overline{\chi}-\frac{\Delta\chi}{2}}^{\overline{\chi}+\frac{\Delta\chi}{2}} d\chi \int_{-\infty}^{\infty} d\tilde{p} P(\tilde{p}) f^2(p-\tilde{p}) \delta_D(\chi-\overline{\chi}) e^{ip(\chi-\overline{\chi})},\\ &= \int_{-\infty}^{\infty} d\tilde{p} P(\tilde{p}) f^2(p-\tilde{p}).\end{aligned} \tag{5.12}$$

This motivates us to define the power spectrum we obtain when considering a finite volume, which we shall denote as $P_{\mathrm{FV}}(p)$:

$$P_{\mathrm{FV}}(p) = \int_{-\infty}^{\infty} \frac{d\tilde{p}}{2\pi\Delta\chi} P(\tilde{p}) f^2(p-\tilde{p}). \tag{5.13}$$

Using our range of tricks and assumptions, we now have a nice comparison between the finite volume result and the standard result. Plugging in some test function for $P(\tilde{p})$ and specifying the parameter $\Delta\chi$ to define $f(p-\tilde{p})$ to the fullest, we can make a plot comparing the finite volume power spectrum with the standard power spectrum. We will first discuss our expected results using our knowledge about the function $f(p-\tilde{p})$ however.

We recall that $f(p-\tilde{p})$ is defined in equation (5.8). We see from this that the function $f^2(p-\tilde{p})$ is peaked at $\tilde{p}=p$ with value $(\Delta\chi)^2$, away from which it drops off like $\frac{1}{(\tilde{p}-p)^2}$. Therefore, the value of $P_{FV}(p)$ will be calculated by an integration of a function that is approximately peaked around $P(p)$. We will see that for large p, we can take $P(\tilde{p}) \approx P(p)$ for the entire domain where the value of $f(\tilde{p}-p)$ is large enough to have an effect in the integration. In that case, the integration over $\tilde{p}$ of $f^2(\tilde{p})$ will yield unity because the function arose from the Fourier transform of a constant. Let us discuss at which $\tilde{p}$ we see that $f^2(\tilde{p}-p)$ becomes much smaller than $f^2(0) \sim (\Delta\chi)^2$.

Let us make the assumption that $\Delta\chi \gg 1$, which we will see is reasonable in the case of our time dependent power spectrum. Moreover, let us assume that in the regime where $f^2(\tilde{p}-p) \ll (\Delta\chi)^2$ the function is dominated by the $\frac{1}{(\tilde{p}-p)^2}$ behavior. Now, we can say that $f^2(\tilde{p}-p) \ll f^2(0)$ if the following holds:

$$\frac{1}{(\tilde{p}-p)^2} \sim \Delta\chi. \tag{5.14}$$

We solve this for $\tilde{p}-p$:

$$\tilde{p}-p \sim \frac{1}{\sqrt{\Delta\chi}}. \tag{5.15}$$

Now, because we require $P(\tilde{p})$ to be approximated by $P(p)$ over this entire domain, we can see for which values of p this is a good approximation. The equivalent requirement would be that $\tilde{p}-p \ll p$. We find that this holds for values of p when $p \sim \left(\frac{1}{\Delta\chi}\right)^{1/4}$.

From our very crude discussion above we see that our finite volume power spectrum is the same as the standard power spectrum for p larger than some scale defined by a power law of the inverse of $\Delta\chi$.[3] If we think about the form our picture will take for p smaller than this, we see that this is defined by

[3]Note that our derivation is very crude, and that the scale below which $P_{FV}(p)$ is different from the standard result can be larger (equivalent to smaller p) than derived here.

the shape of $P(p)$. In general, we can think of this part as being smoothed out by the integration over $\tilde{p}$, such that we lose information about the shape of $P_{FV}(p)$ on very large scale.

Physically we could have expected this of course. If we only take a finite volume in which we try to determine the power spectrum, we cannot get an indication of modes that have a scale larger than our volume. For these modes with real length $x > \Delta\chi$, we thus cannot trust the results. If we transform this length into Fourier modes, we see that this is the case for wavenumbers $p < \frac{2\pi}{\Delta\chi}$. Hence, physically we expect strange results for small p.

To provide ourselves with a more visual version of this discussion here, we have plotted a graph of the finite volume power spectrum together with the normal power spectrum. Please note that we assume here that the one-dimensional power spectrum has the same form as the real three-dimensional power spectrum. The result can be seen in figure 5.2, where we used a volume of $\Delta\chi = 100\text{Mpc } h^{-1}$.

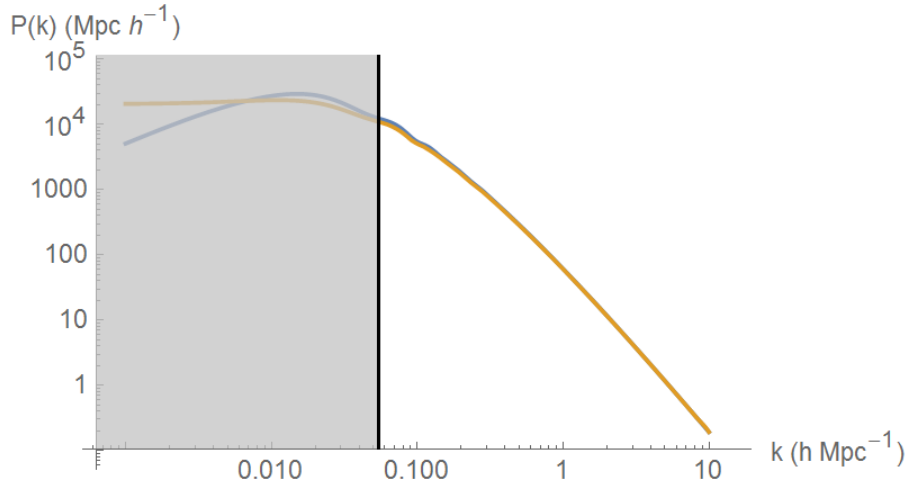

Figure 5.2: The finite volume power spectrum plotted together with the normal power spectrum. We can see that the result for the finite volume case and the original result coincide for large k. In this case $\Delta\chi = 100\text{Mpc } h^{-1}$. Hence, we greyed out the k axis for $k < \frac{2\pi}{\Delta\chi}$.

This visual description of the effect confirms for us the smoothing on large scale (small p), because of which we cannot trust our results there. Therefore, in such a finite volume description we can only consider the effects at shorter scales.

5.3 Perturbation theory on the light cone in Einstein-de Sitter

Now that we have gained an intuition for the effect of a finite volume Fourier transform on our calculations, we can continue with our real cause: a description of the light cone effect. We recall that the linear power spectrum in SPT is given by:

$$P_L(k,\tau) = P_L(k)(D^{(+)}(\tau))^2. \tag{5.16}$$

In this equation, for each individual linear density field the time dependence is described by the linear term of the growth function. We can see from this that the linear result will always come with a growth function squared. Moreover, we remember that the perturbative expansion for the time dependent density field in EdS was given by:

$$\delta(\vec{k},\tau) = \sum (D^{(+)}(\tau))^n \delta^n(\vec{k}). \tag{5.17}$$

Now, we will continue by introducing the light cone effect. We recall that in our normal formulation of SPT we define our Fourier transformed density based on the real density field $\delta(\vec{x},\tau)$. When observing on the past light cone, there is an explicit dependence of the time component of this field on the radial distance χ. Therefore, we can parametrize both the distance and time dependence using $\delta(\mathbf{x},\chi)$, where $\mathbf{x}$ is a two-dimensional vector instead of the three-dimensional vector $\vec{x}$. The value of χ also fully defines the cosmological conformal time τ at which we should consider the density.

The considerations above combined with the parametrization of our time dependence in equations (5.16) and (5.17) motivates us to define a reduced density field in real space:

$$\tilde{\delta}(\mathbf{x},\chi) \equiv \frac{\delta(\mathbf{x},\chi)}{D(\chi)}. \tag{5.18}$$

Here we chose to divide by the growth function, so that for our linear term in the reduced correlator we do not get a time dependence such as in equation (5.16). Moreover, our growth function continues to have a time dependence, which is parametrized by the dependence of $\chi(\tau)$ on τ. Because time dependence on the light cone is always defined by a radial distance, we will therefore use χ as our time parameter.

Now that we have defined this reduced density on the light cone, we would like to define the power spectrum there. In order to do this, we need to follow the same steps as in the SPT case. Hence, we first need to calculate the Fourier transform of our reduced overdensity and then start calculating the two point function. To obtain useful perturbative results, we need to expand our reduced density afterwards. After that, we can try to find a suitable definition for our power spectrum.

Let us first consider the Fourier transform of our reduced density in equation (5.18). We recall that in the χ direction we use the finite volume definition from equation (5.1), whereas in our $\mathbf{x}$ coordinates we use the standard definition of the Fourier transform from equation (3.27). We find:

$$\begin{aligned}\tilde{\delta}(\mathbf{k},p) &= \int_{-\infty}^{\infty} d^2\mathbf{x} \int_{\overline{\chi}-\frac{\Delta\chi}{2}}^{\overline{\chi}+\frac{\Delta\chi}{2}} d\chi \tilde{\delta}(\mathbf{x},\chi) e^{-i\mathbf{k}\mathbf{x}} e^{-ip\chi}, \\ &= \int_{-\infty}^{\infty} d^2\mathbf{x} \int_{\overline{\chi}-\frac{\Delta\chi}{2}}^{\overline{\chi}+\frac{\Delta\chi}{2}} d\chi \frac{\delta(\mathbf{x},\chi)}{D(\chi)} e^{-i\mathbf{k}\mathbf{x}} e^{-ip\chi}.\end{aligned} \tag{5.19}$$

We check that the normal relation for the complex conjugate holds:

$$\begin{aligned}\tilde{\delta}^*(\mathbf{k},p) &= \int_{-\infty}^{\infty} d^2\mathbf{x} \int_{\overline{\chi}-\frac{\Delta\chi}{2}}^{\overline{\chi}+\frac{\Delta\chi}{2}} d\chi \tilde{\delta}(\mathbf{x},\chi) e^{i\mathbf{k}\mathbf{x}} e^{ip\chi}, \\ &= \tilde{\delta}(-\mathbf{k},-p).\end{aligned} \tag{5.20}$$

Note that in the above equations the Fourier mode $\mathbf{k}$ is two-dimensional, and together with p it spans the three-dimensional Fourier mode $\vec{k}$.

Now, we consider the two point correlation function. We recall that statistical homogeneity normally implies that $\langle \delta(\vec{k})\delta(\vec{k}') \rangle$ only depends on the size of $\vec{k}$ and that the only nonzero modes are those where $\vec{k} = -\vec{k}'$. However, in this case we break statistical homogeneity along the line of sight. Therefore, we rewrite our three-dimensional coordinate $\vec{k}$ in terms of a two-dimensional Fourier mode $\mathbf{k}$, which parametrizes the position perpendicular to the line of sight of an observable in the sky, and in terms

of the one-dimensional Fourier modes p and p', which describe radial distance along the line of sight. Moreover, we retain the property that nonzero results follow only for $\mathbf{k} = -\mathbf{k}'$. However, p and p' can be chosen arbitrarily.

The last property leads to a lot of difficulty. Normally, the $\vec{k} = -\vec{k}'$ requirement automatically ensures that the correlation function is real. However, in our case our two-point correlation function is typically complex, with a dependence on a phase factor $(p + p')$. Only in the case where we require modes with $p = -p'$ reality is ensured:

$$\begin{aligned}\langle\tilde{\delta}(\mathbf{k}, p)\tilde{\delta}(\mathbf{k}', p')\rangle^* &= \langle\tilde{\delta}(-\mathbf{k}, -p)\tilde{\delta}(-\mathbf{k}', -p')\rangle, \\ &= \langle\tilde{\delta}(\mathbf{k}', p')\tilde{\delta}(\mathbf{k}, p)\rangle, \\ &= \langle\tilde{\delta}(\mathbf{k}, p)\tilde{\delta}(\mathbf{k}', p')\rangle.\end{aligned} \tag{5.21}$$

Because we have no meaningful way of comparing our complex results with real results, we will therefore only consider modes with $p = -p'$ when we move to the actual calculations. Before we start writing down the perturbative expansion of our two point correlation function, we need to define the way our reduced density will look when expanded. Therefore, we write down the Fourier transformed reduced density, and expand the standard density we integrate over. Our result then depends on the Fourier transform of the $(n-1)^{\text{th}}$ order growth function and the n^{th} order density field:

$$\begin{aligned}\tilde{\delta}(\mathbf{k}, p) &= \int_{-\infty}^{\infty} d^2\mathbf{x} \int_{\overline{\chi}-\frac{\Delta\chi}{2}}^{\overline{\chi}+\frac{\Delta\chi}{2}} d\chi \frac{\delta(\mathbf{x}, \chi)}{D(\chi)} e^{-i\mathbf{k}\mathbf{x}} e^{-ip\chi}, \\ &= \int_{-\infty}^{\infty} d^2\mathbf{x} \int_{\overline{\chi}-\frac{\Delta\chi}{2}}^{\overline{\chi}+\frac{\Delta\chi}{2}} d\chi \sum_n \frac{D^n(\chi)\delta^{(n)}(\mathbf{x}, \chi)}{D(\chi)} e^{-i\mathbf{k}\mathbf{x}} e^{-ip\chi}, \\ &= \sum_n \int \frac{dq}{2\pi} D_{n-1}(q)\delta^{(n)}(\mathbf{k}, p-q),\end{aligned} \tag{5.22}$$

where $D_n(q)$ is the Fourier transform of $D^n(\chi)$. Now, we can continue by calculating the full correlator:

$$\langle\tilde{\delta}(\mathbf{k}, p)\tilde{\delta}(\mathbf{k}', p')\rangle = \langle\sum_n \int \frac{dq}{2\pi} D_{n-1}(q)\delta^{(n)}(\mathbf{k}, p-q) \sum_{n'} \int \frac{dq'}{2\pi} D_{n'-1}(q')\delta^{(n')}(\mathbf{k}', p'-q')\rangle. \tag{5.23}$$

We can then use some tricks to simplify equation (5.23) tremendously. First of all, we recall the Wick theorem. As our initial $\delta(\mathbf{k}, p)$ is sourced by a stochastic gaussian field, only terms with an even value of $(n + n')$ survive. Hence, once more, we will have the P_{22} and P_{13} terms at one-loop order. Moreover, we can take the correlation brackets inside the integral, because the correlation is only between the densities. Because we have the normal density fields within the integrand, we can actually write our correlation function as an integral over growth functions and a power spectrum.

Let us make these considerations a little more concrete, by first looking at the linear order results for our reduced density correlator. We recall equation (5.16), and see that our reduced density correlator simply gives:

$$\langle\tilde{\delta}(\mathbf{k}, p)\tilde{\delta}(\mathbf{k}', p')\rangle_{11} = \langle\delta_1(\mathbf{k}, p)\delta_1(\mathbf{k}', p')\rangle = (2\pi)^3\delta_D^2(\mathbf{k} + \mathbf{k}')\delta_D(p + p')\frac{P_L(k, \overline{\chi})}{D^2(\overline{\chi})}. \tag{5.24}$$

Here we see that the linear result has is simply rescaled by the growth function, where we evaluate the growth function using the comoving distance $\overline{\chi}$ at the middle of our bin. A further discussion of the linear results including redshift space distortions and bias effects can be found in [53].

For our purposes however, we would like to investigate what happens in the perturbative case. Our redefinition of the density in equation (5.18) simplified the first order results, but the one-loop correlators are not so trivial. We consider those terms in the correlation function:

$$\begin{aligned}\langle\tilde{\delta}(\mathbf{k},p)\tilde{\delta}(\mathbf{k}',p')\rangle_{22} &= \langle\int\frac{dq}{(2\pi)}\frac{dq'}{(2\pi)}D_1(q)\delta^{(2)}(\mathbf{k},p-q)D_1(q')\delta^{(2)}(\mathbf{k}',p'-q')\rangle,\\ &= \int\frac{dq}{(2\pi)}\frac{dq'}{(2\pi)}D_1(q)D_1(q')\langle\delta^{(2)}(\mathbf{k},p-q)\delta^{(2)}(\mathbf{k}',p'-q')\rangle,\\ &= \int\frac{dq}{(2\pi)}\frac{dq'}{(2\pi)}D_1(q)D_1(q')(2\pi)^3\delta_D^2(\mathbf{k}+\mathbf{k}')\delta_D(p-q+p'-q')P_{22}(\mathbf{k},p-q),\\ &= 2\pi\delta_D^2(\mathbf{k}+\mathbf{k}')\int dqD_1(q)D_1(p+p'-q)P_{22}(\mathbf{k},p-q).\end{aligned} \tag{5.25}$$

$$\begin{aligned}\langle\tilde{\delta}(\mathbf{k},p)\tilde{\delta}(\mathbf{k}',p')\rangle_{13} &= \langle\int\frac{dq}{(2\pi)}D_2(q)\delta^{(3)}(\mathbf{k},p-q)\delta^{(1)}(\mathbf{k}',p')\rangle,\\ &= \int\frac{dq}{(2\pi)}D_2(q)\langle\delta^{(3)}(\mathbf{k},p-q)\delta^{(1)}(\mathbf{k}',p')\rangle,\\ &= \int\frac{dq}{(2\pi)}D_2(q)(2\pi)^3\delta_D^2(\mathbf{k}+\mathbf{k}')\delta_D(p-q+p')P_{13}(\mathbf{k},p-q),\\ &= (2\pi)^2\delta_D^2(\mathbf{k}+\mathbf{k}')D_2(p+p')P_{13}(\mathbf{k},-p').\end{aligned} \tag{5.26}$$

Here we define any $P_{ij}(\mathbf{k},p)$ as:

$$P_{ij}(\mathbf{k},p) \equiv P_{ij}(\sqrt{k^2+p^2}). \tag{5.27}$$

Before we continue with our discussion, we symmetrize our correlation functions in p and p'. For P_{22} this is a trivial operation, since the term was already manifestly symmetric from its definition; in other words, we only make it explicit for this term. For P_{13} we see that the growth function part of the expression does not change. For any realization of P_{13} where the size of p and the size of p' are different, this symmetrization changes the term. Because we will set $p=-p'$ later in our discussion, this does not affect our results.

After symmetrization, the P_{22}-like term takes the form:

$$\langle\tilde{\delta}(\mathbf{k},p)\tilde{\delta}(\mathbf{k}',p')\rangle_{22} = 2\pi\delta_D^2(\mathbf{k}+\mathbf{k}')\int dqD_1(q)D_1(p+p'-q)\left(\frac{P_{22}(\mathbf{k},p-q)+P_{22}(\mathbf{k},p'-q)}{2}\right), \tag{5.28}$$

and the P_{13}-like term takes the form:

$$\langle\tilde{\delta}(\mathbf{k},p)\tilde{\delta}(\mathbf{k}',p')\rangle_{13} = (2\pi)^2\delta_D^2(\mathbf{k}+\mathbf{k}')D_2(p+p')\left(\frac{P_{13}(\mathbf{k},-p')+P_{13}(\mathbf{k},-p)}{2}\right). \tag{5.29}$$

From this, we first realize that these results are in fact exact. If we are then able to write down an exact function for the Fourier transform of the growth function and explicitly integrate out q, we would have an exact result for the P_{22}-like two point correlation function. The same holds for the P_{13}-like term if we have a nice expression for the Fourier transform of our growth function squared. Alas, because of the complicated form of the power spectrum and the fact that our Fourier transform of the growth function is defined in a bin along the line of sight cf. equation (5.1), we are not able to write down such an analytic result.

We deal with these difficulties when calculating the Fourier transform of our growth functions by making an approximation. The growth function can be an arbitrarily complicated function depending

on cosmology, and therefore a Taylor approximation makes sense. Because we are working in bin along the line of sight with average comoving distance $\overline{\chi}$ and width $\Delta\chi$, it makes sense to approximate our growth function in the following way:[4]

$$D(\chi) = D(\overline{\chi}) + D'(\overline{\chi})(\chi - \overline{\chi}) + \mathcal{O}((\chi - \overline{\chi})^2). \tag{5.30}$$

For equation (5.30) makes use of a Taylor-expansion with respect to comoving distance $\overline{\chi}$, we need to consider where we can trust the results. Since in Einstein-de Sitter $D(\chi)$ has a polynomial form, we realize that each following order in $(\chi - \overline{\chi})$ scales like $\frac{\Delta\chi}{\overline{\chi}}$, where we entered the bin width because it gives an upper bound on the size of $(\chi - \overline{\chi})$. Hence, we need to require that $\Delta\chi$ is small with respect to $\overline{\chi}$. Because we are working within bins, this approximation is reasonable; it only breaks down in the case where $\Delta\chi$ is of the order of $\overline{\chi}$.

Now, because we are faced with the Fourier transform of the growth function in our expressions (5.25) and (5.26) we proceed by calculating the Fourier transform of equation (5.30). We find that the Fourier transform of the growth function is given by:

$$D(p) \simeq D(\overline{\chi})\frac{2\sin\left(\frac{p\Delta\chi}{2}\right)}{p}e^{-ip\overline{\chi}} + D'(\overline{\chi})\left(\frac{i\Delta\chi}{p}\cos\left(\frac{p\Delta\chi}{2}\right) - \frac{2i}{p^2}\sin\left(\frac{p\Delta\chi}{2}\right)\right)e^{-ip\overline{\chi}}. \tag{5.31}$$

We also need to calculate the Fourier transform of the growth function squared, because we this function is a part of equation (5.26). We find that:

$$\begin{aligned} D_2(p) \simeq D^2(\overline{\chi})\frac{2\sin\left(\frac{p\Delta\chi}{2}\right)}{p}e^{-ip\overline{\chi}} + D'(\overline{\chi})D(\overline{\chi})\left(\frac{2i\Delta\chi}{p}\cos\left(\frac{p\Delta\chi}{2}\right) - \frac{4i}{p^2}\sin\left(\frac{p\Delta\chi}{2}\right)\right)e^{-ip\overline{\chi}} \\ + D'^2(\overline{\chi})\left(\frac{\sin\left(\frac{p\Delta\chi}{2}\right)(\Delta\chi)^2}{2p} + \frac{2\Delta\chi}{p^2}\cos\left(\frac{p\Delta\chi}{2}\right) - \frac{4}{p^3}\sin\left(\frac{p\Delta\chi}{2}\right)\right)e^{-ip\overline{\chi}}. \end{aligned} \tag{5.32}$$

Now that we have equations (5.31) and (5.32), we can look at the expressions for our reduced density correlators. Note that we will consider results up to second order following equation (5.30) from here on out. We first give the expression (up to second order) for the P_{22}-like term:

[4] We ignore terms of second and higher order in $(\chi - \overline{\chi})$ from here on out. This implies we will miss a term proportional to $D(\overline{\chi})D''(\overline{\chi})(\Delta\chi)^2$ in our final results, which is of the same order as the $D'^2(\overline{\chi})(\Delta\chi)^2$ term. We recommend that an extension is made to this thesis to include this term.

$$
\begin{aligned}
\langle\tilde{\delta}(\mathbf{k},p)\tilde{\delta}(\mathbf{k}',p')\rangle_{22} = \delta_D^2(\mathbf{k}+\mathbf{k}')(2\pi)\int dq\,\Bigg[& D^2(\overline{\chi})\frac{4\sin\left(\frac{q\Delta\chi}{2}\right)\sin\left(\frac{(p+p'-q)\Delta\chi}{2}\right)}{q(p+p'-q)}e^{-i(p+p')\overline{\chi}} \\
& + D(\overline{\chi})D'(\overline{\chi})\left(\frac{2i\Delta\chi\sin\left(\frac{q\Delta\chi}{2}\right)\cos\left(\frac{(p+p'-q)\Delta\chi}{2}\right)}{q(p+p'-q)} - \frac{4i\sin\left(\frac{q\Delta\chi}{2}\right)\sin\left(\frac{(p+p'-q)\Delta\chi}{2}\right)}{q(p+p'-q)^2}\right)e^{-i(p+p')\overline{\chi}} \\
& + D'(\overline{\chi})D(\overline{\chi})\left(\frac{2i\Delta\chi\cos\left(\frac{q\Delta\chi}{2}\right)\sin\left(\frac{(p+p'-q)\Delta\chi}{2}\right)}{q(p+p'-q)} - \frac{4i\sin\left(\frac{q\Delta\chi}{2}\right)\sin\left(\frac{(p+p'-q)\Delta\chi}{2}\right)}{q^2(p+p'-q)}\right)e^{-i(p+p')\overline{\chi}} \\
& + D'^2(\overline{\chi})\left(\frac{-(\Delta\chi)^2\cos\left(\frac{q\Delta\chi}{2}\right)\cos\left(\frac{(p+p'-q)\Delta\chi}{2}\right)}{q(p+p'-q)} + \right. \\
& + \frac{\Delta\chi\left[2q\cos\left(\frac{q\Delta\chi}{2}\right)\sin\left(\frac{(p+p'-q)\Delta\chi}{2}\right) + 2(p+p'-q)\sin\left(\frac{q\Delta\chi}{2}\right)\cos\left(\frac{(p+p'-q)\Delta\chi}{2}\right)\right]}{q^2(p+p'-q)^2} \\
& \left. - \frac{4\sin\left(\frac{q\Delta\chi}{2}\right)\sin\left(\frac{(p+p'-q)\Delta\chi}{2}\right)}{q^2(p+p'-q)^2}\right)e^{-i(p+p')\overline{\chi}}\Bigg]\frac{1}{2}\Big(P_{22}(\mathbf{k},p-q)+P_{22}(\mathbf{k},p'-q)\Big).
\end{aligned}
\tag{5.33}
$$

Obviously, equation (5.33) is messy and not very informative. To simplify the expression, we first redefine the arguments of the sinoids:

$$
\begin{aligned}
\alpha &= \frac{q\Delta\chi}{2}, \\
\beta &= \frac{(p+p'-q)\Delta\chi}{2}.
\end{aligned}
\tag{5.34}
$$

Having done this, we need to apply the following trigonometric identities to simplify our result:

$$
\begin{aligned}
\sin(\alpha)\sin(\beta) &= \frac{\cos(\alpha-\beta)-\cos(\alpha+\beta)}{2}, \\
\cos(\alpha)\sin(\beta) &= \frac{\sin(\alpha+\beta)-\sin(\alpha-\beta)}{2}, \\
\cos(\beta)\sin(\alpha) &= \frac{\sin(\beta+\alpha)-\sin(\beta-\alpha)}{2}, \\
\cos(\alpha)\cos(\beta) &= \frac{\cos(\alpha-\beta)+\cos(\alpha+\beta)}{2}.
\end{aligned}
\tag{5.35}
$$

After applying the identities from equation (5.35) and resubstituting the momentum modes back into the expression, we find the following:

$$\langle\tilde{\delta}(\mathbf{k},p)\tilde{\delta}(\mathbf{k}',p')\rangle_{22} = \delta_D^2(\mathbf{k}+\mathbf{k}')(2\pi)\int dq \left[D^2(\overline{\chi})\frac{2\cos\left(\frac{(2q-p-p')\Delta\chi}{2}\right) - 2\cos\left(\frac{(p+p')\Delta\chi}{2}\right)}{q(p+p'-q)}e^{-i(p+p')\overline{\chi}} \right.$$
$$+ D(\overline{\chi})D'(\overline{\chi})\left(\frac{2i\Delta\chi\sin\left(\frac{(p+p')\Delta\chi}{2}\right)}{q(p+p'-q)} - \frac{p+p'}{2}\frac{2i\cos\left(\frac{(2q-p-p')\Delta\chi}{2}\right) - 2i\cos\left(\frac{(p+p')\Delta\chi}{2}\right)}{q^2(p+p'-q)^2}\right)e^{-i(p+p')\overline{\chi}}$$
$$+ D'^2(\overline{\chi})\left(\frac{-(\Delta\chi)^2\left[\frac{1}{2}\cos\left(\frac{(2q-p-p')\Delta\chi}{2}\right) + \frac{1}{2}\cos\left(\frac{(p+p')\Delta\chi}{2}\right)\right]}{q(p+p'-q)}\right.$$
$$+ \frac{\Delta\chi\left[2(p+p')\sin\left(\frac{(p+p')\Delta\chi}{2}\right) + (p+p'-2q)\sin\left(\frac{(2q-p-p')\Delta\chi}{2}\right)\right]}{q^2(p+p'-q)^2}$$
$$\left.\left. - \frac{2\cos\left(\frac{(2q-p-p')\Delta\chi}{2}\right) - 2\cos\left(\frac{(p+p')\Delta\chi}{2}\right)}{q^2(p+p'-q)^2}\right)e^{-i(p+p')\overline{\chi}}\right] \frac{1}{2}\Big(P_{22}(\mathbf{k},p-q) + P_{22}(\mathbf{k},p'-q)\Big). \tag{5.36}$$

Now, we have an equation for the P_{22}-like term we cannot simplify further without making assumptions. Also, entering equation (5.32) into (5.26) we find that:

$$\langle\tilde{\delta}(\mathbf{k},p)\tilde{\delta}(\mathbf{k}',p')\rangle_{13} = (2\pi)^2\delta_D^2(\mathbf{k}+\mathbf{k}')\left(\frac{P_{13}(\mathbf{k},-p') + P_{13}(\mathbf{k},-p)}{2}\right)e^{-i(p+p')\overline{\chi}}$$
$$\left[D^2(\overline{\chi})\frac{2\sin\left(\frac{(p+p')\Delta\chi}{2}\right)}{(p+p')} + D'(\overline{\chi})D(\overline{\chi})\left(\frac{2i\Delta\chi\cos\left(\frac{(p+p')\Delta\chi}{2}\right)}{(p+p')} - \frac{4i\sin\left(\frac{(p+p')\Delta\chi}{2}\right)}{(p+p')^2}\right)\right.$$
$$\left. + D'^2(\overline{\chi})\left(\frac{\sin\left(\frac{(p+p')(\Delta\chi}{2}\right)(\Delta\chi)^2}{2(p+p')} + \frac{2\Delta\chi\cos\left(\frac{(p+p')\Delta\chi}{2}\right)}{(p+p')^2} - \frac{4\sin\left(\frac{(p+p')\Delta\chi}{2}\right)}{(p+p')^3}\right)\right]. \tag{5.37}$$

Even though we managed to simplify our expressions somewhat, the results in equations (5.36) and (5.37) do not help us to quantify the results. The equations all have a complex phase factor $e^{-i(p+p')\overline{\chi}}$ and are therefore impossible to compare with the results we get in normal SPT. Moreover, we have some dependence on our bin width $\Delta\chi$ which is hard to think about analytically. However, if we recall our one-dimensional toy model with a finite volume Fourier transform, we can think of ways to come to meaningful results.

First of all, we realize that no matter how smartly we integrate the expression in equation (5.36) or how cleverly we rewrite equation (5.37), we will always be stuck with a complex result. To make a meaningful comparison with SPT, we need to demand that the result is real, so we put $p = -p'$ by hand. We realize that this is equivalent to throwing away information about our power spectrum, but it is necessary in order to be able to compare. However, if one were to find a meaningful physical attribution for the complex parts of our expressions this would be a valuable extension of the theory.

Also, when we think about the expression for the normal P_{22}- and P_{13}-term for the correlator, we see that this is equal to the power spectrum multiplied by a *three*-dimensional Dirac delta function. In our reduced correlator, we only have a two-dimensional Dirac delta function. Hence, we need to find a way to get rid of the Dirac delta function in $p+p'$ so that we do not compare a distribution with a function.

To do that, we recall the trick we used in our toy model.

Let us first consider a double integral applied to the P_{22}-like term of the normal density correlator:

$$\begin{aligned}\int_{\overline{\chi}-\frac{\Delta\chi}{2}}^{\overline{\chi}+\frac{\Delta\chi}{2}} d\chi \int_{-\infty}^{\infty} dp' \langle \delta(\mathbf{k},p)\delta(\mathbf{k}',p')\rangle_{22} e^{i(p+p')(\chi-\overline{\chi})} = \\ = \int_{\overline{\chi}-\frac{\Delta\chi}{2}}^{\overline{\chi}+\frac{\Delta\chi}{2}} d\chi \int_{-\infty}^{\infty} dp' P_{22}(\mathbf{k},p)(2\pi)^3\delta_D^2(\mathbf{k}+\mathbf{k}')\delta_D(p+p')e^{i(p+p')(\chi-\overline{\chi})}, \\ = (2\pi)^3\Delta\chi P_{22}(\mathbf{k},p)\delta_D^2(\mathbf{k}+\mathbf{k}').\end{aligned} \tag{5.38}$$

Of course, we can apply the same double integral to the P_{22}-like term of the reduced density correlator, where we set $p=-p'$ by hand as we did before:

$$\begin{aligned}\int_{\overline{\chi}-\frac{\Delta\chi}{2}}^{\overline{\chi}+\frac{\Delta\chi}{2}} d\chi \int_{-\infty}^{\infty} dp' \langle \tilde{\delta}(\mathbf{k},p)\tilde{\delta}(\mathbf{k}',-p)\rangle_{22} e^{i(p+p')(\chi-\overline{\chi})} = \\ = (2\pi)^2\delta_D^2(\mathbf{k}+\mathbf{k}')\int dq D(q)D(-q)\left(\frac{P_{22}(\mathbf{k},p-q)+P_{22}(\mathbf{k},p+q)}{2}\right).\end{aligned} \tag{5.39}$$

Now, if we remember our definition for the reduced density field from equation (5.18), we recall that we need to take into account a factor of $D^2(\overline{\chi})$ in our expression for the normal correlator to be able to really compare the two. Moreover, we need to take into account the time dependence of the one-loop correction to the standard power spectrum as well. If we do this, we can define the reduced version of the P_{22} term in the one-loop power spectrum by:

$$\tilde{P}_{22}(\mathbf{k},p) \equiv \frac{1}{2\pi\Delta\chi D^2(\overline{\chi})}\int dq D(q)D(-q)\left(\frac{P_{22}(\mathbf{k},p-q,\overline{\chi})+P_{22}(\mathbf{k},p+q,\overline{\chi})}{2}\right). \tag{5.40}$$

We can obtain the integrand on the right-hand side of the equation by setting $p+p'$ to 0 in equation (5.36). If we apply the same trick for the P_{13}-like term, we see that we can define:

$$\tilde{P}_{13}(\mathbf{k},p) \equiv \frac{1}{\Delta\chi D^2(\overline{\chi})} D_2(0) P_{13}(\mathbf{k},p,\overline{\chi}). \tag{5.41}$$

Once again, the right-hand side of the equation can be obtained by setting $p+p'$ to 0 in equation (5.37). Now that we have obtained these definitions for our reduced power spectrum, we can look at the expressions we obtain using the Fourier transform of our approximation from equation (5.30). We find the following for $\tilde{P}_{22}$:

$$\boxed{\begin{aligned}\tilde{P}_{22}(\mathbf{k},p) = \frac{1}{2\pi\Delta\chi D^2(\overline{\chi})}\int dq \left[D^2(\overline{\chi})\frac{2\cos(q\Delta\chi)-2}{-q^2} - D'^2(\overline{\chi})\left(\frac{-(\Delta\chi)^2[\frac{1}{2}\cos(q\Delta\chi)+\frac{1}{2}]}{q^2} + \right.\right. \\ \left.\left. + \frac{2\Delta\chi q\sin(q\Delta\chi)}{q^4} + \frac{2\cos(q\Delta\chi)-2}{q^4}\right)\right]\frac{P_{22}(\mathbf{k},p-q,\overline{\chi})+P_{22}(\mathbf{k},p+q,\overline{\chi})}{2},\end{aligned}} \tag{5.42}$$

and we find for $\tilde{P}_{13}$ that:

$$\boxed{\tilde{P}_{13}(\mathbf{k},p) = P_{13}(\mathbf{k},p,\overline{\chi})\left[1+\frac{D'^2(\overline{\chi})}{D^2(\overline{\chi})}\frac{(\Delta\chi)^2}{12}\right]}. \tag{5.43}$$

Note that the result from equation (5.43) is the central result which describes the correction due to the light cone effect for the P_{13} term. The result in equation (5.42) is our central result for the P_{22} term,

but we will see that its form can be written more elegantly when doing the numerics, with which we will continue.

Let us first obtain some intuition for $\tilde{P}_{22}$. We recall from our finite volume 1d toy model that the Fourier of a constant function in our finite volume definition yields a result that deviates from the standard result only for small p. Here, the same property holds for the first term of equation (5.42). Since we approximated our growth function using equation (5.30), the term that multiplies $D^2(\overline{\chi})$ is exactly the same as the function $f^2(p-\tilde{p})$ from equation (5.13),[5] where now we evaluate the term in q instead. Hence, the first term just describes the standard power spectrum with a finite volume effect.

Then, the deviation from the standard finite volume result is quantified by the terms multiplying $D'^2(\overline{\chi})$. If we consider the relative size of these terms with respect to the $D^2(\overline{\chi})$-term, we have a measure for the inaccuracy of the normal SPT results. However, we have to be careful if we want to attribute the full deviation to our dependence on the growth function. The correction terms are also plagued by finite volume effects after all, as we have obtained them using our finite volume Fourier transform. Therefore, we can only trust the correction effects in the case when p is large, or equivalently, only at scales that are not too long.

To see the structure of the actual results, we will have to do the calculations using numerical methods. In order to do these calculations, we need to define the growth function in the (EdS) cosmology we are working with as a function of comoving distance χ and we need to investigate which average comoving distance $\overline{\chi}$ and which comoving width $\Delta\chi$ surveys into the large scale structure of the universe typically envelop. In that way, we can obtain results for the length scales we are typically confronted with in cosmology.

We start by recalling the relation between the comoving distance and the redshift in EdS from chapter 2, where we reintroduce the speed of light c so that our dimensions work out:

$$\chi(z) = \frac{2c}{H_0}\left(1 - \frac{1}{\sqrt{1+z}}\right). \tag{5.44}$$

Following this, we recall that the growing mode of the growth function in EdS is given by:

$$D(z) = \frac{1}{1+z}. \tag{5.45}$$

Using equation (5.44) we rewrite this as:

$$D(\chi) = \left(1 - \frac{H_0\chi}{2c}\right)^2. \tag{5.46}$$

In our discussion, we want to look at distances typical for the next generation of surveys. Following [52], we consider surveys of redshift up to $z = 5$ with bin width $\Delta z \approx 0.3$. Because we are working with the comoving distance χ as our main parameter, we use equation (5.44) to convert these redshifts and bin widths into comoving distances. Doing this yields that redshifts in the range $1 \leq z \leq 5$ correspond to distances in the range of 1500Mpc $h^{-1} \leq \overline{\chi} \leq$ 3500Mpc h^{-1}. Moreover, the bin widths range from $\Delta\chi \approx$ 300Mpc h^{-1} at $z = 1$, to $\Delta\chi \approx$ 60Mpc h^{-1} at $z = 5$. Hence, we will look at comoving distances in this range of values.

Moreover, we need to find a way to deal with the separate dependence on $\mathbf{k}$ and p in our expressions, because our normal expression for P_{22} depends only on the size k of the three-dimensional vector $\mathbf{k}$. We can fix this in a number of ways, where each time the key is to ensure that the total argument of our power spectrum $\tilde{P}(\mathbf{k}, p)$ equals k. In this thesis, we have looked at $|\mathbf{k}| = \frac{k}{\sqrt{2}}, |p| = \frac{k}{\sqrt{2}}$; $|\mathbf{k}| = 0, |p| = k$

[5] This is not so difficult to show using the trigonometric identities from equation (5.35).

and at $|\mathbf{k}| = k, |p| = 0$.

After doing multiple calculations for various comoving distances and bin sizes, we find that our results are qualitatively the same and all have a form similar to figure 5.3 regardless of coordinate choice. In this figure, we see that the correction effects, which are the terms which go like $D'^2(\overline{\chi})$, have the same shape as the first order term, which goes like $D^2(\overline{\chi})$. Moreover, as we have seen before in our 1d toy model, the first order term (which is only affected by our finite volume definition of the Fourier transform) completely agrees with the normal result for large enough k.

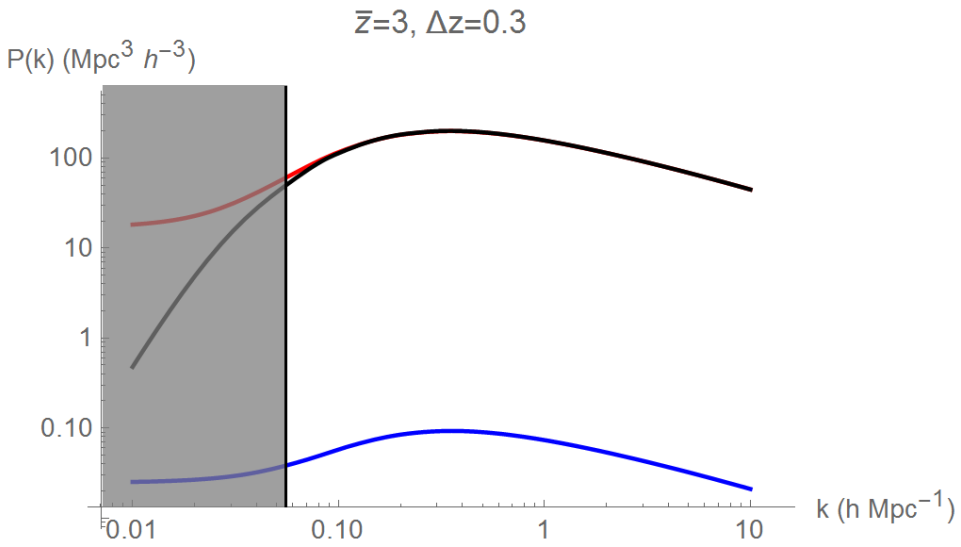

Figure 5.3: The time dependent $\tilde{P}_{22}$ terms first order (red line) and correction (blue line) contribution plotted together with the standard P_{22} power spectrum (black line) for average redshift $\overline{z} = 3$ and bin width $\Delta z = 0.3$. We see that the correction term and the first order term have the same shape, implying that the light cone effect does not affect the shape of the power spectrum. Note that as before we can only trust the result for $k > \frac{2\pi}{\Delta\chi}$ because of finite volume effects. It turns our that the finite volume effect becomes negligible around $k = k_{\mathrm{NL}}$.

Now that we know that the $D'^2(\overline{\chi})$-like correction term follows the shape of the $D^2(\overline{\chi})$-like first order P_{22} term, we are interested in calculating how big they are relative to the size of the time-independent effect. Plotting the size of the correction divided by the size of the first order term, we find that their ratio is very close to $\frac{D'^2(\overline{\chi})(\Delta\chi)^2}{D^2(\overline{\chi})12}$ for the large k at which our finite volume does not have an effect, which was the result we found for $\tilde{P}_{13}$ as well. We have plotted the ratio for the same example in figure 5.4, where we used (5.44) to calculate the bin width $\Delta\chi$.

In order to see why the ratio between the normal (finite volume) term, and the time dependent correction takes this value, we need to further inspect our expressions. More specifically, we want to find an expression for the correction term as a fraction of our first order term. This motivates us to further investigate the ratio between the correction terms and the first order term within the integrand, a quantity which we will call $R(q, \Delta\chi)$:

$$R(q,\Delta\chi) = -D'^2(\overline{\chi})\left(\frac{-(\Delta\chi)^2[\frac{1}{2}\cos(q\Delta\chi)+\frac{1}{2}]}{q^2} + \frac{2\Delta\chi q\sin(q\Delta\chi)}{q^4} + \frac{2\cos(q\Delta\chi)-2}{q^4}\right) \times \left[D^2(\overline{\chi})\frac{2\cos(q\Delta\chi)-2}{-q^2}\right]^{-1}. \tag{5.47}$$

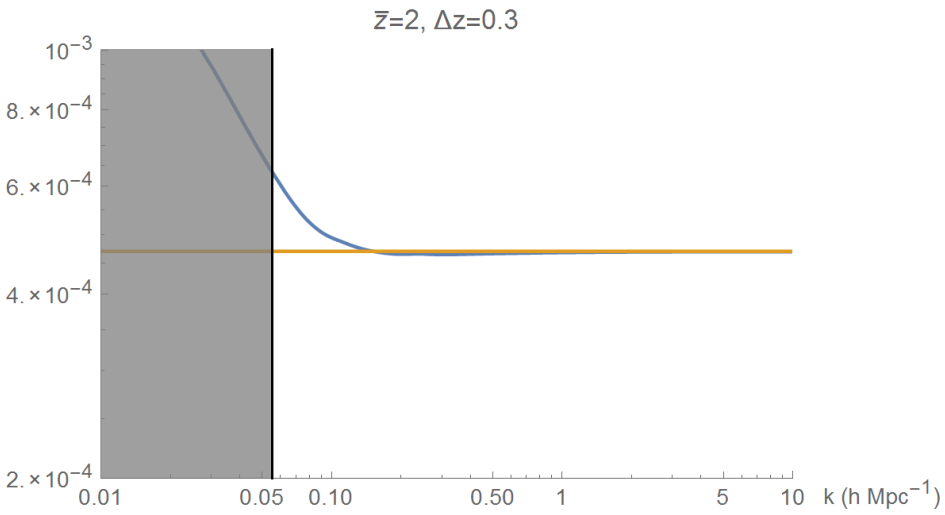

Figure 5.4: The ratio between the correction terms and the first order term in blue, plotted together with the constant $\frac{D'^2(\overline{\chi})(\Delta\chi)^2}{D^2(\overline{\chi})12}$. We see that the values approximately match for k at which there is no finite volume effect, so for $k > \frac{2\pi}{\Delta\chi}$.

To learn more about this fraction, we will expand it in a series. This gives us:

$$R(q,\Delta\chi) = \frac{(\Delta\chi)^2 D'^2(\overline{\chi})}{D^2(\overline{\chi})}\left(\frac{(\Delta\chi)^2 q^2}{144} + \frac{(\Delta\chi)^4 q^4}{4320} + \mathcal{O}(q^6)\right). \tag{5.48}$$

From this equation, we can see a constant which has the same form as our result. The mysterious factor of $\frac{1}{12}$ is not so easily explained unfortunately. The fraction we get from equation (5.48) is the one we obtain if we divide the terms within the integrand, whereas the terms in the actual calculation are integrated over. The only thing pointing to the factor of 12, can be seen when looking at the separate expansions of the first order term and correction terms.

$$\frac{2\cos(q\Delta\chi) - 2}{-q^2} = (\Delta\chi)^2\left(1 - \frac{q^2(\Delta\chi)^2}{12} + \mathcal{O}(q^4)\right), \tag{5.49}$$

$$\frac{-(\Delta\chi)^2[\frac{1}{2}\cos(q\Delta\chi) + \frac{1}{2}]}{q^2} + \frac{2\Delta\chi q\sin(q\Delta\chi)}{q^4} + \frac{2\cos(q\Delta\chi) - 2}{q^4} = (\Delta\chi)^4\left(\frac{(\Delta\chi)^2 q^2}{144} + \mathcal{O}(q^4)\right). \tag{5.50}$$

From this expansion, we see a relative factor of 12 between the correction and the first order term that goes like q^2.

Let us for now assume that the fraction between the correction terms and the first order term in fact always is equal to $\frac{D'^2(\overline{\chi})(\Delta\chi)^2}{D^2(\overline{\chi})12}$. This means that the full expression for $\tilde{P}(\mathbf{k},p)$ is given by:

$$\boxed{\tilde{P}(\mathbf{k},p,\overline{\chi},\Delta\chi) = \frac{1}{D^2(\overline{\chi})}\left(P_L(\mathbf{k},p,\overline{\chi}) + (1 + \frac{D'^2(\overline{\chi})(\Delta\chi)^2}{D^2(\overline{\chi})12})\,[P_{13}(\mathbf{k},p,\overline{\chi}) + P_{22}(\mathbf{k},p,\overline{\chi})]\right)}, \tag{5.51}$$

where in this equation we have explicitly written down the dependence of $\tilde{P}(\mathbf{k},p)$ on $\overline{\chi}$ and $\Delta\chi$. We can consider this equation to really be our final result for the thesis, where we found the factor analytically for $\tilde{P}_{13}$, and numerically for $\tilde{P}_{22}$.

Then, the question arises at which redshift this term is of a significant size. To investigate this, we plot the ratio $\frac{D'^2(\overline{\chi})(\Delta\chi)^2}{D^2(\overline{\chi})12}$ for average comoving distance $\overline{\chi} \in (1000, 4000)$ Mpc h^{-1} and bin width $\Delta\chi \in (0, 500)$ Mpc h^{-1} in figure 5.5. Note that the bin widths from typical surveys are no larger than $\Delta\chi \approx 300$ Mpc h^{-1} for small comoving distance χ and $\Delta\chi \approx 60$ Mpc h^{-1} for large comoving distance χ [52]. However, we chose a domain beyond those values in order to investigate where the effect does become significant.

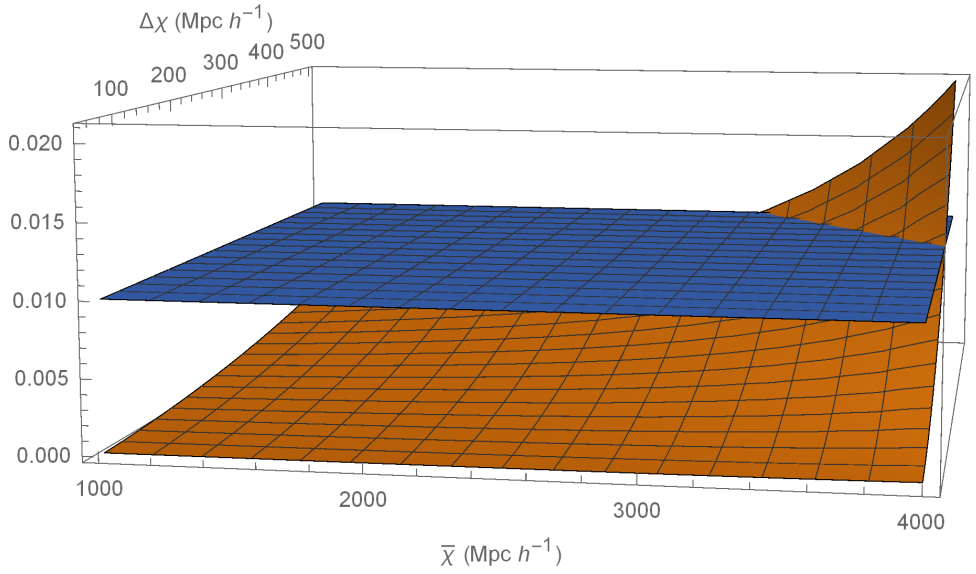

Figure 5.5: The ratio between the correction terms and the first order term, plotted for $\overline{\chi} \in (1000, 4000$ Mpc $h^{-1})$ and $\Delta\chi \in (0, 500)$ Mpc h^{-1} together with the 1% plane. The large bin width results at large comoving distance are not realistic, as bin width decreases with comoving distance.

From figure 5.5 we can see that there is some domain in terms of $\overline{\chi}$ and $\Delta\chi$ in which the light cone effect is larger than order 1%. This means that we can conceive surveys for which the light cone effect needs to be taken into account in the analysis. To further clarify which areas those are, we have also made a contour plot of this ratio in figure 5.6.

However, in cosmology the comoving distance χ is not a quantity that is often used to express radial distances. It has served the objective of this thesis well in the derivation thus far, but to obtain an equivalent of figure 5.6 that speaks to the observational cosmologist, we have to make a plot using the redshift z. Therefore, we use equation (5.44) to express the ratio that corrects the perturbative terms in equation (5.51) in terms of redshift z and redshift bin width Δz. Doing this, we see that:

$$\frac{D'^2(\overline{\chi})}{12D^2(\overline{\chi})} = \frac{H_0^2}{12c^2}(1+z), \tag{5.52}$$

$$(\Delta\chi)^2 = \frac{4c^2}{H_0^2}\left[\frac{1}{\sqrt{1+z-\Delta z/2}} - \frac{1}{\sqrt{1+z+\Delta z/2}}\right]^2, \tag{5.53}$$

such that:

$$\frac{D'^2(\overline{\chi})(\Delta\chi)^2}{D^2(\overline{\chi})12} = \frac{1+z}{3}\left[\frac{1}{\sqrt{1+z-\Delta z/2}} - \frac{1}{\sqrt{1+z+\Delta z/2}}\right]^2. \tag{5.54}$$

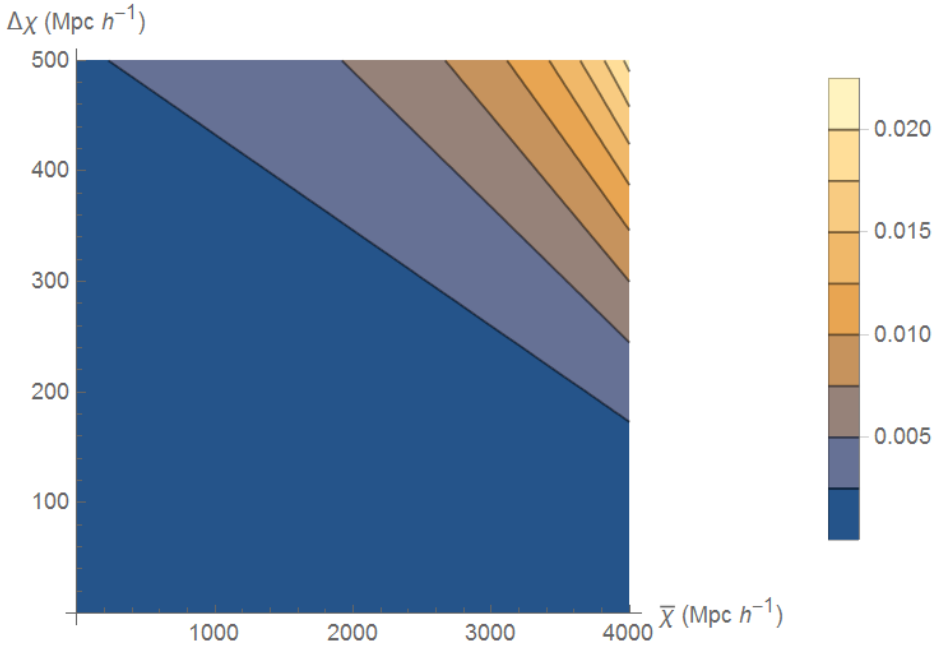

Figure 5.6: A contour plot of the fraction shown in figure 5.5.

If we use these equations to plot the correction in a contour plot for different redshifts and bin widths, we find the picture in figure 5.7. We see that only surveys which have large redshift bins Δz at low redshift z need to take into account the light cone effect.

Moreover, we recall that the light cone effect only corrects the one-loop perturbative terms for the power spectrum. Therefore, the light cone effect only contributes for k where one-loop contributions are the dominant contribution to the power spectrum.

5.4 Summary

We have seen that to take into account the light cone effect, we need to follow a number of steps. First, we need to specify a redshift bin in which we are working, because usually redshift surveys approximate the cosmological evolution of objects by evaluating the growth function at the average time within the bin. To relate to this, we need to redefine our Fourier transform to be defined over a finite volume along the line-of-sight direction. Our discussion of the 1d toy model shows that we can do this, but that our results are only valid for wavelengths shorter than the volume of our bin $\Delta\chi$, or equivalently $k > \frac{2\pi}{\Delta\chi}$.

To describe observations on the light cone, we defined the reduced density field $\tilde{\delta}(\mathbf{x}, \chi)$. Following this, we followed the SPT framework to find expressions which describe the result for our reduced power spectrum. In general, the results we obtained were complex because we broke statistical homogeneity, but we can deal with this by demanding that the wavenumbers p and p' along the line of sight obey $p = -p'$. Doing the calculations within a normal EdS cosmology, we find that the linear results only differ trivially from the SPT results, but that the $\tilde{P}_{13}$ and $\tilde{P}_{22}$ results get the same additional factor, which we found analytically for $\tilde{P}_{13}$ and which we obtained through numerics on the analytic result for $\tilde{P}_{22}$. In general, we found that our one-loop EdS result on the light cone is given by:

$$\boxed{\tilde{P}(\mathbf{k}, p, \overline{\chi}, \Delta\chi) = \frac{1}{D^2(\overline{\chi})}\left(P_L(\mathbf{k}, p, \overline{\chi}) + (1 + \frac{D'^2(\overline{\chi})(\Delta\chi)^2}{D^2(\overline{\chi})12})\left[P_{13}(\mathbf{k}, p, \overline{\chi}) + P_{22}(\mathbf{k}, p, \overline{\chi})\right]\right)}. \tag{5.55}$$

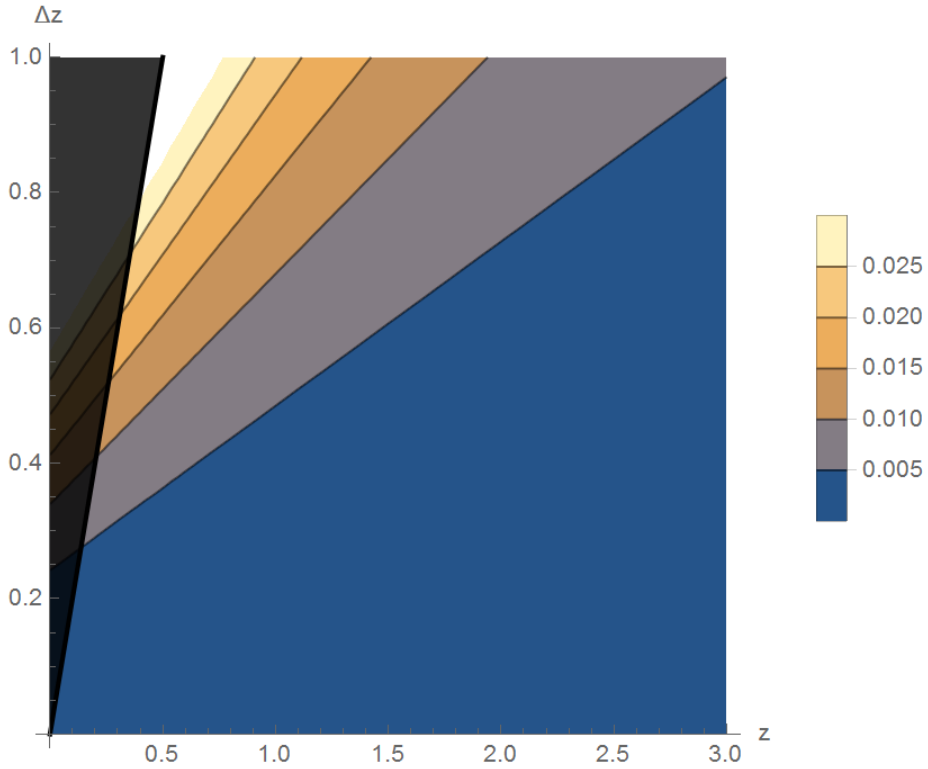

Figure 5.7: A contour plot of the correction in terms of redshift. The greyed out area is the area where $\Delta z > 2z$. We see that in redshift space, only large bins at low redshift induce a significant effect. More specifically, the effect is of order 1% for $\Delta z \gtrsim 0.35(1+z)$.

At last, we looked at the typical size of the correction term that is associated with $\tilde{P}_{22}$ and $\tilde{P}_{13}$. We see that this effect only becomes of order 1% when the redshift bin is relatively large compared to the average redshift; $\Delta z \gtrsim 0.35(1+z)$, as is shown in figure 5.7.

Chapter 6

Conclusion

6.1 Summary

We started this thesis by giving introducing what large scale structure entails, and why it is relevant to study it. Moreover, we gave a short description of the light cone effect, which is an effect that arises because we observe galaxies on our past light cone. We continued with a crash course in the basics of modern cosmology to make the reader familiar with the relevant concepts, and then started describing the standard theory that is used to describe the large scale structure of the universe. We saw that within this Standard Perturbation Theory (SPT) framework, we can think of the matter within the universe as a classical fluid, which we can describe using the Euler and continuity equations. We showed how we can approximate the solution to this equation perturbatively if we make a few reasonable assumptions, and explained how we can use a statistical description to deal with the complications that arise when observing our universe.

After discussing SPT, we gave some further motivation to study large scale structure in detail, by describing the importance of large scale structure as a cosmological probe. We explained that large scale structure observations may give insight in the mysterious components that make up most of the universe, and showed that they can also help us to understand the very early universe better. In addition, we discussed some of the key next generation observations that will provide us with the necessary data to do so.

Then, we moved on to include the light cone effect in SPT applied to observations. In the standard theory, the light cone effect is neglected within observation bins along the line of sight. We, however, explicitly included the effect by evaluating the growth functions for the density fields on the past light cone within these bins. We studied bins in a 1d toy model to see what the implication of working within a finite volume was with respect to the normal treatment in which the volume is assumed to be infinite. To make a good comparison between this finite volume result and the normal result, we saw that we had to require $p = -p'$ for the one-dimensional Fourier modes, and that we needed to employ a double integration to deal with a Dirac delta function that hinders comparison of the two. We found that for a finite volume discussion, we can trust the results only for wavenumbers $p > \frac{2\pi}{\Delta\chi}$, where $\Delta\chi$ parametrizes the bin size. We explained that this makes sense physically, because within a finite volume we are not able to observe long wavelengths (or equivalently, small wavenumbers).

After this, we calculated the light cone effect up to one-loop order. We found that the linear result depends in a trivial way on the approximated result for linear volume, but at one-loop order the results were more complicated. In general, we saw that because the inclusion of the light cone effect is equivalent to breaking the statistical homogeneity of the observed universe, we can no longer assume that our results for the power spectrum are real. Typically, the results turn out to be complex. We solved this by requiring that the Fourier modes along the line of sight were chosen in a way that ensured the reality

of our resulting power spectrum, analogously to the requirement we made in our discussion of the 1d toy model. To be able to compare our results with the standard result, we also had to apply the double integral trick we used for the 1d toy model once more.

Having applied this combination of tricks, we found that the light cone effect correction of the one-loop result is quantified by a typical factor depending on the bin width and the growth function at the center of the bin. This result is given in equation (5.51). For the $\tilde{P}_{13}$-term, we were able to derive this analytically, whereas for the $\tilde{P}_{22}$ result we saw from numerical evaluation of the analytic result that the correction takes the same form for the entire one-loop result. We considered the significance of the effect by plotting the correction factor for typical comoving distances and bin widths employed in galaxy surveys. By looking at the results in redshift space, we found that the effect is significant for $\Delta z \gtrsim 0.35(1+z)$.

6.2 Outlook

There are a number of areas which are still to be explored by future research on the light cone effect. Given that the effect we quantified is specifically important for observations, every extension which includes other observational effects would add to the value of this work. In addition, we recommend an extension of the work to higher order correlation functions. Finally, we would recommend an extension to a ΛCDM cosmology, because Einstein-de Sitter is a poor approximation for galaxies that are very close by.

For observations, the inclusion of redshift space distortions would be a great addition. After all, many of the observations of large scale structure are done in redshift space. Besides, galaxy bias, a quantity we have not discussed in this thesis, also needs to be included. In a theoretical derivation which includes redshift space distortions and bias, we will have much more precision in our predictions for the power spectrum.

Following an inclusion of such distortions we suggest an extension of the theory to different large scale structure observables. The bispectrum in particular would be a good extension of this work, because the bispectrum is a key probe of primordial non-gaussianity. For similar reason, an extension to the trispectrum might be helpful.

Lastly, a similar derivation in ΛCDM would be very valuable. Einstein-de Sitter is a good model for most of the large scale structure observations, but we really need to quantify the effect of dark energy when probing the universe at redshift $z < 0.4$. Because large scale structure observations also probe the universe at those redshifts, an extension would be highly valuable.

As a small addendum, we realize that requiring $p = -p'$ in order to make our results real is equivalent to throwing out information about the inhomogeneity of the universe we observe due to time dependence. Because in this thesis we were trying to obtain results that can be compared to the normal theory it was a pure necessity, but we encourage readers to think about the physical meaning of the complex parts of our results. If one were to find such a physical meaning, it would be a very valuable extension to the current knowledge we have about large scale structure.

Acknowledgements

I would first and foremost like to thank dr. Enrico Pajer for being my supervisor in writing this thesis. He was a great help in keeping focus throughout this project, and was always able to take a step back when I was lost in formulas. Moreover, he taught me to think about physics in a deeper and more meaningful way by pushing me to develop a physical intuition for the mathematical difficulties. In addition, his sharp questions helped me to really take the next step in understanding the subject matter, whereas I might have been satisfied with less than full understanding otherwise.

I would also like to thank Yvette Welling for the enjoyable discussions, the help whenever I encountered a difficulty, and the pointed questions when discussing results of derivations.

Finally I would like to thank my parents and housemates for their interest in the thesis, which helped me in thinking about the subject matter in an accessible way, and which reinforced my sense of wonder about our universe.

Bibliography

[1] http://s980.photobucket.com/user/phanhienqt2/media/2014-Tram-Vu-tru-hoc-hien-dai/32.jpg.html. Accessed: 3 December 2016.

[2] http://www.damtp.cam.ac.uk/user/db275/TEACHING/INFLATION/Lectures.pdf. Accessed:15 December 2016.

[3] P. A. R. Ade et al. Planck 2013 results. XVI. Cosmological parameters. *Astron. Astrophys.*, 571:A16, 2014.

[4] Shadab Alam et al. The clustering of galaxies in the completed SDSS-III Baryon Oscillation Spectroscopic Survey: cosmological analysis of the DR12 galaxy sample. *Submitted to: Mon. Not. Roy. Astron. Soc.*, 2016.

[5] Marcelo Alvarez et al. Testing Inflation with Large Scale Structure: Connecting Hopes with Reality. 2014.

[6] Luca Amendola et al. Cosmology and fundamental physics with the Euclid satellite. *Living Rev. Rel.*, 16:6, 2013.

[7] C. Armendariz-Picon, Viatcheslav F. Mukhanov, and Paul J. Steinhardt. A Dynamical solution to the problem of a small cosmological constant and late time cosmic acceleration. *Phys. Rev. Lett.*, 85:4438–4441, 2000.

[8] Valentin Assassi, Daniel Baumann, Enrico Pajer, Yvette Welling, and Drian van der Woude. Effective theory of large-scale structure with primordial non-Gaussianity. *JCAP*, 1511:024, 2015.

[9] B. Bassett and R. Hlozek. *Baryon acoustic oscillations*, page 246. 2010.

[10] Daniel Baumann. Inflation. In *Physics of the large and the small, TASI 09, proceedings of the Theoretical Advanced Study Institute in Elementary Particle Physics, Boulder, Colorado, USA, 1-26 June 2009*, pages 523–686, 2011.

[11] F. Bernardeau, S. Colombi, E. Gaztanaga, and R. Scoccimarro. Large scale structure of the universe and cosmological perturbation theory. *Phys. Rept.*, 367:1–248, 2002.

[12] R. R. Caldwell, Rahul Dave, and Paul J. Steinhardt. Cosmological imprint of an energy component with general equation of state. *Phys. Rev. Lett.*, 80:1582–1585, 1998.

[13] S. M. Carroll, W. H. Press, and E. L. Turner. The cosmological constant. *Annual review of astronomy and astrophysics*, 30:499–542, 1992.

[14] Xingang Chen. Primordial Non-Gaussianities from Inflation Models. *Adv. Astron.*, 2010:638979, 2010.

[15] Matthew Colless. Cosmological results from the 2df galaxy redshift survey. In *Measuring and modeling the universe. Proceedings, Symposium, Pasadena, USA, November 17-22, 2002*, pages 196–206, 2003.

[16] Antonio J. Cuesta, Viviana Niro, and Licia Verde. Neutrino mass limits: robust information from the power spectrum of galaxy surveys. *Phys. Dark Univ.*, 13:77–86, 2016.

[17] K. S. Dawson, D. J. Schlegel, C. P. Ahn, S. F. Anderson, É. Aubourg, S. Bailey, R. H. Barkhouser, J. E. Bautista, A. Beifiori, A. A. Berlind, V. Bhardwaj, D. Bizyaev, C. H. Blake, M. R. Blanton, M. Blomqvist, A. S. Bolton, A. Borde, J. Bovy, W. N. Brandt, H. Brewington, J. Brinkmann, P. J. Brown, J. R. Brownstein, K. Bundy, N. G. Busca, W. Carithers, A. R. Carnero, M. A. Carr, Y. Chen, J. Comparat, N. Connolly, F. Cope, R. A. C. Croft, A. J. Cuesta, L. N. da Costa, J. R. A. Davenport, T. Delubac, R. de Putter, S. Dhital, A. Ealet, G. L. Ebelke, D. J. Eisenstein, S. Escoffier, X. Fan, N. Filiz Ak, H. Finley, A. Font-Ribera, R. Génova-Santos, J. E. Gunn, H. Guo, D. Haggard, P. B. Hall, J.-C. Hamilton, B. Harris, D. W. Harris, S. Ho, D. W. Hogg, D. Holder, K. Honscheid, J. Huehnerhoff, B. Jordan, W. P. Jordan, G. Kauffmann, E. A. Kazin, D. Kirkby, M. A. Klaene, J.-P. Kneib, J.-M. Le Goff, K.-G. Lee, D. C. Long, C. P. Loomis, B. Lundgren, R. H. Lupton, M. A. G. Maia, M. Makler, E. Malanushenko, V. Malanushenko, R. Mandelbaum, M. Manera, C. Maraston, D. Margala, K. L. Masters, C. K. McBride, P. McDonald, I. D. McGreer, R. G. McMahon, O. Mena, J. Miralda-Escudé, A. D. Montero-Dorta, F. Montesano, D. Muna, A. D. Myers, T. Naugle, R. C. Nichol, P. Noterdaeme, S. E. Nuza, M. D. Olmstead, A. Oravetz, D. J. Oravetz, R. Owen, N. Padmanabhan, N. Palanque-Delabrouille, K. Pan, J. K. Parejko, I. Pâris, W. J. Percival, I. Pérez-Fournon, I. Pérez-Ràfols, P. Petitjean, R. Pfaffenberger, J. Pforr, M. M. Pieri, F. Prada, A. M. Price-Whelan, M. J. Raddick, R. Rebolo, J. Rich, G. T. Richards, C. M. Rockosi, N. A. Roe, A. J. Ross, N. P. Ross, G. Rossi, J. A. Rubiño-Martin, L. Samushia, A. G. Sánchez, C. Sayres, S. J. Schmidt, D. P. Schneider, C. G. Scóccola, H.-J. Seo, A. Shelden, E. Sheldon, Y. Shen, Y. Shu, A. Slosar, S. A. Smee, S. A. Snedden, F. Stauffer, O. Steele, M. A. Strauss, A. Streblyanska, N. Suzuki, M. E. C. Swanson, T. Tal, M. Tanaka, D. Thomas, J. L. Tinker, R. Tojeiro, C. A. Tremonti, M. Vargas Magaña, L. Verde, M. Viel, D. A. Wake, M. Watson, B. A. Weaver, D. H. Weinberg, B. J. Weiner, A. A. West, M. White, W. M. Wood-Vasey, C. Yeche, I. Zehavi, G.-B. Zhao, and Z. Zheng. The Baryon Oscillation Spectroscopic Survey of SDSS-III. *The Astronomical Journal*, 145:10, January 2013.

[18] Scott Dodelson. *Modern cosmology.* Academic Press, San Diego, CA, 2003.

[19] A. Einstein. Die Feldgleichungen der Gravitation. *Sitzungsberichte der Königlich Preußischen Akademie der Wissenschaften (Berlin), Seite 844-847.*, 1915.

[20] D. J. Eisenstein, D. H. Weinberg, E. Agol, H. Aihara, C. Allende Prieto, S. F. Anderson, J. A. Arns, É. Aubourg, S. Bailey, E. Balbinot, and et al. SDSS-III: Massive Spectroscopic Surveys of the Distant Universe, the Milky Way, and Extra-Solar Planetary Systems. *The Astronomical Journal*, 142:72, September 2011.

[21] Daniel J. Eisenstein and Wayne Hu. Power spectra for cold dark matter and its variants. *Astrophys. J.*, 511:5, 1997.

[22] Daniel J. Eisenstein, Hee-jong Seo, and Martin J. White. On the Robustness of the Acoustic Scale in the Low-Redshift Clustering of Matter. *Astrophys. J.*, 664:660–674, 2007.

[23] A. Friedmann. Über die Krümmung des Raumes. *Zeitschrift fur Physik*, 10:377–386, 1922.

[24] J. N. Fry. The Galaxy correlation hierarchy in perturbation theory. *The Astrophysical Journal*, 279:499–510, April 1984.

[25] M. Fukugita and P. J. E. Peebles. The Cosmic Energy Inventory. *The Astrophysical Journal*, 616:643–668, December 2004.

[26] M. H. Goroff, B. Grinstein, S.-J. Rey, and M. B. Wise. Coupling of modes of cosmological mass density fluctuations. *The Astrophysical Journal*, 311:6–14, December 1986.

[27] S.W. Hawking. The development of irregularities in a single bubble inflationary universe. *Physics Letters B*, 115(4):295 – 297, 1982.

[28] D. J. Heath. The growth of density perturbations in zero pressure friedmannlematre universes. *Monthly Notices of the Royal Astronomical Society*, 179(3):351–358, 1977.

[29] A. F. Heavens and A. N. Taylor. A spherical harmonic analysis of redshift space. *Monthly Notices of the Royal Astronomical Society*, 275(2):483–497, 1995.

[30] Mark P. Hertzberg. Effective field theory of dark matter and structure formation: Semianalytical results. *Phys. Rev.*, D89(4):043521, 2014.

[31] G. Hinshaw, D. Larson, E. Komatsu, D. N. Spergel, C. L. Bennett, J. Dunkley, M. R. Nolta, M. Halpern, R. S. Hill, N. Odegard, L. Page, K. M. Smith, J. L. Weiland, B. Gold, N. Jarosik, A. Kogut, M. Limon, S. S. Meyer, G. S. Tucker, E. Wollack, and E. L. Wright. Nine-year Wilkinson Microwave Anisotropy Probe (WMAP) Observations: Cosmological Parameter Results. *The Astrophysical Journal Supplement*, 208:19, October 2013.

[32] Cullan Howlett, Antony Lewis, Alex Hall, and Anthony Challinor. CMB power spectrum parameter degeneracies in the era of precision cosmology. *JCAP*, 1204:027, 2012.

[33] E. Hubble. A Relation between Distance and Radial Velocity among Extra-Galactic Nebulae. *Proceedings of the National Academy of Science*, 15:168–173, March 1929.

[34] J. C. Jackson. A critique of Rees's theory of primordial gravitational radiation. *MNRAS*, 156:1P, 1972.

[35] Raul Jimenez, Carlos Pena-Garay, and Licia Verde. Neutrino footprint in Large Scale Structure. *Phys. Dark Univ.*, 15:31–34, 2017.

[36] N. Kaiser. Clustering in real space and in redshift space. *MNRAS*, 227:1–21, July 1987.

[37] Martin Kunz and Domenico Sapone. Dark Energy versus Modified Gravity. *Phys. Rev. Lett.*, 98:121301, 2007.

[38] Ofer Lahav, Per B. Lilje, Joel R. Primack, and Martin J. Rees. Dynamical effects of the cosmological constant. *Monthly Notices of the Royal Astronomical Society*, 251(1):128–136, 1991.

[39] Antony Lewis, Anthony Challinor, and Anthony Lasenby. Efficient computation of CMB anisotropies in closed FRW models. *Astrophys. J.*, 538:473–476, 2000.

[40] Juan Martin Maldacena. Non-Gaussian features of primordial fluctuations in single field inflationary models. *JHEP*, 05:013, 2003.

[41] Colin McGill. The redshift projection i. caustics and correlation functions. *Monthly Notices of the Royal Astronomical Society*, 242(3):428–438, 1990.

[42] Enrico Pajer and Matias Zaldarriaga. On the Renormalization of the Effective Field Theory of Large Scale Structures. *JCAP*, 1308:037, 2013.

[43] Nathalie Palanque-Delabrouille et al. Neutrino masses and cosmology with Lyman-alpha forest power spectrum. *JCAP*, 1511(11):011, 2015.

[44] Will J. Percival. Large Scale Structure Observations. In *Proceedings, International School of Physics 'Enrico Fermi': New Horizons for Observational Cosmology: Rome, Italy, June 30-July 6, 2013*, volume 186, pages 101–135, 2015. [,317(2015)].

[45] Planck Collaboration, P. A. R. Ade, N. Aghanim, M. I. R. Alves, C. Armitage-Caplan, M. Arnaud, M. Ashdown, F. Atrio-Barandela, J. Aumont, H. Aussel, and et al. Planck 2013 results. I. Overview of products and scientific results. *Astronomy and Astrophysics*, 571:A1, November 2014.

[46] Romn Scoccimarro, H. M. P. Couchman, and Joshua A. Frieman. The bispectrum as a signature of gravitational instability in redshift space. *The Astrophysical Journal*, 517(2):531, 1999.

[47] Alexei A. Starobinsky. Dynamics of Phase Transition in the New Inflationary Universe Scenario and Generation of Perturbations. *Phys. Lett.*, B117:175–178, 1982.

[48] Masahiro Takada, Eiichiro Komatsu, and Toshifumi Futamase. Cosmology with high-redshift galaxy survey: neutrino mass and inflation. *Phys. Rev.*, D73:083520, 2006.

[49] Max Tegmark et al. Cosmological Constraints from the SDSS Luminous Red Galaxies. *Phys. Rev.*, D74:123507, 2006.

[50] N. Turok and D. N. Spergel. Scaling solution for cosmological sigma models at large N. *Physical Review Letters*, 66:3093–3096, June 1991.

[51] Obinna Umeh, Sheean Jolicoeur, Roy Maartens, and Chris Clarkson. A general relativistic signature in the galaxy bispectrum. 2016.

[52] Yvette Welling, Drian van der Woude, and Enrico Pajer. Lifting Primordial Non-Gaussianity Above the Noise. *JCAP*, 1608(08):044, 2016.

[53] Kazuhiro Yamamoto, Hiroaki Nishioka, and Yasushi Suto. The cosmological light cone effect on the power spectrum of galaxies and quasars in wide-field redshift surveys. *Astrophys. J.*, 527:488–497, 1999.

[54] D. G. York, J. Adelman, J. E. Anderson, Jr., S. F. Anderson, J. Annis, N. A. Bahcall, J. A. Bakken, R. Barkhouser, S. Bastian, E. Berman, W. N. Boroski, S. Bracker, C. Briegel, J. W. Briggs, J. Brinkmann, R. Brunner, S. Burles, L. Carey, M. A. Carr, F. J. Castander, B. Chen, P. L. Colestock, A. J. Connolly, J. H. Crocker, I. Csabai, P. C. Czarapata, J. E. Davis, M. Doi, T. Dombeck, D. Eisenstein, N. Ellman, B. R. Elms, M. L. Evans, X. Fan, G. R. Federwitz, L. Fiscelli, S. Friedman, J. A. Frieman, M. Fukugita, B. Gillespie, J. E. Gunn, V. K. Gurbani, E. de Haas, M. Haldeman, F. H. Harris, J. Hayes, T. M. Heckman, G. S. Hennessy, R. B. Hindsley, S. Holm, D. J. Holmgren, C.-h. Huang, C. Hull, D. Husby, S.-I. Ichikawa, T. Ichikawa, Ž. Ivezić, S. Kent, R. S. J. Kim, E. Kinney, M. Klaene, A. N. Kleinman, S. Kleinman, G. R. Knapp, J. Korienek, R. G. Kron, P. Z. Kunszt, D. Q. Lamb, B. Lee, R. F. Leger, S. Limmongkol, C. Lindenmeyer, D. C. Long, C. Loomis, J. Loveday, R. Lucinio, R. H. Lupton, B. MacKinnon, E. J. Mannery, P. M. Mantsch, B. Margon, P. McGehee, T. A. McKay, A. Meiksin, A. Merelli, D. G. Monet, J. A. Munn, V. K. Narayanan, T. Nash, E. Neilsen, R. Neswold, H. J. Newberg, R. C. Nichol, T. Nicinski, M. Nonino, N. Okada, S. Okamura, J. P. Ostriker, R. Owen, A. G. Pauls, J. Peoples, R. L. Peterson, D. Petravick, J. R. Pier, A. Pope, R. Pordes, A. Prosapio, R. Rechenmacher, T. R. Quinn, G. T. Richards, M. W. Richmond, C. H. Rivetta, C. M. Rockosi, K. Ruthmansdorfer, D. Sandford, D. J. Schlegel, D. P. Schneider, M. Sekiguchi, G. Sergey, K. Shimasaku, W. A. Siegmund, S. Smee, J. A. Smith, S. Snedden, R. Stone, C. Stoughton, M. A. Strauss, C. Stubbs, M. SubbaRao, A. S. Szalay, I. Szapudi, G. P. Szokoly, A. R. Thakar, C. Tremonti, D. L. Tucker, A. Uomoto, D. Vanden Berk, M. S. Vogeley, P. Waddell, S.-i. Wang, M. Watanabe, D. H. Weinberg, B. Yanny, N. Yasuda, and SDSS Collaboration. The Sloan Digital Sky Survey: Technical Summary. *The Astronomical Journal*, 120:1579–1587, September 2000.

[55] S. Zaroubi and Y. Hoffman. Clustering in Redshift Space: Linear Theory. *The Astrophysical Journal*, 462:25, May 1996.